OsloMet – Oslo Metropolitan University

Department of Civil Engineering & Energy Technology
Section of Civil Engineering

Master Program in Structural Engineering & Building Technology

MASTER THESIS

SUMMARY / SYNOPSIS
This study has investigated the effects of scaled distance, façade thickness, Young's modulus and density on the reaction forces of a façade element subjected to blast load, and to what extent an empirical equation can predict the response. The parametric study is done using numerical analyses. Curve fitting is used on the results of the numerical analyses, to find the empirical equation. It is shown that the response of the system is highly dependent on both stiffness and mass of the system in addition to the scaled distance. The results also showed that it is possible to express the response by a simple, yet, accurate empirical equation, which can be useful for an early design stage. However, more detailed equations describing the response is also suggested. The results in this thesis may function as a preliminary study or building block for further research, for example to develop design guidelines for blast resistant structures.

Preface

This thesis is written by Åshild Øyro and Marense Louise Thomassen. The thesis, written in the spring of 2022, is our final project in the master's degree program of Structural Engineering and Building Technology, with specialization in Structural Engineering, at the Department of Civil Engineering and Energy Technology, Faculty of Technology, Arts and Design, Oslo Metropolitan University.

We would like to thank our internal supervisor at Oslo Metropolitan University, Professor Aase Reyes, for guidance and support throughout our project. Further we would like to thank Emrah Erduran at Oslo Metropolitan University, for valuable academic guidance and assistance. We would also like to thank Rune Orderløkken at Oslo Metropolitan University for essential technical support and guidance regarding licencing acquirements.

Further, we would like to thank our external supervisors at the Norwegian Defence Estates Agency, dr. Ole Vestrum and dr. Sumita Dey, for insightful guidance regarding the problem definition, as well as availability and inspiring engagement in our many meetings.

We would also like to thank our families and friends for support and motivation.

Oslo, 24th of May 2022

Åshild Øyro

Marense Louise Thomassen

Table of contents

Figures

Tables

Nomenclature

T_n	Natural period of vibration
ω_n	Natural circular frequency of vibration
f_n	Natural cyclic frequency of vibration
P_{s0}	Peak incident pressure
P_0	Ambient pressure
$P_{\bar{s}o}$	Peak negative pressure
P_r	Reflected pressure
i_s	Positive phase impulse
i_r	Reflected impulse
t_0	Duration of positive phase
t_{0**}	Duration of negative phase
t_a	Arrival time
U_s	Shock velocity
L_w	Wavelength of shock wave
R	Stand-off distance
W	Charge weight
Z	Scaled distance
E_A	Artificial strain energy
E_I	Internal energy
E_W	External work
E_{KE}	Kinetic energy
E_E	Strain energy
E_V	Viscous dissipation energy
E_{FD}	Fictional dissipation energy
E_{IHE}	Internal heat energy
E_{PW}	Contact penalty work
E_{CW}	Constraint penalty work
E_{MW}	Work done by propelling added mass
E_{HF}	External heat energy
E_P	Plastic dissipation
E_{CD}	Creep dissipation energy
E_{DMD}	Damage dissipation energy
E_{DC}	Distortion control dissipation energy
E_{FC}	Fluid cavity energy
δ	Deflection
c	Speed of sound
ζ	Damping ratio
w	Width of façade element
h	Height of façade element
t	Thickness of façade element
E	Young's modulus
ρ	Density

v	Poison's ratio
D	Flexural rigidity
q	Evenly distributed load
t_{cr}	Critical time increment
$\varDelta t$	Time increment
ω_{max}	Highest eigenvalue
L	Plate length between supports
L_e	Length of mesh element

1. Introduction

1.1   Background

There has been an increased interest of protection from intentional and accidental explosions because of earlier catastrophes and the present potential of an explosion occurring. Subsequently, the interest of designing blast resistant structures has increased [1].

Structural design in Europe is largely based on equations and specifications given in the European Standards, provided by The European Commission. These standards are compiled of ten main standards, Eurocodes, covering aspects such as structural safety, serviceability and durability, general actions on structures, geotechnical and seismic design, as well as design and detailing of building materials [2]. The Eurocodes thoroughly describe how to design load bearing structures to resist both dynamic loads and accidental actions. Yet, design and detailing specifications of structures subjected to external explosions are lacking within the Eurocodes.

Some guidelines and manuals do, however, exist. The European Commission has published a technical manual regarding actions on structures from external explosions, giving some detailing on design of structures to resist these actions. This technical report was developed as the topic is not sufficiently covered by the Eurocodes [3]. Further, the American Department of Defence has published a manual covering aspects such as calculations of loads due to explosions and calculation procedures regarding dynamic response and construction details [4]. However, both these manuals focus on a structure's global response to blast loading, with little emphasis on the load transfer from façades to the supporting structure.

The Norwegian Defence Estates Agency (NDEA) is a governmental administrative agency that works with buildings in the defence sector. Amongst other they offer expert knowledge on securing buildings [5]. It is both costly and time consuming to model buildings subjected to blast loads in detail. Therefore, NDEA is interested in researching the possibility of developing guidelines for design against external explosions, in a similar fashion to design codes developed by The European Commission. In the development phase of such a guideline, preliminary research must be completed to uncover aspects important aspects, such as the response of structural components and façades.

1.2   Objectives and scope

When a structure is subjected to a blast load, the façade is the first component encountered by the load. Thus, in terms of designing structures to resist actions from external explosions, it is

important to understand how the different factors that govern the load transfer from the façade to the supporting structure. Deriving an empirical equation describing this load transfer can be highly useful to predict the response, and the subsequent damage due to a blast load. Moreover, an empirical equation reduces the need to detail model a structure, which simplifies the early stages of the structural design. Based on this the following research question is established:

What are the effects of varying the scaled distance, façade thickness, Young's modulus, and density, on the reaction forces of a façade element subjected to a blast load, and to what extent can the response be expressed by an empirical equation?

Figure 1 provides an illustration of the research question. The figure shows how the blast pressure wave, P(t), relates to the reaction forces, F(t), where the box represents the unknown effects different factors have on the behaviour of the reaction forces.
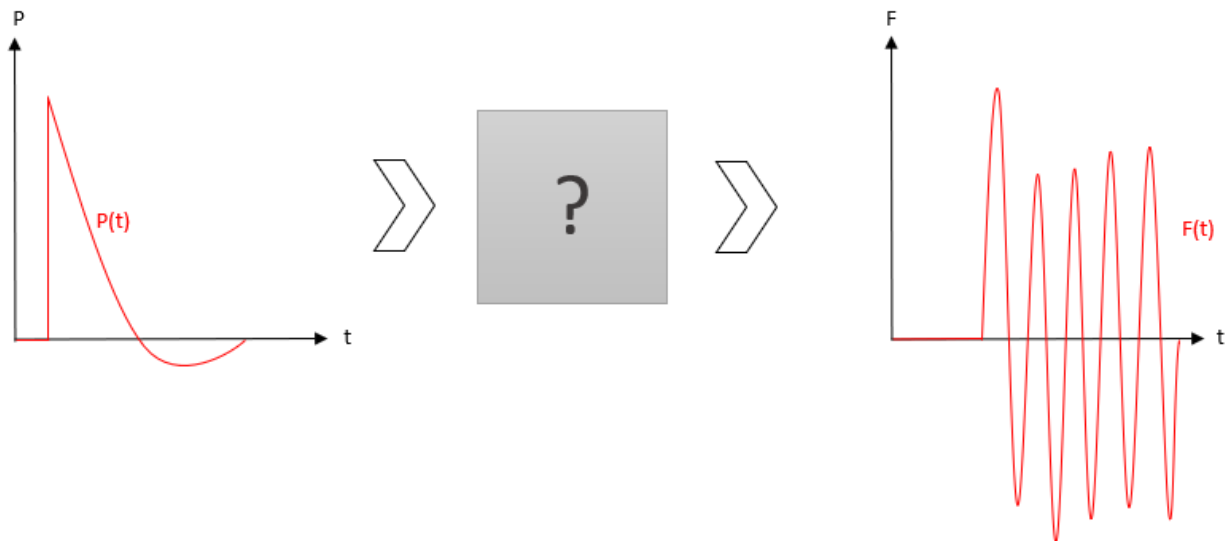
Figure 1: Black box from blast load to reaction forces

The main objective of this thesis is to answer the stated research question. A parametric study of a façade element subjected to blast load is conducted through numerical analyses, using the Finite Element (FE) software Abaqus. The parameters of interest in this parametric study are the thickness of the façade element, the material properties (Young's modulus and density) and, the scaled distance (the relationship between the charge weight of the explosives and the distance from the explosion). From the numerical analyses the reaction forces are obtained, and it is possible to evaluate the different parameters effect on the response, without conducting costly physical experiments.

To analyse the time history of the reaction forces Fast Fourier Transform (FFT) is utilized. This allows for a structured analysis of the parameters, giving a more detailed understanding of the time history of the reaction forces and the effect of the parameters. The FFT is conducted in MATLAB.

To investigate if it is possible to develop an empirical equation describing the response of the façade element, curve fitting is utilized. Different simplified general expressions are evaluated.

1.2.1   Delimitations

Some delimitations regarding the complexity of the material, model and the load are specified. It is expected that the reader has a basic understanding of key concepts and principles related to the topic of structural engineering.

The material properties are specified as linear elastic, disregarding the plastic response of the façade element. Damping is not included in the model of the façade element, as damping is not expected to impact the peak response [6]. Disregarding damping is also favourable for the analysis of the free vibration phase of the response.

The analyses focuses on pressure waves from physical external explosions, therefore explosions due to nuclear and chemical events are disregarded. To simplify the analyses, the negative phase of the blast load is neglected. This is a common simplification as the magnitude of the negative phase is very small compared to the positive phase. Hence, the phase after the peak response is reached, is referred to as the free vibration phase. Further, the analysis only covers lateral loading of the façade element, disregarding explosions occurring at an angle from the façade face.

1.3   Outline

Chapter 2 presents theory cover numerical analysis of a façade subjected to a single pulse load at high velocity. Here, the software utilized in this analysis and a state-of-the-art literature review of a numerical analysis of a plate subjected to blast load using Abaqus is included. Chapter 3 describes the method used. Chapter 4 and 5 presents the results, and the analysis of the results respectively, prior to the discussion in Chapter 6. The conclusion is given in Chapter 7, then some recommendations for further work are given in Chapter 8.

2.   Theory

This chapter gives an overview of important theory regarding rapid dynamic loading, and ways of both calculating and modelling this. The theory is divided into three distinct parts. The first part focuses on the response of a façade element using plate theory and introduces the concept of blast loading. It also contains theory regarding dynamic loading, and briefly introduces mathematical ways of describing complex physical signal. The second part of the theory focuses on how the physical state of a structure and load, can be calculated using the finite element method (FEM). Further, detailing how FEM is implemented in the modelling software Abaqus, and different features regarding Abaqus. Lastly, a state-of-the-art literature review is presented, focusing on the existing research on plates subjected to blast loads.

2.1   Plate theory

A plane geometrical shape can be regarded as a plate if one of its three dimensions are much smaller than the other [7]. To determine the response of such geometrical shapes plate theory is utilized. A plate can be categorized as either a thick or a thin plate, where the limit for being categorized as a thin plate is $t \leq 1/10$ of spanwise dimensions, where t is the thickness of the plate [8].

Thin plates are further categorized based on the maximum deflection of the plate. Plate theory of both thick plates and thin plates with small deflections requires an elastic response, and the theory is based on the Bernoulli-Navier hypothesis of plane cross-sections and Hooke's law [7]. For thin plates with small deflections the load is transmitted by the means of flexural rigidity. However, when the deflection of a plate becomes large compared to the thickness, the curvature naturally increases, leading to loads being transmitted by both flexural rigidity and membrane action. When the deflection of a plate becomes high compared to the thickness, plasticity is introduced in the form of membrane action [9].

Further, a plate can be categorized as either a one-way or a two-way plate, based on how the plate carries loads. When a plate is subjected to a lateral load, three internal moments, M_x, M_y and M_{xy}, occurs as a consequence of the curvature produced by the loading. In two-way plates all three of these moments are significant, whereas a one-way plate is only able to carry these internal moments in the shortest span [7]. Thus, the bending of a thin one-way plate can be described as "bending to a cylindrical surface", illustrated in Figure 2 [9].

Figure 2: Bending to a cylindrical surface

As thin plates are considered to carry lateral loads in a very similar manner as a beam, i.e., by the means of bending, the assumption of thin plate theory resembles the Euler-Bernoulli beam theory [8]. Therefore, the equation of deflection due to bending is derived in a similar way as for a beam. Thus, using plate theory the maximum deflection, occurring in the middle plane, of a one-way plate subjected to an evenly distributed lateral load is calculated by Equation (1) [9],

$$\delta_{max} \approx \frac{5}{384} * \frac{qL^4}{D} \qquad (1)$$

where q is the evenly distributed load, L is the length between the supports, and D is the flexural rigidity, calculated by Equation (2) [8]. In Equation (2) E is the Young's modulus and v is the Poisson's ratio. Note that the flexural rigidity of a plate corresponds to the bending stiffness, EI, of a beam.

$$D = \frac{Et^3}{12(1 - v^2)} \qquad (2)$$

2.2   Blast load calculations

The chemical reaction of explosives creates heat and gases, the fast expansion of this gas creates a pressure wave known as a blast wave [10]. When an explosion occurs the pressure wave generated will expand radially, increasing in size at supersonic velocity [11]. The pressure wave will propagate from its centre at a high speed, with a dilatational form as shown in Figure 3 [12]. The maximum pressure, referred to as the peak pressure, will be highest at the wavefront [10].

The magnitude of a blast load depends on the amount of explosives, and the distance from the centre of the explosion, referred to as stand-off distance [12]. Further, the explosive device's orientation in space, e.g., air blast or surface blast, effects the behaviour of the pressure wave.

The amount of energy released in an explosion, expressed in Joules, is used to determine the magnitude of the explosion. This is expressed by the energy generated in an explosion of TNT, which is approximately 4680 Joules per gram [13]. Therefore, to generalize calculations of blast loads, the weight of explosive is given in the TNT equivalent weight.
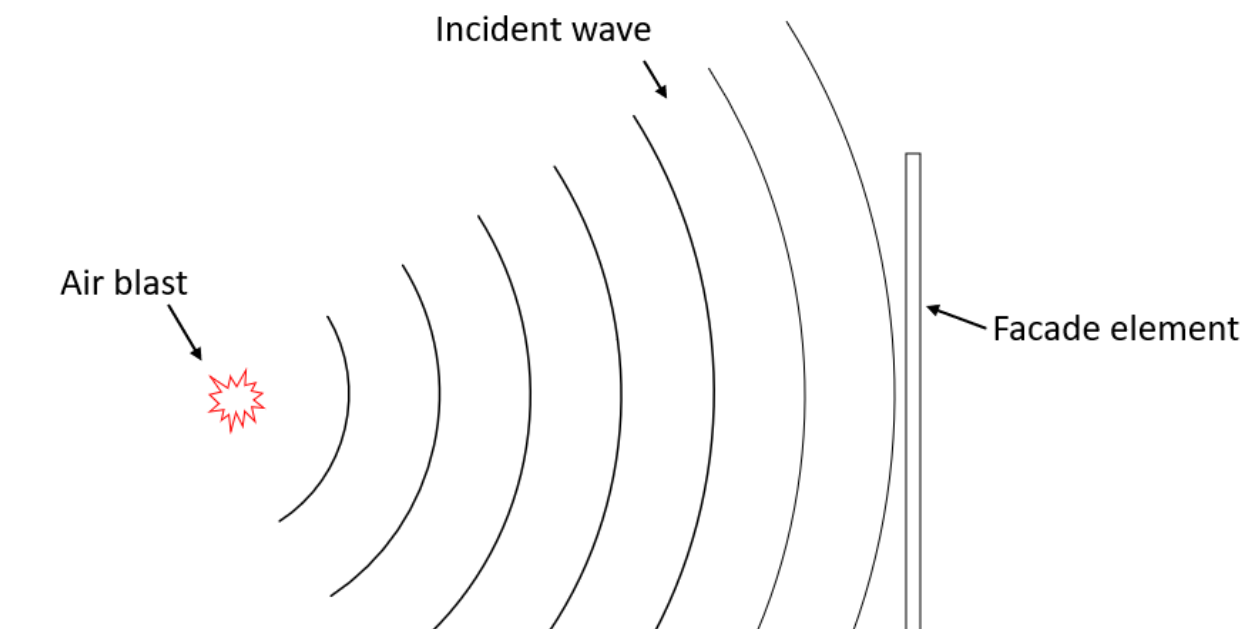
Figure 3: Wave propagation from an air blast

A wave propagating from an explosion is referred to as an incident wave, shown in Figure 3. When the incident blast wave encounters a structure, it will be reflected. Due to a change of momentum when the incident wave reflects, the pressure increase above the incident pressure wave [10]. This additional pressure is referred to as reflected pressure and is quite high compared to the incident pressure [12]. The reflected pressure is dependent of the angle which the incident wave strikes the structure. For a pressure wave perpendicular to a surface, meaning an angle of 0°, the whole surface will be subjected to the peak reflected pressure [13].

2.2.1   Friedlander equation

The Friedlander equation defines a blast wave in simple terms by the initial pressure and its subsequent decaying motion. The equation has proven to be valid for a vast range of explosive sizes. The Friedlander equation is given in Equation (3) [14],

$$p_s(t) = p_{s0}\left(1 - \frac{t}{t_0}\right)e^{-b\frac{t}{t_0}} \qquad (3)$$

where p_{s0} is the peak incident pressure, t is the time, t_0 is the duration of the positive phase and b is the decay coefficient.

Figure 4 shows the pressure time profile of an incident pressure wave, as given by the Friedlander equation. Where p_0 is the ambient pressure, i_s is the impulse, p_{s0}^- is the peak negative pressure, t_0^- is the duration of the negative phase, and t_a is the arrival time of the shock front at a given location. A negative pressure phase, t_0^-, will follow the blast pressure wave as a result from vacuum and reversal of gas in the centre of the blast. The positive pressure phase will be quite high in magnitude but with a rapid duration. The negative pressure phase, on the other hand, will have a smaller magnitude and longer duration. As a result, the consequences due to the positive phase are more severe, and the negative phase is often neglected [12]. If this incident pressure wave reflects of a structure, the pressure time profile will have a similar shape. However, the peak pressure will be higher [1].
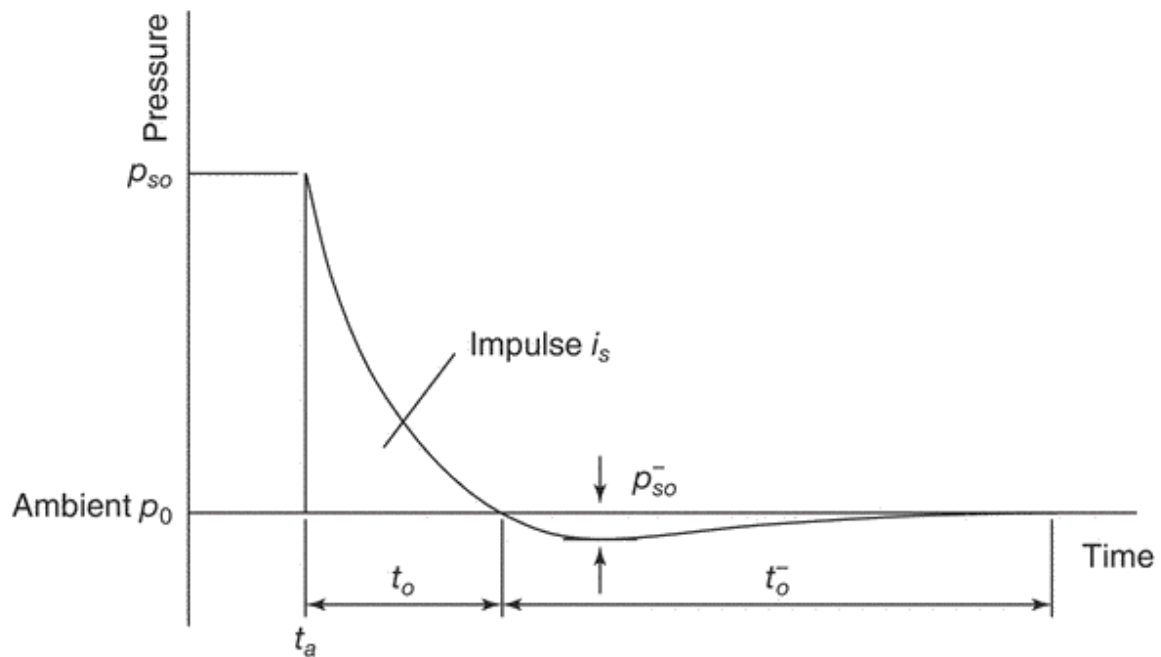
Figure 4: Friedlander pressure-time history curve [5]

2.2.2   Hopkinson-Cranz scaling

To easily determine more complex parameters of a blast wave, scaling laws are frequently used. Hopkinson-Cranz is the most widely used scaling law when determining blast wave parameters. This law, often referred to as cube root scaling, suggests that the relationship between two independent explosions can be defined by a scaled distance, Z [3].

The concept of cube root scaling is based on the energy released in an explosion and the propagation of the blast wave. As blast waves expand spherically, its volume is found by Equation (4),

$$V = \frac{4}{3}\pi R^3 \tag{4}$$

where R is the distance to the centre of the explosion, called stand-off distance. The blast wave parameters are found to be proportional to the energy per unit volume [1]. From this, it is found that the relationship between explosion with alike charge shapes and stand-off distance is constant, as shown in Equation (5). [10], where W is the charge weight of the explosive.

$$\frac{R_1}{W_1^{1/3}} = \frac{R_2}{W_2^{1/3}} \tag{5}$$

9

Scaled distance uses the relationship between two different explosions to define a constant Z. This constant can be used to calculate the magnitude of R or W for a different explosion, with similar shape. The scaled distance, Z, is shown in Equation (6) [10].

$$Z = \frac{R}{W^{1/3}} \tag{6}$$

Experimental results have shown that using scaled distance is valid for charge weights ranging from grams to tonnes [1]. Note, cube root scaling does not directly apply for close in explosions, as the shape of the wave front in close proximities is highly dependent on the charge shape [1]. Scaled distances with a value lower than 0.4 should be used with caution, as the procedure might not capture the real behaviour the explosion [15]. Moreover, scaled distance can be used to find blast parameters related to both incident and reflected blasts waves.

2.2.3 Kingery-Bulmash

As calculation of blast loads parameters are quite complex, most equations are derived from empirical data [16]. The most widely acknowledged approach for calculating blast parameters is the Kingery-Bulmash procedure [15].

The calculation procedure developed by Kingery-Bulmash are quite complex, stating equations and estimations for the shape and blast parameters. The Kingery-Bulmash equations have been satisfactory verified by numerous experiments [14]. Moreover, the equations have been implemented in graphs, as shown in Figure 5 [4]. These graphs use the relationship between scaled distance and the empirical data to determine the different blast parameters.

Figure 5 shows the shock velocity, U_s, wavelength of the shock wave, L_w, reflected pressure, p_r, reflected impulse, i_r, dynamic drag pressure, q_s, and particle velocity behind the wavefront, $\bar{u}$. The additional parameters p_{s0}, i_s, t_a, and t_0 are defined previously[10].
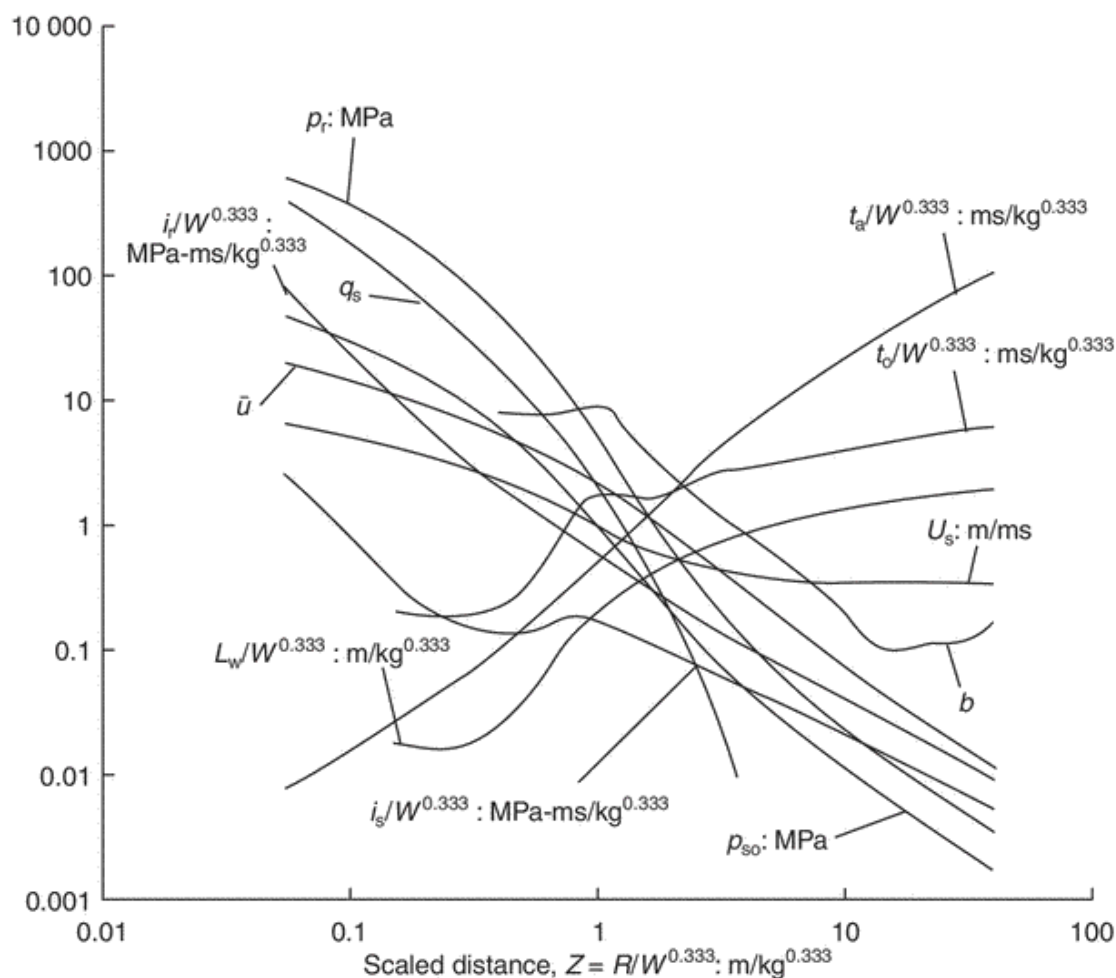
Figure 5: Blast wave parameters of incident and reflected blast wave [1]

2.3 Structural dynamics

The next sections will go through some common definitions in structural dynamics, followed by some aspects of the dynamic response of a system.

2.3.1 Definitions

When the magnitude, direction or position of a load vary with time, it is referred to as a dynamic load. If a structure is subjected to a transient load it will start to vibrate. A structure exposed to dynamic loading can undergo forced and free vibration. A structure undergoes forced vibration when the external force is working [17]. The structure undergoes free vibration if it is moved from its static equilibrium, and then is free to vibrate without being influenced by an external force.

11

The time it takes for the system to complete one cycle in the free vibration phase is referred to as the natural period of vibration, T_n. The natural cyclic frequency of vibration, f_n, is expressed by T_n, as shown in Equation (7) [6].

$$f_n = \frac{1}{T_n} = \frac{\omega_n}{2\pi} \tag{7}$$

Both the T_n and f_n is related to the natural circular frequency of vibration, ω_n, as shown in Equation (8), where k is the stiffness and m is the mass[6].

$$\omega_n = \sqrt{\frac{k}{m}} \tag{8}$$

In the free vibration phase a structure will vibrate with a distinctive circular natural frequency in multiple shapes, referred to as mode shapes. Therefore, for a multi degree of freedom system, the total vibrating response of the system is defined as a sum of the natural circular frequencies of all mode shapes [18].

2.3.2   Dynamic response

A blast load can be considered as a moving pulse load. This means that both the duration and the magnitude of the blast load is time dependent, causing different parts of the structure to be affected by the varying load at different times [11]. This time dependency implies that the pressure from a blast wave is imposed as a dynamic load [13]. Yet, given the high velocity of a blast wave, the properties of the resulting load is quite different from load types known from conventional structural dynamics.

Blast waves from explosions can be viewed as a dynamic single pulse excitation and may be idealized with a simple pulse shape, e.g., rectangular, half cycle or triangular pulse. The response of the system is determined in the forced vibration phase and the free vibration phase. The response of the system will be dependent on the peak pressure load, p_{s0}, positive phase duration, t_0, and the natural period of vibration, T_n [6]. Calculation in structural dynamics can become quite complex. Thus, dynamic response of structures can be analysed in different finite element software programs, such as Abaqus and LS-DYNA. These programs can calculate both the blast wave as well as the dynamic response of the structure [15].

2.4　Fourier

2.4.1　Fourier series

By using Fourier series, an arbitrary periodic function, or signal, may be written mathematically as a sine and cosine function with n terms. A Fourier series is calculated using three Fourier coefficients a_0, a_n, and b_n, the frequency, ω_0, and the period of the function, T. The equation of a Fourier series is stated in Equation (9) [19].

$$F(t) = a_0 + \sum_{n=1}^{0} (a_n \cos n\omega_0 t + b_n \sin n\omega_0 t) \tag{9}$$

The Fourier coefficient a_0, a_n, and b_n calculated by Equation (10), (11), and (12) respectively [19].

$$a_0 = \frac{2}{T} \int_{-T/2}^{T/2} f(t)\, dt \tag{10}$$

$$a_n = \frac{2}{T} \int_{-T/2}^{T/2} f(t)\cos(n\omega_0 t)\, dt \qquad n = 0, 1, 2, \dots \tag{11}$$

$$b_n = \frac{2}{T} \int_{-T/2}^{T/2} f(t)\sin(n\omega_0 t)\, dt \qquad n = 1, 2, 3, \dots \tag{12}$$

The weight of each individual term of a Fourier series, is described by the values of a_n and b_n. For arbitrary periodic functions and signals described as a function of time, the values of a_0, a_n, and b_n can be directly determined.

2.4.2　Fast Fourier Transform

To produce a mathematical model of an arbitrary physical signal composed by sampled data, Fourier transforms can be used. When analysing a physical signal, e.g., the signal of a vibrating plate, Fourier transforms can be a powerful tool, enabling the transformation of the signal to a mathematical model. A physical continuous-time signal must be transformed into a discrete-time signal, meaning the continuous-time signal is transformed into several discrete data points [19].

When a physical signal is sampled, thereby consisting of discrete-time signals, the Fourier constant must be calculated by the data points of this sample. In such cases the signal, which

consists of discrete-time data points, is directly converted from discrete-time to the frequency domain of the given signal. This is what is known as Discrete Fourier Transforms (DFT) [19]. When the number of measurements, denoted as N, become large the calculations in a DFT results in many cumbersome operations which in turn leads to many round-off errors. A common way of simplifying a DFT is by using algorithms based on factorisation of N, thus minimizing the calculations. This process is known as Fast Fourier Transform (FFT) [19].

2.5   Finite element method

Basic engineering problems can be solved analytically using commonly known equations describing the laws of physics. However, as problems grow in complexity these equations can become demanding, and even impossible, to solve analytically. The FEM enables the solution of such complex engineering problems. The FEM is based on discretization of the initial problem, i.e., dividing the original configuration into smaller parts [20]. This discretization introduces the concept of nodes, elements, and mesh. Each element is defined by nodes on the boundary of the element. The pattern of these nodes and elements is what defines the mesh. A FEM model is analysed by solving systems of equations at defined integration points [20].

As FEM is based on approximations, the output will also be defined as such. However, the accuracy of the output is naturally dependent on the accuracy of the input. Therefore, by increasing accuracy of the mesh used in the computation, the accuracy of the output may be enhanced [20].

2.5.1   Mesh

Given that the output from a FE model is dependent on the mesh, it is important to understand the appropriate measures that must be undertaken before a mesh can be deemed appropriate for a given problem. This can be done by ensuring convergence of the calculated output, through mesh refinement. Mesh refinement can be undertaken based on different approaches. The arguably easiest, both with regards to computational cost and time, is to reduce the size of the elements, and thus increasing the total number of elements in the mesh [20]. Further, the accuracy of the output can be increased by utilizing full integration, as opposed to reduced integration. Reduced integration uses *one* integration point, extrapolating the calculated output to the nodes. On the other hand, full integration uses an increased number of integration points to obtain a more accurate output at the nodes. The computational cost is higher using full integration, due to the increased number of calculation points [21].

2.6   Abaqus

Abaqus/CAE (Complete Abaqus Environment) is a FE software. To execute an analysis in Abaqus, a procedure is defined by dividing the problem history into steps, where each step defines a unique phase of the problem history. The analysis procedure in each unique step can differ, as the specified analysis is only executed in its belonging step [21]. The state of the model, i.e., the computed stresses and strains, is computed from the previous step and accounted for in the next step in the analysis.

Abaqus allows for both standard and explicit analysis, where Abaqus/Standard and Abaqus/Explicit are two independent modules of the program. The two modules are based on different data structures, where the calculations are based on different theories and analysis methods [21].

Abaqus enables the modelling of blast wave parameters and wave propagation. The equations used in the software is based on the Kingery-Bulmash procedure [15]. Pressure waves produced by an explosion, are modelled in Abaqus as an incident dilatational wave field. This can be done using the CONWEP model in Abaqus/Explicit. By defining the stand-off distance and charge weight of the explosives, measured in TNT, Abaqus gives empirical blast load parameters that describe the time history pressure load. Both the incident and reflected pressure is included in the time history pressure load [22].

2.6.1   Element type

Abaqus enables the use of a wide range of element types. The available element types are dependent on the geometry of the model problem, and solver chosen (explicit or standard) for the analysis. The elements in Abaqus are all based on numerical integration, with either full or reduced integration. Additionally, elements can either use first order (linear) or second order (quadratic) interpolation [21].

For 3D models the standard volume element used in Abaqus is a type of hexahedral solid element. A type of solid isoperimetric element offered in both Abaqus/Standard and Abaqus/Explicit is a hexahedral called C3D8. The element is defined as a "brick" with eight nodes, as illustrated in Figure 6, where each node has three degrees of freedom. The element utilise full integration, which means it will have eight integration points within the element [21].
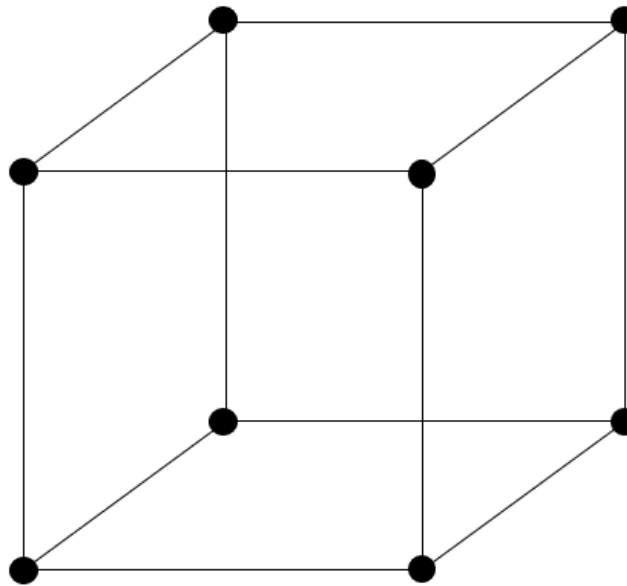
Figure 6: Eight node solid element – C3D8 [16]

2.6.2   Explicit dynamic analysis

Explicit dynamic analysis in Abaqus is based on explicit direct integration methods, commonly used in structural dynamics [21]. Utilizing an explicit integration method is preferable when analysing wave propagation related to blast or impact loading [20]. An explicit dynamic analysis is computed using lumped mass matrices, coupled with central difference integration [21]. In the central difference integration method, the kinematic state of a system is calculated based on times $i - 1/2$ and $i + 1/2$. The integration method can be explicit by using the state of the system from a previous increment, to advance the state in the next increment [20]. It is important to note that the central difference integration method in Abaqus is not considered to be "self-starting", which means that a value for velocity at $\dot{u}^{\left(i-\frac{1}{2}\right)}$ needs to be specified. If this is not specifically defined, the software assumes $\dot{u}=0$ at time zero [21]. Further, in direct integration methods the response history of a system is computed through stepwise integration over a time period [20].

Time increment

An explicit analysis utilizes many small time increments when integrating over a time period [21]. The stability of a time increment is based on a stability limit. The time increment used, must be smaller than the stability limit, shown in Equation (13) [20]. Here L_e is the length of the element, c is the speed of sound in the material and ω_{max} is the highest eigenvalue of the system.

$$t_{cr} \leq \frac{L_e}{c} = \frac{2}{\omega_{max}} \qquad (13)$$

If the time increment exceeds this limit, the calculations will fail, however if the time increment is too small the calculations can become unnecessarily comprehensive and costly [20]. Thus, the explicit integration methods are defined as conditionally stable [21]. Abaqus theory manual states that "stable time increment size is precisely the transit time of a dilatational wave across the element" [21]. This stable time increment is computed automatically by Abaqus [21].

2.7   State of the art – Numerical studies

The calculation procedures of Kingery-Bulmash, described in Section 2.2.3, are largely based on experimental results [15]. However, executing an experiment of a realistic blast load environment requires scrupulous preparation beforehand, access and security clarence to explosives, and complex safety procedures during the experiment. In addition, the right equipment is needed to measure the response, especially since visual inspection is not always possible. Thus, such an experiment is both time consuming and costly. Therefore, numerical simulations can be a good alternative to physical experiments, when researching various effects of blast load

As this thesis uses Abaqus, a small sample of literature covering "plates/façade elements subjected to blast loads in Abaqus" is presented. The research examines different aspects of blast load environment and response, resulting in a somewhat broad focus area. Examples of this include examining the bending stress in a concrete plate, and effects of using inhomogeneous cross-sections [23-25]. The general trends and key findings of this literature study is presented in the following paragraphs.

The literature study shows that simulating blast loads in Abaqus is a recognized practice, as results exhibit high correlation with physical experiments [24-26]. Dharmasena et al. and

Henchie et al. performed explosive test, comparing the results with a numerical analysis from Abaqus, using CONWEP. Both studies found a clear overlap between the simulation in Abaqus and physical results [25, 26]. This observation is supported by the findings of Markose and Rao, where the result of their numerical simulation in Abaqus, were compared with results of physical experiments completed by Ackland et al [24, 27].

Furthermore, several of the numerical analyses covered in this literature study, utilizes an explicit analysis in Abaqus, described in Section 2.6.2 [24-26, 28-31]. Indicating that an explicit analysis is most common when modelling a blast in Abaqus. However, Mendes and Liling are using an implicit analysis [23].

In Abaqus blast loads are commonly modelled in one of two main ways. Either by defining an interaction using a CONWEP definition, as explained in Section 2.6, or by applying the load as an evenly distributed pressure load, using an incident wave with a time history amplitude [23-26, 28, 30, 31]. In a paper from 2014 these two methods are compared and evaluated. The paper found that the CONWEP definition gives a realistic simulation of the blast wave from conventional explosives, by automating important features related to blast loads. However, an incident wave with time history amplitude, permits flexibility by using an amplitude from real life explosion results or vapor cloud explosion, that behaves differently than conventional explosives [32].

The studies indicate that there is no clear trend regarding the orientation, stand-off distance, and charge weight used in the numerical simulations. The experimental studies are relatively small in magnitude, regarding the stand-off distance, and explosives. The stand-off distance varies from around 40 mm to 150 mm, and the amount of TNT ranges from 5 grams to 35 grams of TNT [24, 26, 28, 30]. These can be reviewed as close in blast loads. Dharmasena et al also utilize a small stand-off distance. However, the weight of TNT in this study is noticeably higher, using magnitudes of 1 kg, 2 kg and 3 kg TNT [25]. Yet, even these magnitudes are quite small compared to Mendes and Liling, using a TNT-weight of 275-500 kg [23]. The literature study indicates that most plates are subjected to one blast load, as opposed many blast loads consecutively. However, Henchie et. al tested up to 5 blast loads on the same plate [26]. They found that "Repeated blast loading has insignificant effects on the resultant impulse imparted to the test plates…" [26].

There is a clear trend with regards to the material used. The most commonly used material, when analysing the response of a plate subjected to a blast load, is steel [26, 28-30]. While steel

alloy and polyurea coated steel plates is also analysed [24, 25]. However, Mendes and Liling evaluated a reinforced concrete plate [23].

As metals are strain rate sensitive materials, the effects of high strain rates are commonly included in the material model definition [24-26, 28-31]. Furthermore, Yuen et al also included the effect of temperature in the material model definition, highlighting the benefits of utilizing an approach that includes these effects. They state that "temperature-dependent material properties correlate better with the experiments compared with predictions that excluded temperature dependency" [29].

Further the studies show some variety regarding the thickness and shape, of the different types of plates analysed. The majority of plates investigated are quite thin, ranging from 2-18 mm, except from Dharmasena et al. investigating a 51 mm metallic honeycomb sandwich plate [23-26, 28-31]. The use of a thicker plate in this study is quite appropriate considering the small stand-off distance used combined with TNT-weights of 1 kg, 2 kg and 3 kg. Moreover, Henchie et al. used a circular domex-700 steel plate, with a diameter of 106 mm positioned vertical [26]. Domex-700 steel was also used by Markose and Rao, completing a failure analysis [30]. Later, the effects of making the plate in a composite material of steel and polyurea was investigated. Finding that a layer of polyuria can support a reduction in deformation and impulse transmitted to base structure [24].

The parametric study of Markose and Rao analyse the effect the charge weight and the angle of plate, have on deflection and impulse when a V- plate is subjected to blast. They found that an increase of charge weight results in an increased deflection and impulse, while an increase of the angle results in an increased impulse [30]. Another study by Razak and Alias found that tilting the plate can have a positive effect on the response. However, it is concluded that more research is needed to find the most optimal angle. The deflection of the middle point of the plate was evaluated, as this is where the maximum deflection occurs for a plate with a 0° angle. As the angle of the plate change, the maximum deflection might occur at different locations in the plate. Thus, more research is needed to find the true optimal angle, with regards to the deflection [28].

To conclude, previous numerical studies shows that modelling blast loads in Abaqus is an accepted approach, giving reliable and realistic results. Further, CONWEP is the most used method of modelling blast loads using Abaqus. The studies shows that Abaqus can be used for both close scale explosions and more long-distance explosions. The literature study also shows

that steel is the most used material, where strain rate sensitivity is defined in the material model in most cases. The literature study also indicate that Abaqus can be used to model the effect of blast loads of different magnitudes, on plates with varying thickness, geometrical shape, and orientation

3.   Method

The following sections cover a visualisation of the façade element as a plate, and the method of the analyses and calculations. The description of the method is split into five main parts: A description of the geometry and boundary conditions of the façade element; the composition of the complete Abaqus model; the calculations of the stiffness and natural circular frequency of vibration; Fast Fourier Transform (FFT) of the data to the frequency domain; and curve fitting.

The numerical analysis provides detailed information about the total response of the plate. This response is highly dependent on the stiffness, D, and the natural circular frequency of vibration ω_n. More insight on the total response is gained by evaluating the presence of multiple frequencies in the response, through an FFT. To find a general expression describing the response of the plate, curve fitting is used.

3.1   Visualization

Based on requirements given by SINTEF Building Research Design Guides, regarding minimum exterior height of commercial buildings, the height of the façade element is set to 4 m [33]. The length of the façade element is set to 3 m. Both the height and the length of the façade element is kept constant for every analysis, while the thickness, t, varies. The variation of the thickness is defined in detail in Section 3.2.1. The dimensions of the façade element are illustrated in Figure 7.

Further, Figure 8 gives an illustration of the boundary conditions of the façade element. The top edge is restricted from moving in its length and thickness direction. While the bottom is restricted from moving in all three directions. Consequently, the façade is modelled as a simply supported one-way plate. Therefore, the façade element is henceforth referred to as a plate. Additionally, Figure 8 illustrates how the boundary condition of the element are seen when viewing the cross-section of the element, both in the length direction and in the height direction.
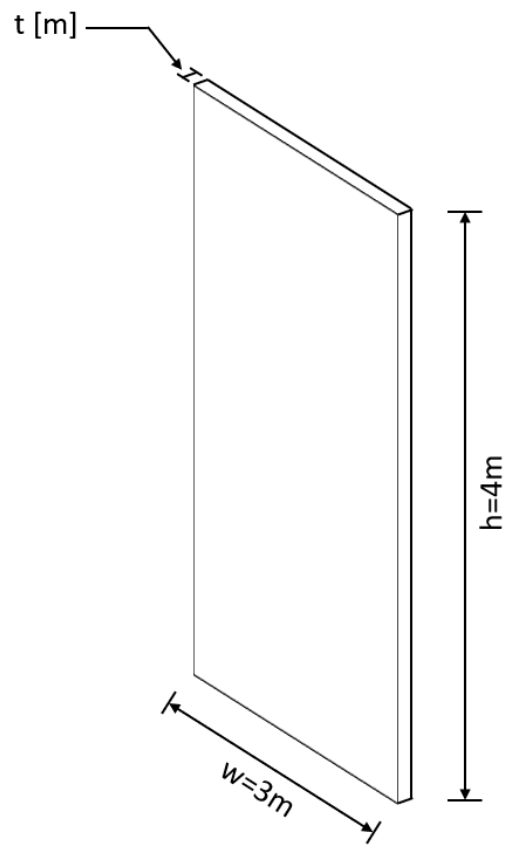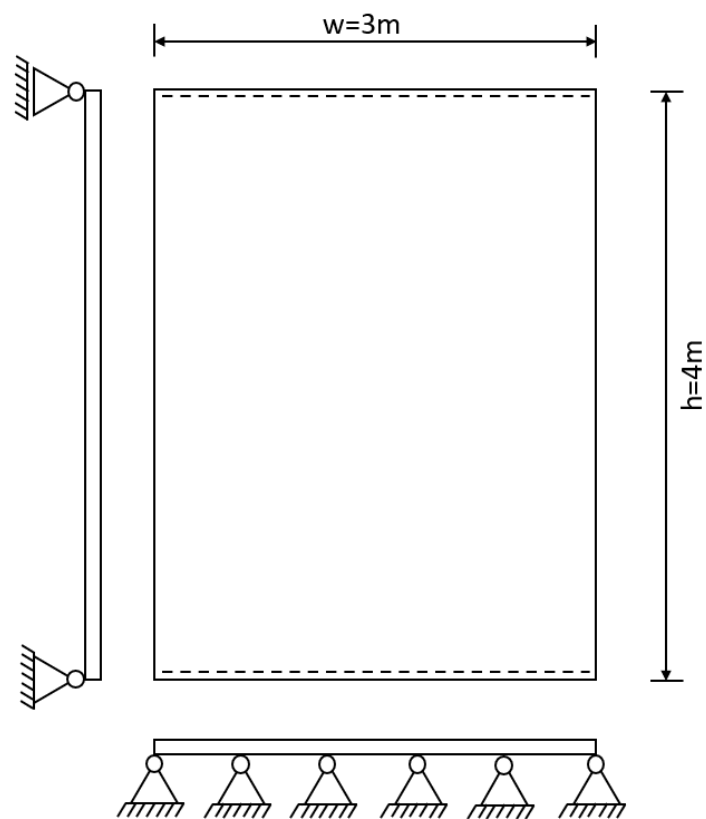
Figure 7: Façade geometry

Figure 8: Boundary conditions

22

3.2   Numerical analyses

For the numerical analyses a model is created in Abaqus, where the information input is defined in a self-consistent set of units, defined in SI-units, i.e., Newton [N], meter [m], kilogram [kg] and second [s]. The numerical model uses a CONWEP definition in Abaqus, aiming at computing the magnitude of a blast pressure wave as realistically as possible. Additionally, the numerical model aims at capturing the behaviour of the load transfer between the façade and the supports, and the material properties affecting this. The analyses of the numerical model is split into nine different datasets. These datasets are described in detailed in Section 3.2.1. Further, to ensure that the model definition and output are satisfactory, some preliminary analyses are conducted. This refinement procedure is described in Section 3.2.2.

3.2.1   Datasets and parameter categories

The analyses are categorized based on the variation of thicknesses and applied load. The geometry is divided into three categories, based on the thickness of the plate. These categories are denoted Thickness 1, Thickness 2, and Thickness 3, with a thickness of 0.125 m, 0.1 m, and 0.075 m respectively. As described in Section 2.1, this is categorized as a thin plate. The thickness is determined based on an evaluation of the computational cost of the analyses, as well consultations with NDEA.

Further, the applied load is divided into three categories, based on the scaled distance, with Load case A using a scaled distance of $Z=4$ m/kg$^{1/3}$, Load case B using $Z=5$ m/kg$^{1/3}$ and Load case C using $Z=6$ m/kg$^{1/3}$. The stand-off distance is kept constant at 100 m in all load cases. The values of scaled distance and stand-off distance are determined in consultation with NDEA, to best simulate the loading environment of interest.

To categorize the analyses in a clear way, the complete parametric study is divided into nine distinct datasets, consisting of every unique combination of the thickness and the applied load. Table 1 shows a detailed summery of all nine datasets. The datasets are named based on the unique combination of thickness and load case, to intuitively describe the parameters in every analysis.

Table 1: Datasets

Dataset	t [m]	Z [m/kg$^{1/3}$]	R [m]	TNT [kg]
1A	0.125	4	100	15625
1B	0.125	5	100	8000
1C	0.125	6	100	4630
2A	0.1	4	100	15625
2B	0.1	5	100	8000
2C	0.1	6	100	4630
3A	0.075	4	100	15625
3B	0.075	5	100	8000
3C	0.075	6	100	4630

Parameter categories

In each dataset the material properties are analysed based on three parameter categories. Each category contains three materials, defined by the Young's modulus, Poison's ratio and the density. In the first category all three material properties vary, with a set interval, ranging from pure steel to pure aluminium. The material of steel and aluminium are chosen as these are commonly used building materials [34, 35]. Moreover. both metals can endure high loading before reaching yield, which is an important aspect in an elastic analysis.

In the second category, the Young's modulus is the only varying material property, using the same interval as in Category 1, while the remaining material properties are unaltered. Similarly, in Category 3 the density is the only varying material property. The material properties of steel are used for the constant material properties in Category 2 and 3. The value of the material properties, at the set intervals, in each category are presented in Table 2.

Table 2: Parameter categories

	CATEGORY 1			CATEGORY 2		CATEGORY 3	
	Steel	*Aluminium*	*Interval 2*	*Interval 1*	*Interval 2*	*Interval 1*	*Interval 2*
Young's modulus [GPa]	210	70	140	70	140	210	210
Poisson's ratio [-]	0.3	0.32	0.31	0.3	0.3	0.3	0.3
Density [kg/m^3]	7800	2700	5250	7800	7800	2700	5250

Given that steel is a constant interval in each of the three categories, there is a total of seven distinct material definition. Meaning every individual dataset contains seven analyses, resulting in a total of 63 analyses.

3.2.2   Modelling in Abaqus

General model definition

The façade element is created as a 3D deformable solid shape, with the dimensions $w \times h = 3m * 4m$, extruded with a thickness of 0.125 m, 0.1 m, or 0.075 m. The section is defined as a solid, homogenous section, and the instance is defined as independent. In addition to the initial step, a dynamic explicit step is defined. A summation of the model definition and input of the dynamic explicit step defined in Abaqus, is given in Table 3.

The boundary conditions of the plate element are modelled as detailed in Section 3.1. Following this, the boundary condition is defined along the upper and lower edge of the model in the Abaqus model, restricting displacement/rotation along the upper and lower edge. In the upper edge this restriction is defined in U1 and U3, and U1, U2 and U3 along the lower edge. The boundary condition is defined in the initial step and is propagated to the following step.

Table 3: Model and step input

PART	*Modelling space*	3D
	Type	Deformable
	Shape	Solid
	Geometry	Extrusion
PART GEOEMTRY	*w [m]*	3
	h [m]	4
	t [m]	0.125, 0.1 0, 0.075
SECTION	*Category*	Solid
	Type	Homogenous
INSTANCE	*Create instance from*	Part
	Instance type	Independent
DYNAMIC EXPLICIT	*Time period [s]*	2
	Nonlinear geometry (nlgeom)	On
	Linear bulk viscosity	0.06
	Quadratic bulk viscosity	1.2
BOUNDARY CONDTION	*Upper edge*	U1, U3
	Lower edge	U1, U2, U3

Interaction

The load from an explosion is modelled by defining an interaction in the interaction module in Abaqus, using the CONWEP definition, explained in Section 2.6. The interaction is defined as an incident wave, occurring in the dynamic explicit step. The wave properties are defined based on an assumption of an in-air explosion, i.e., an air blast. The weight of TNT in each load case, is calculated using Equation (6), and scaled distances of 4 m/kg$^{1/3}$, 5 m/kg$^{1/3}$ or 6 m/kg$^{1/3}$. The centre of the explosion is placed in a reference point with a stand-off distance of 100 m, and at $w/2$ and $h/2$ of the plate dimensions. This gives a placement perpendicular to the plate. The interaction definition from Abaqus is summarized in Table 4.

Table 4: Interaction and CONWEP definition

INTERACTION PROPERTIES	*Step*	Dynamic, Explicit
	Type	Incident wave
	Definition	CONWEP
INCIDENT WAVE PROPERTIES	*Definition*	Air blast
	TNT-equivalent [kg]	15625, 8000, 4630
	R [m]	100
CONWEP DATA	*Time of detonation [s]*	0.001
	Magnitude scale factor	1

Mesh refinement

Mesh refinement is conducted to ensure convergence of the output. The mesh refinement is based only on increasing the total number of elements and is evaluated based on convergence of displacement, at a node located at the centre of the plate. The mesh refinement evaluates element sizes enabling two, three and four rows of elements over the thickness of the plate element. Thus, an individual mesh refinement is completed for all three thicknesses. However, the mesh refinement is only illustrated using Thickness 1.

To reduce computational costs, mesh refinement is completed using a time step of one second for the dynamic explicit step. Further, the load is simplified by extracting the pressure wave from the CONWEP model and using a tabulated value of the pressure-time history as an evenly distributed load defined using a tabulated amplitude. By defining the load using a tabulated amplitude, the time before the load reaches the plate can be disregarded, thus reducing the computational cost. Mesh refinement is only completed for one load case, as the convergence of output is not dependent on the magnitude of the load.

Further, the mesh refinement is analysed based on the displacements in one single time step, as illustrated in Figure 9. The figure shows the displacements after 0.005 seconds, right after the load has reached the plate. As shown in Figure 9 the displacements converge almost instantaneously.

The mesh refinement for Thickness 2 and 3, showed that the appropriate approximate global size of the element is found when three rows of mesh elements is used. However, Thickness 1 needed four rows over the thickness. The final mesh size used for each thickness is presented in Table 5. As described in Section 2.6.2 using the automatic calculation by Abaqus produces the most optimal magnitude of the time increment. Thus, calculation of the stable time increment for each mesh is given by Abaqus, these values are summarized in Table 5.
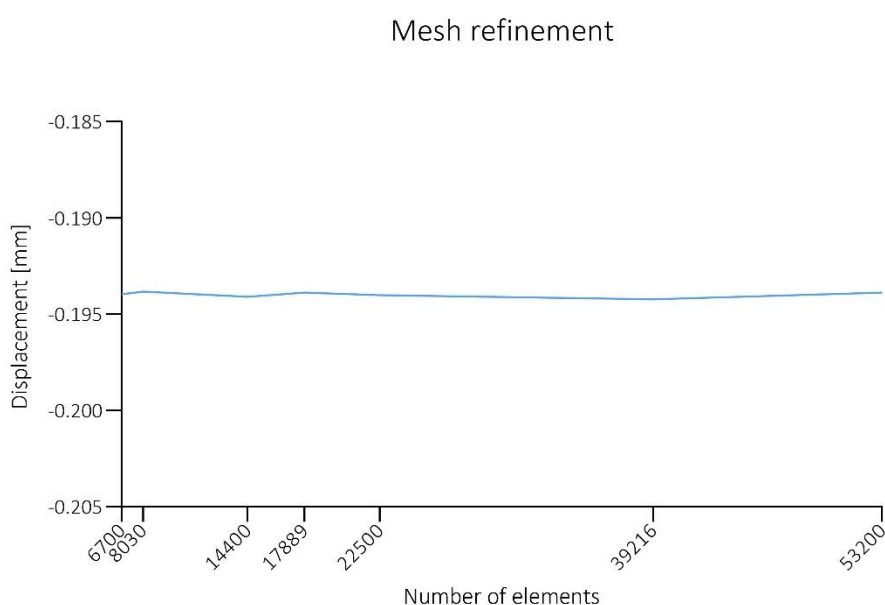

Figure 9: Mesh refinement – displacements

Table 5: Mesh refinement definition

	THICKNESS 1	THICKNESS 2	THICKNESS 3
Global size [m]	0.035	0.0325	0.0275
Number of nodes	50026	46128	64241
Number of elements	39216	33948	47415
Element type	C3D8	C3D8	C3D8
Stable time increment [s]	3.62E-06	4.53e-06	2.88E-06

Output request

The accuracy of the output is highly dependent on the output request. When using a rough output request, some important aspects of the result might be missed, as the requested output do not cover the total response. A rough output request means that the output frequency is low. Thus, to determine that the output request is high enough to cover all important aspects of the response, the output request is refined. The output request is analysed at evenly spaced time intervals of 0.01 seconds, 0.005 seconds and 0.0025 seconds, and is executed for a pure steel plate, using a model with CONWEP load interaction for Dataset 2A (t=0.1 m and Z=4 m/kg$^{1/3}$). The output request is refined based on both the pressure wave and the response of the plate.

Table 6 shows the result of the output request refinement, with regards to the pressure wave. As shown in Table 6, the output request using a higher frequency is able to cover the arrival time of the load more precisely. This can be seen by the arrival time seemingly decreasing with an increased output request. However, the differences are quite small.

Additionally, the magnitude of the incident wave seemingly increases with an increased output. This suggests that a higher output frequency is needed to cover the rapid changes of the load. As clearly shown, an output request of 0.01 s is not able to cover the peak of the incident wave. An output request of 0.005 s could be adequate, as there is a minimal difference between the results found when using an interval of 0.005 s and 0.0025 s.

Table 6: Incident wave information

OUTPUT REQUEST	0.010 s	0.005 s	0.002.5 s
Arrival time [s]	0.17	0.165	0.1625
Peak incident pressure [kN/m²]	79.79	95.76	95.92

Further, the output request is refined based on the reaction forces. Figure 10 shows the time history of the reaction forces, when using an output request of evenly spaced time intervals of 0.01 s. Figure 10 indicates that the peaks of many of the amplitudes are not covered using this output request frequency. This is further illustrated in Figure 11, indicating the possible extension of the peak.
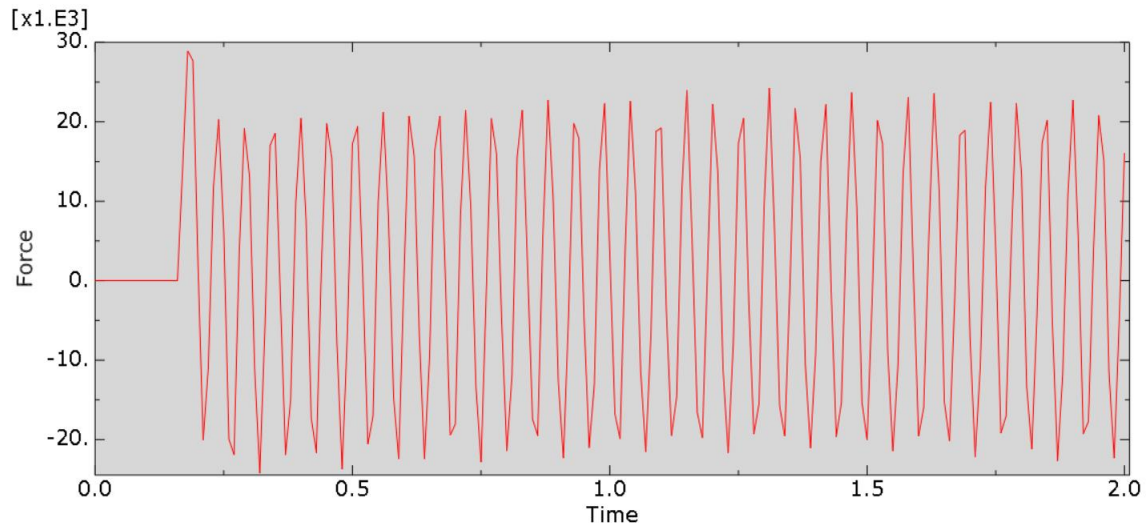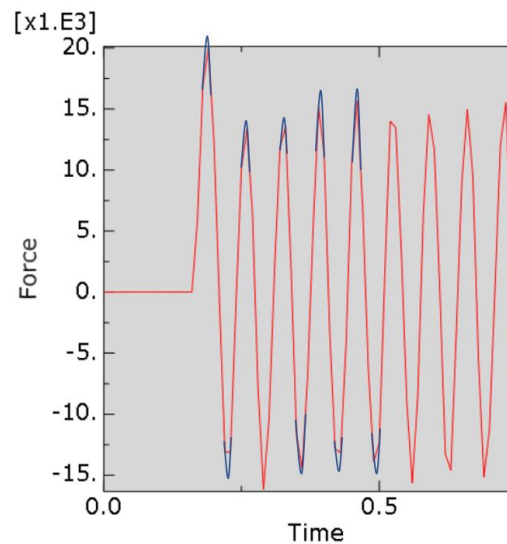
Figure 10: Reaction force – output every 0.01 s

Figure 11: Expansion of peaks

Figure 12 shows the reaction forces for an output frequency, using evenly spaced times intervals of 0.005 s. The figure illustrate that the amplitudes of the reaction force are seemingly more consistent over the duration of the analysis. This indicates that this output frequency can capture more of the actual response. Further, the amplitudes have a sharper angle, indicating that maximum amplitude has been reached for more instances than when using evenly spaced time intervals of 0.01 s.
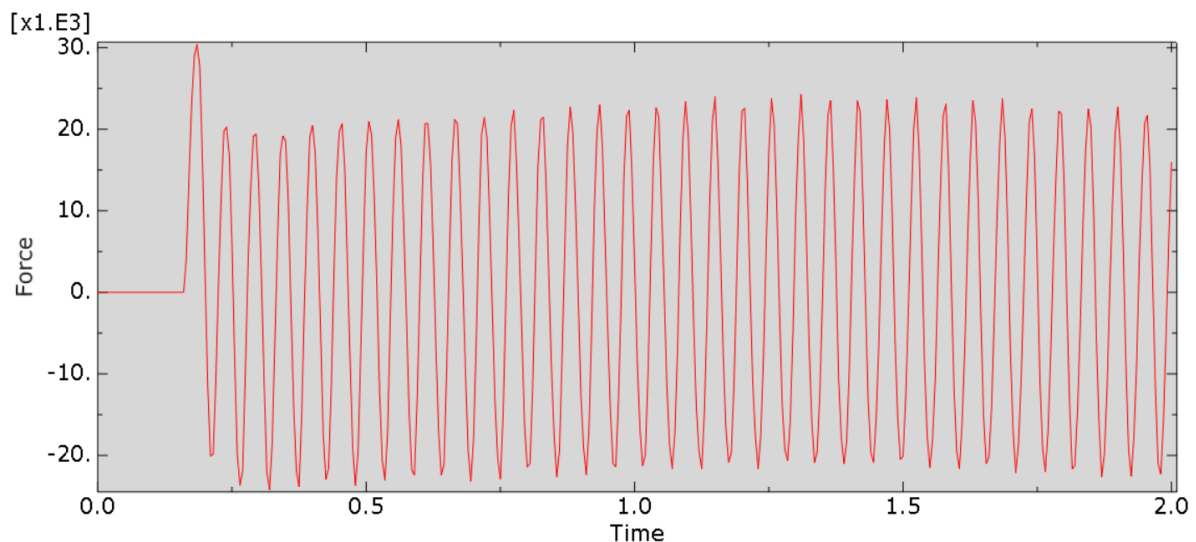
Figure 12: Reaction force – output every 0.005 s

Lastly, Figure 13 shows the reaction force when using an output request with evenly spaced time intervals of 0.0025 s. The figure indicates that an additional vibration frequency is detected, as many of the amplitude peaks are serrated. However, this frequency is small and does not seem to influence the overall response.
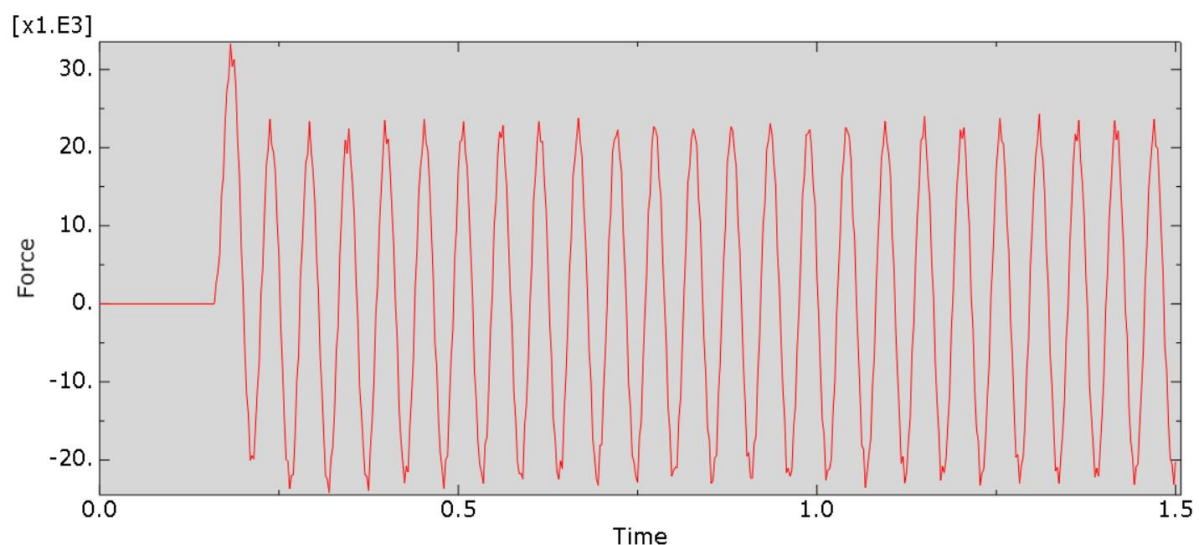

Figure 13: Reaction force – output every 0.0025 s

Table 7 shows the result of the output request refinement, with regards to the peak reaction force. The table highlights both the magnitude and the time of the peak reaction force. As Table 7 shows, the time of the peak reaction force varies, as do the magnitude of the peak reaction force. The results indicate that more precise results are captured when increasing the output frequency. The peak pressure shows minor changes between 0.005 and 0.0025 seconds. As the

30

analysis becomes more computationally expensive when using small intervals, an output request using evenly spaced time intervals of 0.005 seconds is deemed appropriate

Table 7: Output request - peak reaction force

OUTPUT REQUEST	0.01 s	0.005 s	0.0025
Time of peak reaction force[s]	0.18	0.185	0.1825
Peak reaction force [kN]	28.94	30.41	33.26

Field and history output request

The frequency of the output is requested at approximate times, using 400 evenly spaced time intervals (corresponding to evenly spaced time intervals of 0.005 s). The field output request for the plate is given in Table 8. The history output has an equal step, frequency and intervals as the field output request and is also valid for the whole model. However, the history output is only requested for energy related output.

Table 8: Output request definition

OUTPUT REQUEST	*Frequency*	Evenly spaced time intervals
	Interval	400
FIELD OUTPUT	*Timing*	Ouput at apriximate times
	Output variable	RF, U
	Element output	Exterior
	Direction	YES
HISTORY OUTPUT	*Output variable*	ALLAE, ALLCD, ALLDMD, ALLFD, ALLIE, ALLKE, ALLPD, ALLSE, ALLVD, ALLWK,

Step time

The duration of the analysis is established in the step module, as described in Section 3.2.2. A refinement of the step time is completed, to ensure that the step time is long enough to capture the total response. Therefore, step times of 1 s, 1.5 s, and 2 s are analysed. Given that a blast load is a very rapid load, with a short duration, the forced vibration phase is expected to be short. However, the step time must be evaluated to ensure that the total analysis time captures the important aspects of the free vibration phase. From the preliminary analysis, it is shown that 2 seconds of analysis was needed to sufficiently capture different vibrations.

3.2.3   Evaluation of load plate analysis

A brief evaluation consisting of calculations of the energy balance of the model and the maximum deflection of the plate is completed. This is done to ensure that no unwanted effects due to modelling errors, exists in the model. Both evaluations are completed using Dataset 1A (t=0.125 m and Z=4 m/kg$^{1/3}$) and the material properties of pure steel. In addition, an evaluation of yield strength is completed, to ensure that the stress in the material at no point surpasses the elastic domain.

Energy balance

An evaluation of the model, with regards to the energy balance is completed. The evaluation focuses on the fictitious energy modes (spurious modes), controlling that these modes do not govern the response. It is controlled that the energy calculated by Abaqus is approximately constant, meaning no additional energy is created or dissipated throughout the analysis. This is done by calculating the energy balance, over time. The time history of the energy is obtained from the history output, calculated in Abaqus. The values of these energies are then used to calculate the energy balance, as shown in Equation (14).

As shown, the total energy is calculated as the sum of the energy due to external work (E_W), internal energy (E_I), kinetic energy (E_{KE}), strain energy (E_E), viscous dissipation energy (E_V), internal heat energy (E_{IHE}), energy due to contact penalty (E_{PW}), energy due to constraint energy work (E_{CW}), work done by propelling added mass (E_{MW}), and external heat energy (E_{HF}).

$$E_{total} = E_I + E_V + E_{FD} + E_{KE} + E_{IHE} - E_W - E_{PW} - E_{CW} - E_{MW} - E_{HF} \qquad (14)$$

Further, the internal energy (E_I) is calculated as a sum of the elastic strain energy (E_E), the inelastic dissipated energy (E_P), energy dissipated by viscoelasticity (E_{CD}), the artificial strain energy (E_A), the energy dissipated by damage (E_{DMD}), the energy dissipated by distortion control (E_{DC}), the fluid cavity energy (E_{FC}), and distortion control dissipation energy (E_{DC}). This is calculated by Equation (15).

$$E_I = E_E + E_P + E_{CD} + E_A + E_{DMD} + E_{DC} + E_{FC} \qquad (15)$$

Displacements

The model of the plate is evaluated by comparing the maximum deflection calculated by plate theory to the maximum deflection computed in Abaqus. To enable a true comparison the applied load in Abaqus is transformed to an evenly distributed static pressure load. The magnitude of the static load is 95.7 kN/m², which corresponds to the maximum value of the CONWEP blast load calculated in Abaqus. To accommodate a static load analysis in Abaqus, the dynamic explicit step is replaced by a static/general step. The rest of the model is kept identical to the model using the CONWEP load definition.

The maximum deflection, occurring in the middle of the plate, is calculated based on plate theory. Due to the definition of the boundary conditions, the plate is only able to carry loads in one direction, meaning it can be regarded as a one-way plate. Moreover, as $t < h/10$ for Thickness 1, 2 and 3, the plate is regarded as a thin plate. Thus, the maximum deflection is calculated as shown below, using Equation (1), where q is the peak pressure from the blast load of Load case A, and L is the length between the supports,

$$\delta_{max} = \frac{5}{384} * \frac{95.7kN/m^2 * (4m)^4}{3.76 * 10^7 Nm}$$

The stiffness, D, of the plate is calculated by Equation (2), where both the Young's modulus and Poison's ratio correspond to the material properties of steel. And t is the façade thickness defined in Thickness 1.

$$D = \frac{210GPa * (0.125m)^3}{12(1 - 0.3^2)}$$

Yield

The von Mises stress computed in Abaqus is compared to the yield strength, to evaluate whether the results from Abaqus exceeds yield. Since the Abaqus model only consist of elastic material properties, the model is unable to detect and realistically model fracture or plastic behaviour. Therefore, it is important to ensure that the material stress does not exceed yield, as this will produce unrealistic behaviour in the model.

The control is performed for steel and aluminium in Dataset 3A (t=0.075 m and Z=4 m/kg$^{1/3}$). This dataset is used as it is defined with the thinnest plate, subjected to the highest load, resulting in the most critical scenario with regards to yield. Steel and aluminium are controlled as these are "true" materials, with information regarding material strength readily available in the European standards. Moreover, these materials are defined with the extremes of the material definition in parametric study.

The maximum von Mises stress for both materials, is found at 0.2 s, given in Table 9. As the table shows the von Mises stress is higher for the aluminium plate, than the steel plate. However, the von Mises stress for both aluminium and steel is below the yield stress of common steel and aluminium materials used in construction [34, 35].

Table 9: von Mises stress – steel and aluminium

	Steel	Aluminium
von Mises stress [MPa]	278	285

3.3   Stiffness and natural frequency

The stiffness, D, and the natural circular frequency of vibration, ω_n, of every material is calculated. The stiffness is calculated using Equation (2), and the natural circular frequency of vibration is calculated using Equation (8). Henceforth the natural circular frequency of vibration is denoted as circular frequency. The stiffness and the natural frequency relate to the material properties and thickness, thus its independent of the loading. Therefore, the calculations are completed for all materials in Thickness 1, 2, and 3 (t=0.125 m, t=0.1 m, and t=0.075 m respectively). There are seven unique materials defined within each thickness, resulting in a total of 21 calculations of both the stiffness and natural frequency is completed. The material properties are defined in Section 3.2.1.

3.4   Fast Fourier Transform

To analyse the results of the numerical analyses, a FFT of each unique combination of plate thickness and material properties is performed. Using a FFT the amplitude and frequencies of different modes are isolated and clearly visualized. Thus, enabling a deeper understanding of the results, as well as a more precise analysis. Given that the frequencies of the modes are independent of the applied load, it is superfluous to analyse multiple load cases. Therefore,

FFTs are only computed for materials in Thickness 1, 2 and 3 (where t=0.125 m, t=0.1 m, and t=0.075 m respectively), using Load case A (Z=4 m/kg$^{1/3}$). The load will naturally impact the amplitude of the oscillations, however, it does not impact the number of frequencies present, or what frequencies that dominate the response in free vibration. Therefore, the FFT is only completed for one load case.

The FFTs of the data, consisting of discrete-time sampling of the physical signals, are calculated using MATLAB. The FFT script is based on an open-source script computing FFTs, published by MathWorks, the producer of MATLAB [36]. Plots of each FFT are compiled in MATLAB.

3.5   Curve fitting

To find a general expression for the time history of the reaction forces, curve fitting is utilized. Curve fitting is a method of finding a mathematical expression that best emulates the curve of given data points. In this thesis the process of curve fitting is divided into two distinct parts. The first part is based on the evaluation of simple sinusoidal functions. The most appropriate of these simple functions are then curve fitted by the means of visual inspection, before the least squares method is utilized. By using the least squares method, the constants of each function is calculated to ensure that the expression gives the smallest discrepancy between the curve of the data points and the expression emulating this. The curve fitting using simple sine functions is completed in Excel, where the add-in "Solver" is used to compute the least squares.

The second way of curve fitting is by using a Fourier series. The accuracy of the curve found using Fourier series is highly dependent on the number, n, of sine and cosine functions that are added. Naturally, the complexity of the calculations is also impacted by the value of n. Therefore, with regards to the Fourier series, the power of n required to obtain satisfactory output is evaluated. To reduce the complexity of the proposed function when using a Fourier series, the reaction forces are curve fitted for the first 0.5 second. The Fourier coefficients a_n and b_n are found by utilizing an open-source code, provided by Graz University of Technology [37, 38].

The results of the Fourier coefficients are used to calculate the full Fourier series. As the coefficient are calculated from data points, the Fourier series is calculated based on the frequency of the data points, as described in Section 2.4.1. Equation (16) shows the calculation

of the full Fourier series, where N are the number of measurements and Δt is the frequency of the data output [37]. As described in Section 3.2.2, the output from Abaqus is given at every $\Delta t = 0.005$ seconds, resulting in $N = 101$ measurements (including the start point at 0, 0).

$$f(t) = \sum_{n=0}^{n<N/2} a_n \cos\left(\frac{2\pi t}{N\Delta t}\right) + b_n \sin\left(\frac{2\pi t}{N\Delta t}\right) \qquad (16)$$

4.   Results

In this chapter the main results are presented. The result of the numerical analysis is presented, describing the reaction forces of each material. The total response is presented by the time history response, peak reaction force and the average amplitude of the free vibration. Then, the stiffness and natural frequency is presented. Further, the result of the FFT is given, illustrating the different modes and frequencies of each material. Lastly, the results of the curve fitting are presented.

The reaction forces are given in the global z-direction, these are by Abaqus denoted as RF3. Henceforth, these reaction forces are described as reaction forces. The results of the reaction forces calculated in Abaqus, are given for each node along the supports. The reaction forces are only presented for the support at the upper edge of the plate, as the plate is symmetrical. The distribution of the reaction forces along the upper edge of the plate, is illustrated in Figure 14. In the following sections these reaction forces are presented as one sum, i.e., one value representing the sum of the reaction forces of each node along the upper edge.

The material definition is divided into three distinct categories, defined in Section 3.2.1. The results of Category 1 (all parameters varying), Category 2 (varying Young's modulus) and Category 3 (varying density) are described as Category 1, 2 and 3 from this point. Moreover, the materials within each category are described by an abbreviation of the parameter category, meaning the abbreviation C1, C2 and C3 is used when referring to materials in Category 1, 2 and 3 respectively. The seven materials in each dataset are from this point, referred to as steel, C1 Aluminium, C1 Interval 2, C2 Interval 1, C2 Interval 2, C3 Interval 1, and C3 Interval 2. The definitions of the material properties are given in Section 3.2.1.

Reaction force distribution - Steel
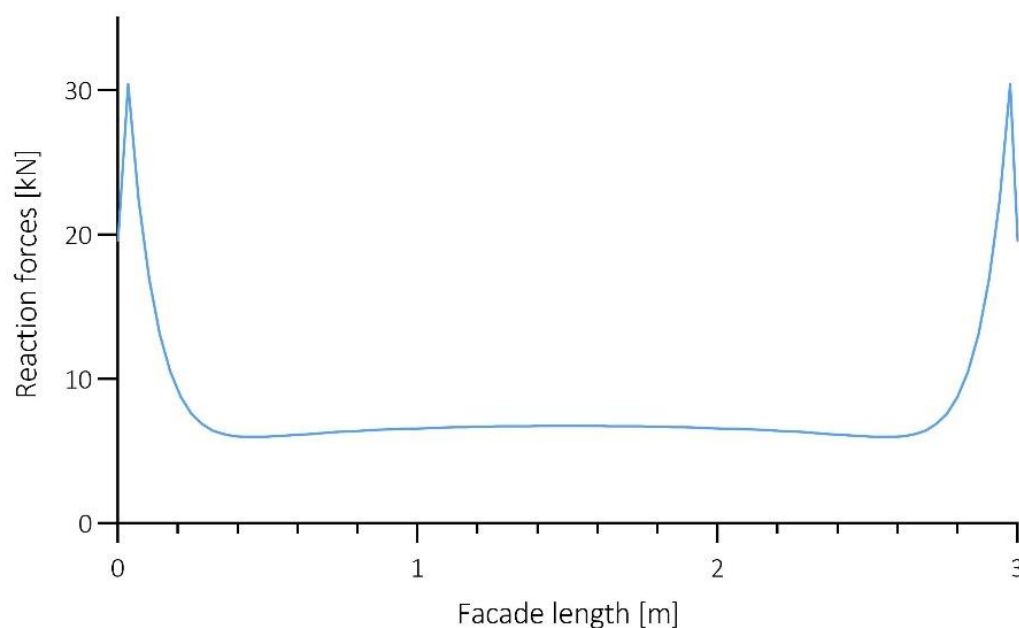
Figure 14: Peak reaction force along the upper edge

4.1 Numerical analysis

In this section the result of the energy balance and the static displacement is given. The pressure wave calculated in Abaqus is presented. The time history of the reaction forces for the different materials are shown. The total time history response is illustrated using figures, as well as presenting the highest peak reaction force and the average amplitude. This illustrates the behaviour of the total response, meaning both the forced and free vibrations.

4.1.1 Energy balance and static displacement

The calculated energy balance of the model shows that the total energy has a magnitude of approximately zero for the whole time step. Given that FEM is based on approximations it is expected that the summation of the energies would not be exactly zero. Meaning, the result of approximately zero total energy throughout the analysis is an acceptable result, and the energy balance is satisfactory. As the external work is equal to the internal work, the model neither produces additional spurious energy nor fictitious dissipation.

Further, the results of the maximum deflection calculated by plate theory, shown in Section 3.2.3, and maximum deflection computed by the static Abaqus model is given in Table 10. The discrepancy between the static model and plate theory is regarded as negligible. Based on these results it is established that the model has a realistic physical behaviour, without producing any unwanted effects.

Table 10: Maximum static deflection, δ_{max}

CALCULATION METHOD	STATIC DEFLECTION, δ_{max} [mm]
Plate theory	8.5
Static model	8.66

4.1.2   Pressure wave

The pressure wave calculated in Abaqus is shown in Figure 15, illustrated using Load case A (Z=4 m/kg$^{1/3}$). As Figure 15 shows the pressure load rapidly increases to the peak and then decrease to a negative phase. Figure 15 shows high similarity to the Friedlander equation described in Section 2.2.1. Load case B and C (Z=5 m/kg$^{1/3}$ and Z=6 m/kg$^{1/3}$ respectively) behave similarly, though differ in magnitude.

The arrival time, the positive phase duration and peak pressure for the different load cases is given in Table 11. Load case A, B and C have the same stand-off distance, but different charge weight. The table shows that the arrival time gets longer, while the pressure gets lower as the scaled distance increases, which is natural as the amount of explosives decreases as *Z* increase. The positive phase duration has the longest duration for Load case A, then decreases. The peak pressure has the highest values for Load case A, followed by Load case B, then C. It is also fitting that the positive phase gets shorter for higher values of *Z*. These findings are reasonable as they follow the relationship presented by Kingery-Bulmash shown in Figure 5, where the different blast parameters are described.
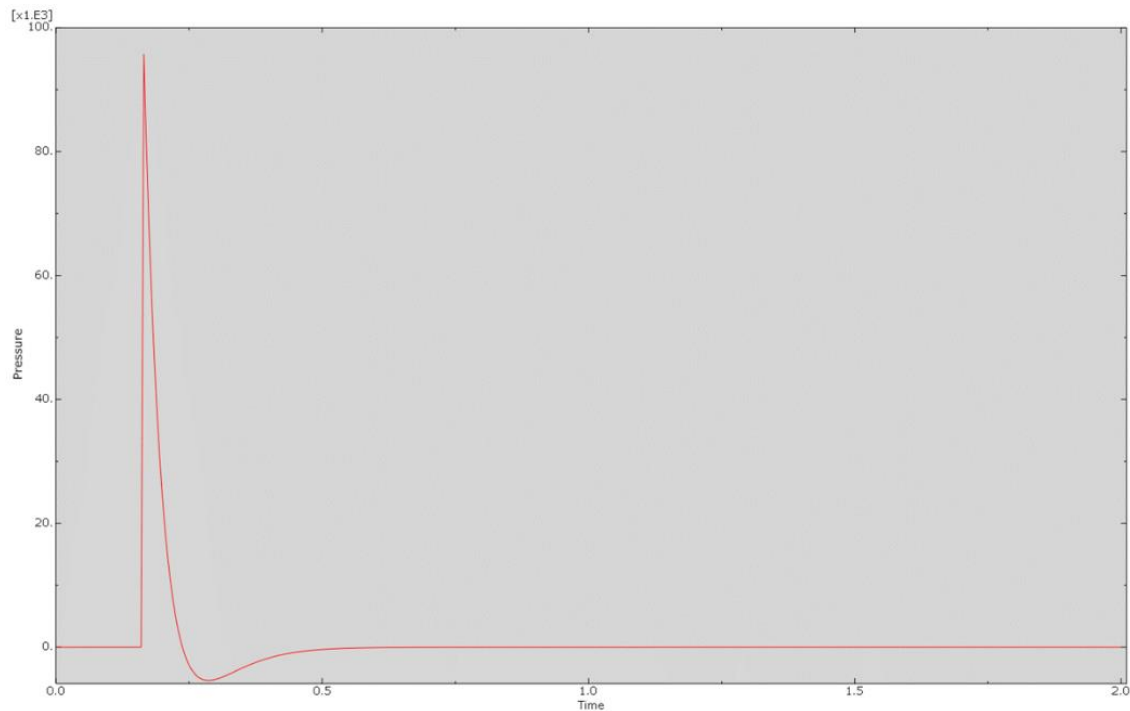
Figure 15: Pressure-time curve – Load case A

Table 11: Load cases

LOAD CASE	A	B	C
Arrival time, t_a [s]	0.165	0.185	0.2
Positive phase duration, t_0 [s]	0.07	0.06	0.055
Peak pressure [kN/m²]	95.76	61.46	44

4.1.3   Time history response

In this section the main results of the time history of the reaction forces are presented, while a detailed analyses of the results is given in Section 5.2. The time history of all seven materials is only illustrated using Dataset 1A (t=0.125 m and Z=4m/kg$^{1/3}$), as varying the scaled distance only impacts the magnitude of the response, not the general behaviour. Moreover, C3 Interval 2 is also illustrated using Thickness 2 (t=0.1 m) and Thickness 3 (t=0.075 m), to demonstrate the general response of all thicknesses. The time history of the remaining materials using Thickness 2 and 3, follows the same general behaviour as described in the following section. The time history of the materials in all datasets is given in Appendix A.

The following sections describe the time history of the reaction forces. The illustration of the time history is presented together after the description, to enable a visual comparison of the response.

Steel

Figure 16 shows the time history of steel. The figure shows that the response starts with a high peak in the forced vibration phase, and then oscillates with a lower amplitude in the free vibration phase. The oscillations in the free vibration phase do not diminish over time, a reasonable result as the system is defined without damping. Figure 16 shows that the free vibration phase exhibit more than one frequency, indicating that more than one mode is present in the response.

C1 Aluminium

Figure 17 shows the time history of C1 Aluminium. It is seen that this material also responds with a peak value in the first oscillation, followed by oscillations with a lower amplitude in the free vibration phase. Furthermore, Figure 17 indicate that the response is composed of more than one frequency: one short frequency, and another longer frequency.

C1 Interval 2

Figure 18 shows the time history of C1 Interval 2. The figure shows that C1 Interval 2 has a similar behaviour as described of both steel and C1 Aluminium regarding the forced and free oscillations. However, the presence of multiple frequencies in the free vibration is not as clearly visible for this material.

C2 Interval 1 – E=70 GPa

Reaction forces of C2 Interval 1 is shown in Figure 19. As shown, this material also responds with a high peak value of the first oscillation, followed by oscillations with a lower amplitude in the free vibration phase. However, as Figure 19 shows this material responds with an additional frequency of a higher value than previous time history responses have shown. This can be seen by the serrated or saw-toothed shape of the time history response. Furthermore, the total vibration oscillates with a lower frequency than what was the case with the materials in Category 1.

C2 Interval 2 – E=140 GPa

The reaction force of C2 Interval 2 is shown in Figure 20. As previous materials, this material also has a peak followed by oscillations with lower amplitudes. More than one frequency is dominating the behaviour of the response, yet for C2 Interval 2 it is not as clear to identify the distinct frequencies as for the previous materials. The clearest vibration of C2 Interval 2 has a higher frequency than C2 Interval 1.

C3 Interval 1 – ρ=2700 kg/m³

Figure 21 shows the reaction forces of C3 Interval 1. This response also has a high peak at the beginning, followed by oscillations in the free vibration phase with a lower amplitude. It also shows more than one vibration, where the clearest vibration has a higher frequency than the responses of the materials in Category 1 and 2.

C3 Interval 2 – ρ=5250 kg/m³

Figure 22 shows the reaction forces for C3 Interval 2. It has a high peak, followed by oscillations in the free vibration phase. There is more than one vibration pattern visible, where one has a noticeably lower frequency than the other. This results in a long waved behaviour of the total vibration.

C3 Interval 1 – ρ=2700 kg/m³

1A - Steel
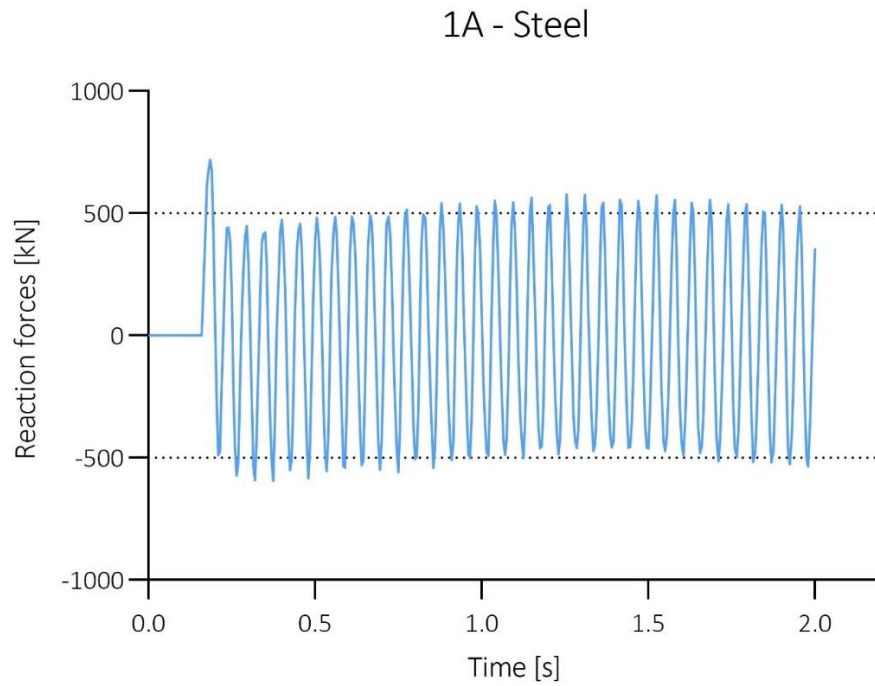
Figure 16: Reaction force – steel
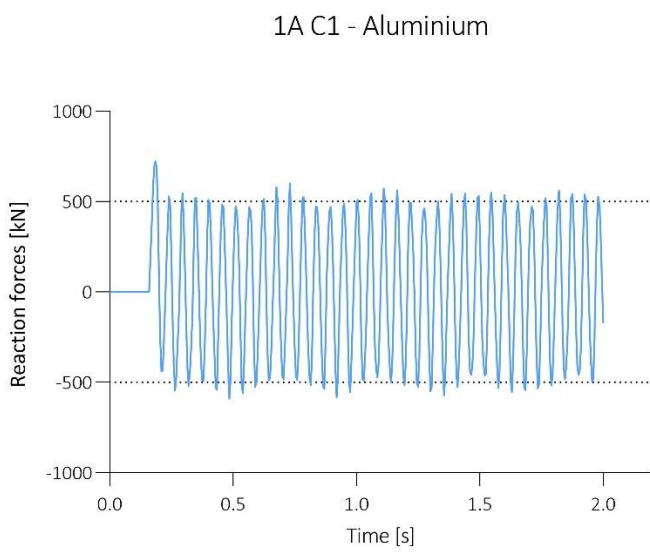
1A C1 - Aluminium

Figure 17: Reaction force – aluminium
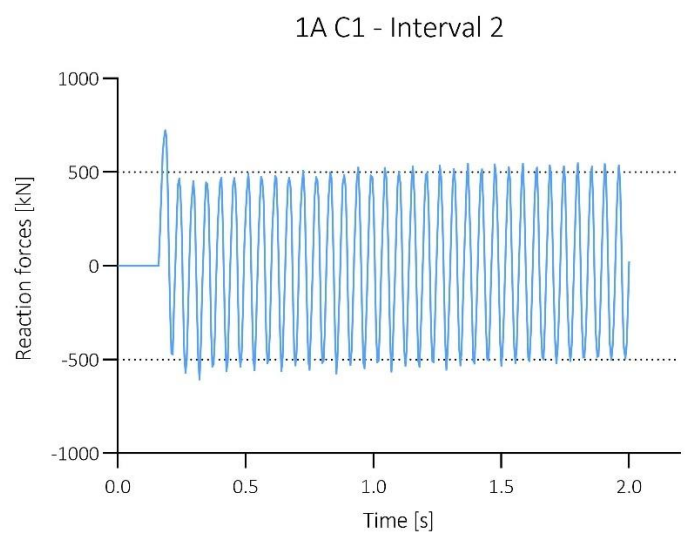
1A C1 - Interval 2

Figure 18: Reaction force – C1 Interval 2

1A C2 - Interval 1
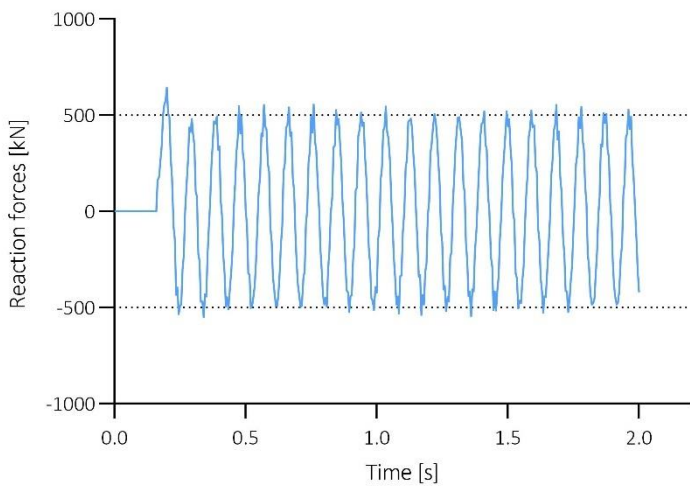
Figure 19: Reaction force – C2 Interval 1

1A C2 - Interval 2
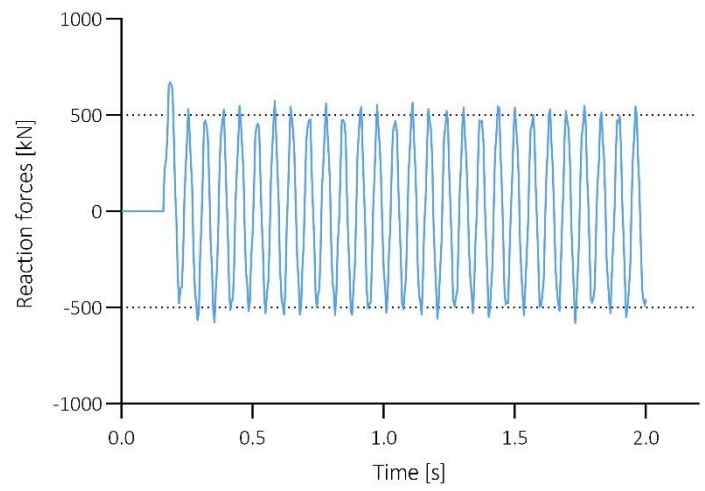
Figure 20: Reaction force – C2 Interval 2

1A C3 - Interval 1
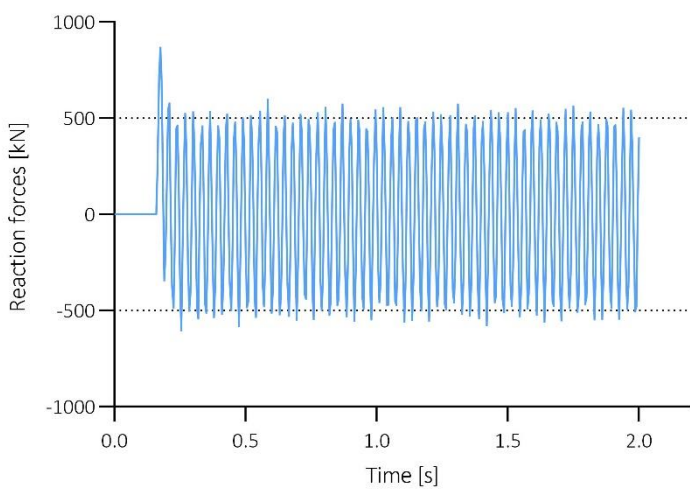
Figure 21: Reaction force – C3 Interval 1

1A C3 - Interval 2
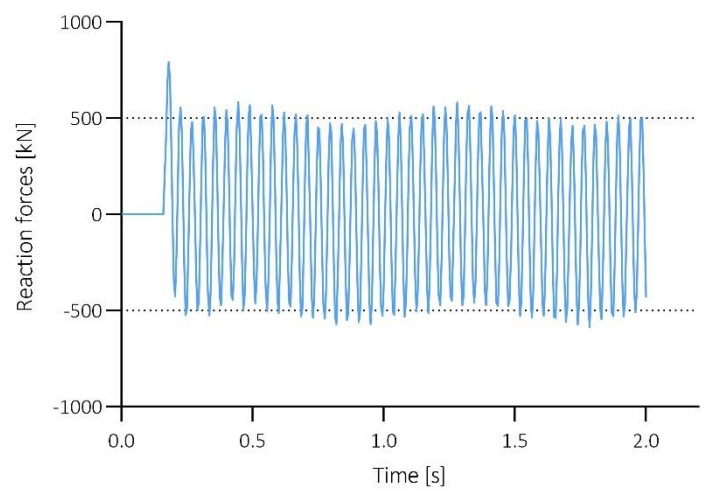
Figure 22: Reaction force – C3 Interval 2

Comparison of Thickness 1, 2 and 3

When the thickness of the plate is changed, the behaviour of the reaction forces changes. Figure 22, Figure 23 and Figure 24 shows the time history response of C3 Interval 2 in Thickness 1, 2 and 3 respectively (t=0.125 m, t=0.1 m and t=0.075 m), using Load case A (Z=4 m/kg$^{1/3}$).

In these figures the response consists of multiple frequencies, where the frequency of the most prominent vibration, the rapid vibration, is seen to decrease as the thickness decreases. Moreover, as the thickness decreases, the additional visible frequency changes. In Figure 22, using t=0.125 m, the additional frequency is much lower than the frequency of the most prominent vibrations. This causes the total response to exhibit one vibration pattern within a longer wave. The same response is visible for t=0.1 m, shown in Figure 23.

However, in the thinnest plate, shown in Figure 24, the total vibrations have changed, exhibiting a serrated form. This indicates that the additional frequency is higher than the most prominent frequency. A similar behaviour is found for all materials when the thickness is varying.
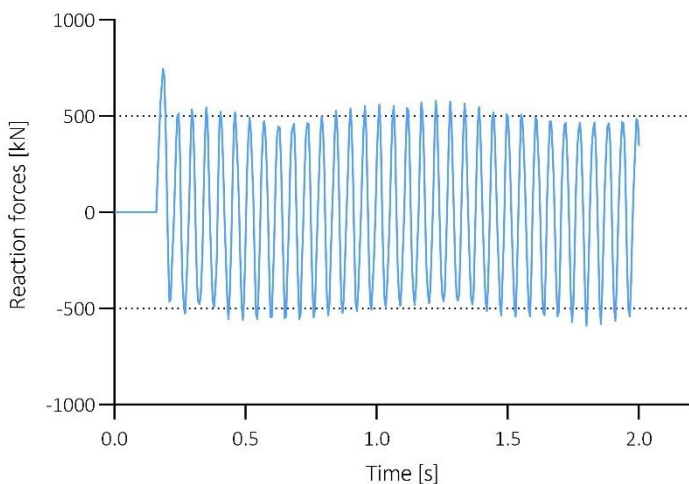
Figure 23: Reaction force – C3 Interval 2 in Dataset 2A
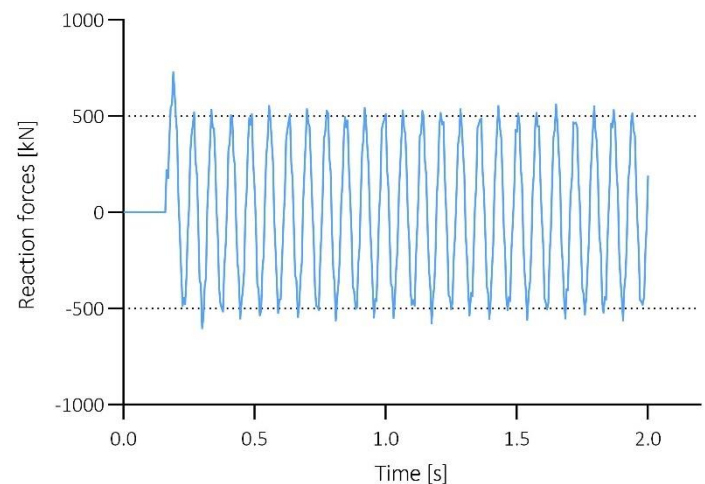
Figure 24: Reaction force – C3 Interval 2 in Dataset 3A

4.1.4 Peak reaction forces

A summary of all peak reaction forces is shown in Table 12. The table shows that the material with lowest density, C3 Interval 1, has the highest peak reaction force of all datasets. Whereas the material with lowest Young's modulus, C2 Interval 1, has the lowest reaction forces of all datasets. The peak reaction forces are analysed in further detail in Section 5.1.

Table 12: Maximum reaction forces [kN]

Dataset	1A	1B	1C	2A	2B	2C	3A	3B	3C
Steel	716.81	465.85	327.43	677.89	437.43	309.31	678.93	437.79	309.05
Aluminium	721.32	464.99	330.44	681.62	441.24	310.42	696.38	447.41	316.05
C1 Interval 2	721.93	466.81	330.64	676.64	435.93	309.06	686.65	443.63	311.18
C2 Interval 1	642.20	416.17	289.47	579.36	374.12	260.81	497.71	328.07	235.89
C2 Interval 2	668.57	427.74	308.08	689.70	446.02	313.76	607.87	392.58	272.66
C3 Interval 1	865.69	557.99	397.31	885.25	566.91	407.92	760.36	487.49	348.86
C3 Interval 2	790.30	508.59	363.57	744.72	479.52	340.69	728.24	468.74	332.43

4.1.5 Amplitude of free vibration

Table 13 shows a summary of the positive average amplitude values for all datasets. The averaged amplitude is found by disregarding the amplitude of the first oscillation, i.e., the forced vibration. With other words, Table 13 shows the average amplitude of the free vibration phase.

The average amplitude is highest in Dataset 1A (t=0.125 m and Z=4 m/kg$^{1/3}$). The variation in the amplitude is somewhat affected by the thickness of the plate. However, as shown in Table 13 the variation in load case influence the average amplitude more notably. Furthermore, for Thickness 1 and 2 (t=0.125 m and t=0.1 m) the averaged amplitude is found to be higher for Category 2 than 3. However, for Thickness 3 (t=0.075 m) the averaged amplitude is found to have smaller variations between Category 2 and 3.

Table 13: Average amplitude of free vibration [kN]

Dataset	1A	1B	1C	2A	2B	2C	3A	3B	3C
Steel	518.83	329.60	237.06	517.32	332.31	237.54	524.13	336.07	241.17
Aluminium	519.54	330.14	237.11	523.41	333.31	239.84	525.12	339.53	241.20
C1 Interval 2	505.64	323.39	230.72	525.76	334.86	240.65	525.28	337.78	241.96
C2 Interval 1	521.79	336.65	241.91	504.66	328.01	236.34	477.76	317.28	227.84
C2 Interval 2	521.39	332.67	236.83	524.50	336.58	242.15	517.24	335.16	241.26
C3 Interval 1	510.06	322.53	231.22	514.60	326.92	233.65	514.41	328.27	233.92
C3 Interval 2	512.48	325.00	233.40	508.93	325.52	233.44	521.26	334.00	240.33

4.2   Stiffness and natural frequency

This section presents the stiffness, D, and the natural frequency ω_n, of the plates with different materials. Table 14 present the stiffness, as calculated by Equation (2). As illustrated in this equation, the stiffness is influenced by the plate thickness, t, the Young's modulus, E, and Poison's ratio, ν. This can also be seen by the results in Table 14, where the highest stiffness is found for the thickest plate, with the highest value of the Young's modulus.

Since the density is the only material property varying in Category 3, the remaining material properties of this category corresponds to the material properties of steel, as described in Section 3.2.1. Moreover, as the density does not affect the stiffness, the magnitude of the stiffness is equal for steel, C3 Interval 1, and C3 Interval 2. However, this is not true for Category 2, as the magnitude of the Young's modulus is not constant in this category.

Table 14: Stiffness, D [kNm]

	Thickness 1	Thickness 2	Thickness 3
Steel	37560.10	19230.77	8112.98
Aluminium	12692.99	6498.81	2741.69
C1 Interval 2	25209.05	12907.03	5445.15
C2 Interval 1	12520.03	6410.26	2704.33
C2 Interval 2	25040.06	12820.51	5408.65
C3 Interval 1	37560.10	19230.77	8112.98
C3 Interval 2	37560.10	19230.77	8112.98

The calculated natural frequencies, ω_n, of the different materials in Thickness 1, 2, and 3, is shown in Table 15. As illustrated in Equation (8), the natural frequency is influenced by both the mass and the stiffness of the plate. This means that the natural frequency is dependent on the thickness and the Young's modulus, as this defines the stiffness of the plate. It also means that natural frequency is dependent on the density and thickness combined, as this defines the total mass of the plate.

This means that the thickness influences both the mass and the stiffness of the plate. However, in the calculations of the natural frequency it is shown that the thickness impacts the stiffness most. This is shown by the calculation of the natural frequency, illustrated in the equation below.

Table 15 shows that the lowest natural frequency is found in the thinnest plate, with the lowest

Youngs modulus, i.e., C2 Interval 1. The table also shows that when the density is low, the natural frequency increases, as shown by the frequencies in C3 Interval 1 and C3 Interval 2.

$$\omega_n = \sqrt{\frac{D}{m}} = \sqrt{\frac{\frac{Et^3}{12(1-v^2)}}{\rho A t}} = \sqrt{\frac{Et^2}{12(1-v^2)(\rho A)}}$$

Table 15: Natural frequency, ω_n [rad/s]

	Thickness 1	Thickness 2	Thickness 3
Steel	56.66	45.33	33.99
Aluminium	55.98	44.79	33.59
C1 Interval 2	56.58	45.26	33.95
C2 Interval 1	32.71	26.17	19.63
C2 Interval 2	46.26	37.01	27.76
C3 Interval 1	96.30	77.04	57.78
C3 Interval 2	69.06	55.25	41.44

4.3   Fast Fourier Transform

Fast Fourier Transforms are completed for Dataset 1A, 2A and 3A (t=0.125 m, t=0.1 m, and t=0.075 m respectively, and Z=4 m/kg$^{1/3}$). As described in Section 2.4.2, a FFT isolates the frequencies present in a signal consisting of datapoints and transforms this into the frequency domain. In this way, an FFT is used to find the multiple frequencies occurring in the total response.

Figure 25 shows the results of the FFT for steel in Dataset 1A. The figure illustrates the distinct frequencies present in the total vibration of the plate, where the sharp peaks indicate the distinct frequencies occurring in the response. Figure 25 shows, the steel plate vibrates with four distinct frequencies, all with varying amplitude. The amplitude of the lowest frequency is most pronounced, with an amplitude of 357 kN and a frequency of 18.45 Hz. This is followed by the frequency of approximately 36.9 Hz and an amplitude of 42 kN. The two remaining frequencies both exhibit quite low amplitudes. A complete analysis of the frequencies in the total response is given in Section 5.2.

Figure 26 gives the result of Category 2 and 3 in the same dataset. The additional FFTs are given in Appendix B. The figure illustrates that the presence of multiple frequencies varies between materials. However, all materials vibrate with more than one frequency.
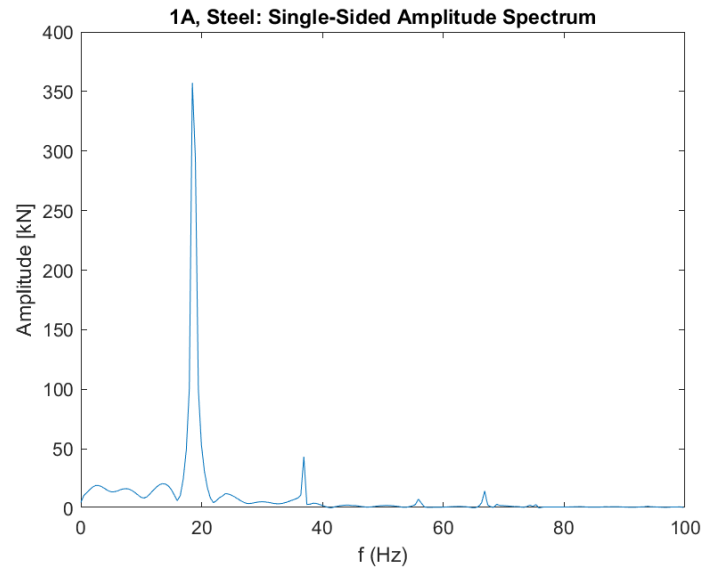
Figure 25: FFT – steel
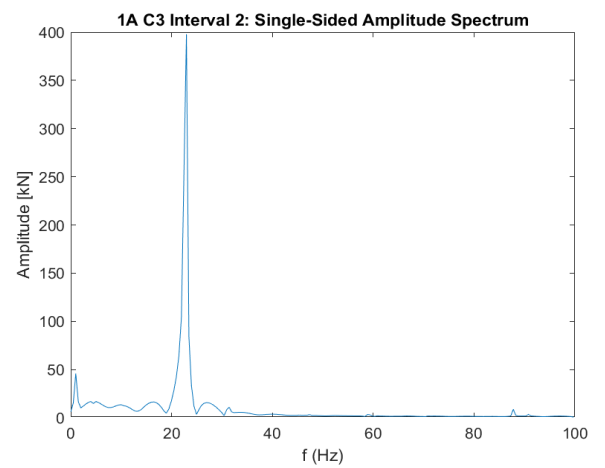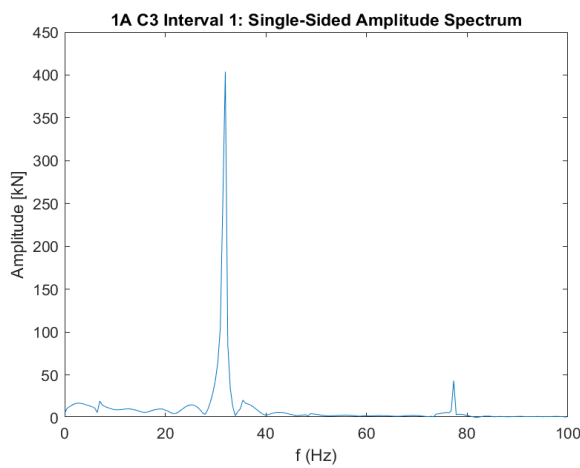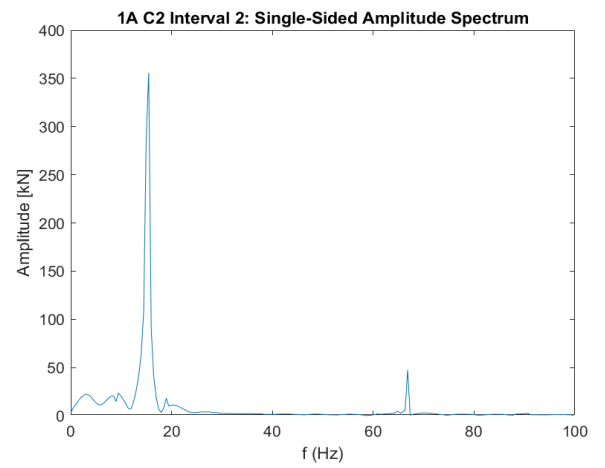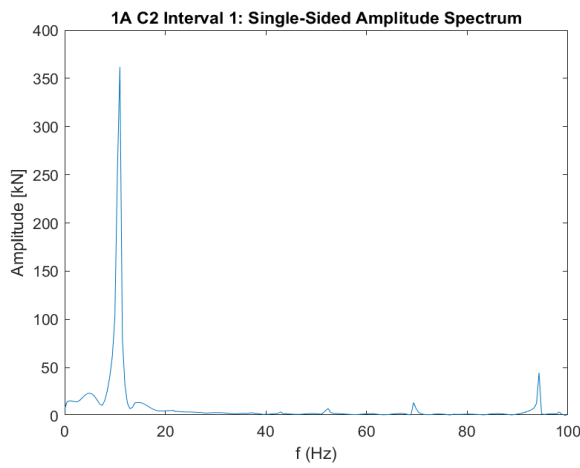
Figure 26: FFT – Category 2 and 3

4.4   Curve fitting

Three different types of equations are evaluated, in the process of finding a general equation that adequately describes the response of the system. These three types are a sine equation using three equation constants, a sine equation with an exponential term and four equation constants, and Fourier series. The following sections include a presentation of the different equations, and an evaluation of the most fitting equation. The following figures illustrating the different equations are showing Dataset 1A (t=0.125m and Z=4m/kg$^{1/3}$).

4.4.1   Sine equation

The first equation, General equation (1), is a sine function using three equation constants. Equation constant A describes the amplitude of the system, while B describes the phase, and C describes the phase change. The Equation constants are first approximated by visual means, then the least squares method is used to find the most fitting value of each constant.

$$F(t) = A\sin(Bt - C)$$ *General equation (1)*

Figure 27 illustrates how General equation (1) follow the curve of the reaction forces of a steel plate. General equation (1) generally fits the oscillation of the response quite well. Yet, there are some main discrepancies to note. General equation (1) is unable to detect the first peak response, as well as the maximum value of some of the oscillations in the free vibration phase.

As the curve fitting uses the least squares method, the constants are meant to result in the least discrepancy between the actual reaction force and the general equation describing the response. Therefore, the period of the first oscillation, which is due to forced vibration, is not completely accounted for and the equation will start with negative values. Further, as shown in Section 4.1.3 and 4.3 the time history response for the different materials has more than one vibration pattern. This extra vibration pattern is not captured by General equation (1).

As the equation does not include any damping and only consists of one single sine oscillation, it will produce oscillations prior to the arrival of the pressure wave. This means that the equation is unable to detect when the pressure wave reaches the plate surface. Though the equation can follow the oscillation in the free vibration phase very well, it might be preferable to have an equation that capture peak reaction forces.

Curve fitting 1A - Steel
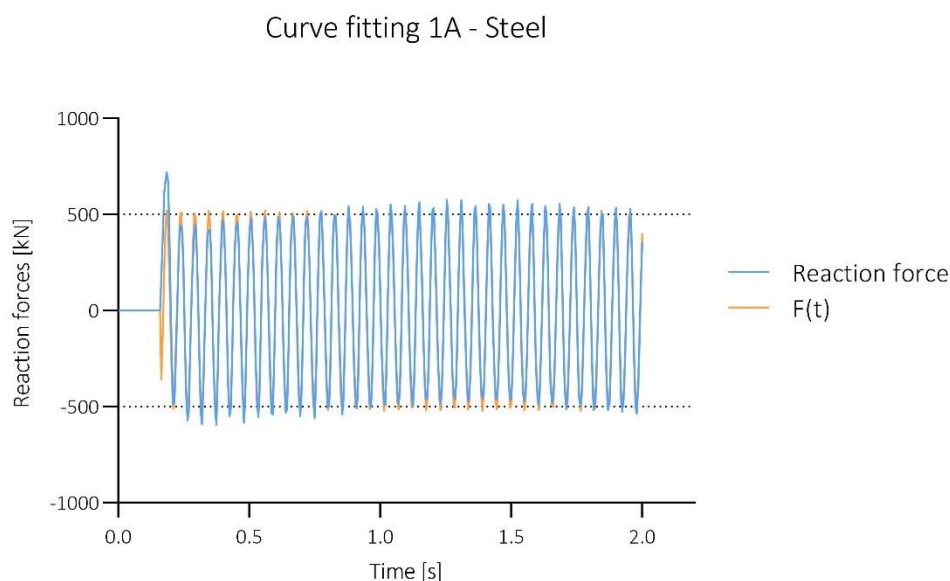
Figure 27: Curve fitting – General equation (1)

4.4.2   Sine equation with an exponential term

General equation (2), is a sine function using four equation constants. Equation constant A, B and C describe the same behaviour as in General equation (1), while Equation constant D determines the contribution of the exponential term, which is decaying over time. As described in Section 2.2.1 t_a is the arrival time of the pressure wave, while t is the time.

$$F(t) = A\sin(Bt - C)\, e^{(Dt_a/t)^2}$$

General equation (2)

Figure 28 shows how General equation (2) follow the curve of the reaction forces, illustrating that this equation is able to detect more of the response than General equation (1). When an exponential term is included in the equation, it is able to detect the peak response in the first oscillation. Thus, the maximum reaction force can be calculated using this equation.

The function does, however, deviate from the actual response at three points. The amplitude of the oscillations following the peak are exaggerated until the exponential has reached its final value of 1.

Like General equation (1) this equation also starts with negative values. Further, when including the exponential part these negative values are amplified by the exponential function. Therefore the "error" in the beginning is larger.

51

Lastly, this equation also results in values of the reaction forces before the arrival time of the load, which due to the exponential part is increasing in magnitude. Yet, this equation is a good approximation of the response, giving the possibility of finding both the maximum load, and the subsequent oscillations.
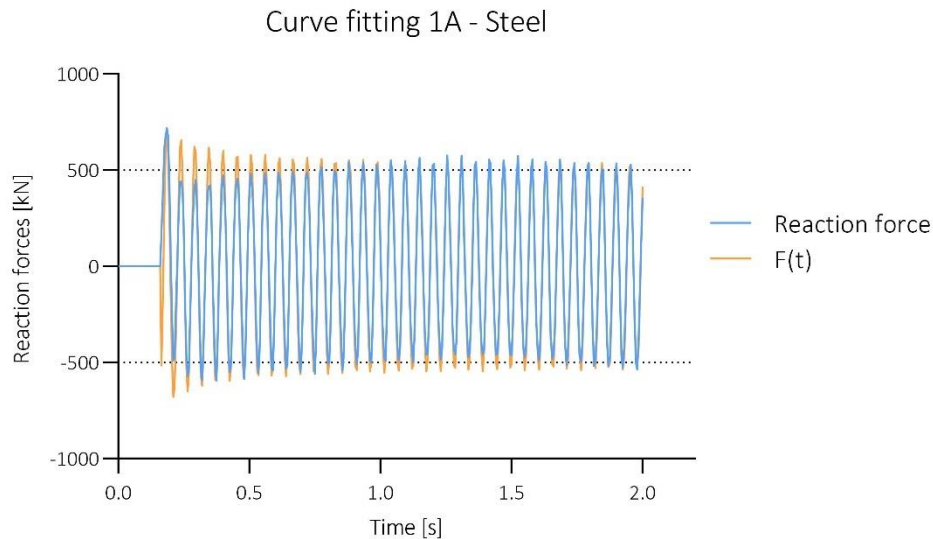
Figure 28: Curve fitting – General equation (2)

General equation (2) is deemed as the most fitting equation to describe the reaction forces. However, as the equation only yields viable results after the arrival of the load, General equation (2) is supplemented with a term defining the time. Therefore, the general equation proposed is as stated in General equation (3).

All nine datasets are curve fitted using General equation (3). Table 16 give the four calculated equation constants of every material in all nine datasets. Using the equation constants and General equation (3) gives the reaction force in kN.

$$F(t) = \begin{cases} 0, & t < t_a \\ A\sin(Bt - C)\, e^{(Dt_a/t)^2}, & t \geq t_a \end{cases} \qquad \textit{General equation (3)}$$

Table 16: Equation constants

Dataset 1A

Load case	A	B	C	D
Steel	518.96	117.32	1.27	0.181
Aluminium	519.31	115.37	0.95	0.184
C1 Interval 2	519.49	116.87	1.20	0.184
C2 Interval 1	472.13	68.19	0.00	0.199
C2 Interval 2	512.26	95.77	4.02	0.154
C3 Interval 1	529.24	199.43	2.04	0.265
C3 Interval 2	526.00	143.62	0.00	0.233

Dataset 1B

Load case	A	B	C	D
Steel	333.096	117.312	3.630	0.186
Aluminium	333.326	115.355	3.273	0.185
C1 Interval 2	333.388	116.868	3.550	0.187
C2 Interval 1	321.047	67.701	0.729	0.155
C2 Interval 2	329.729	95.771	5.950	0.148
C3 Interval 1	335.790	199.608	0.000	0.300
C3 Interval 2	335.297	143.009	2.054	0.232

Dataset 1C

Load case	A	B	C	D
Steel	240.04	117.31	5.37	0.171
Aluminium	240.20	115.35	4.99	0.176
C1 Interval 2	240.25	116.86	5.28	0.175
C2 Interval 1	231.51	67.70	1.73	0.146
C2 Interval 2	237.82	95.77	1.09	0.132
C3 Interval 1	243.41	199.43	2.74	0.261
C3 Interval 2	241.76	143.01	4.18	0.225

Dataset 2A

Load case	A	B	C	D
Steel	511.15	93.79	3.73	0.163
Aluminium	505.49	92.40	3.65	0.193
C1 Interval 2	507.25	92.68	3.22	0.185
C2 Interval 1	472.36	53.99	3.32	0.130
C2 Interval 2	500.39	76.13	0.65	0.191
C3 Interval 1	525.00	160.51	2.90	0.295
C3 Interval 2	517.36	114.88	1.08	0.221

Dataset 2B

Load case	A	B	C	D
Steel	329.52	93.78	5.62	0.162
Aluminium	325.86	92.37	5.52	0.188
C1 Interval 2	326.62	92.65	5.08	0.179
C2 Interval 1	311.12	53.97	4.41	0.126
C2 Interval 2	324.52	76.12	2.19	0.185
C3 Interval 1	336.00	160.64	0.00	0.290
C3 Interval 2	332.14	114.86	3.36	0.218

Dataset 2C

Load case	A	B	C	D
Steel	233.20	94.12	0.94	0.169
Aluminium	235.07	92.35	0.60	0.174
C1 Interval 2	235.96	92.64	0.17	0.170
C2 Interval 1	224.63	53.96	5.19	0.093
C2 Interval 2	233.89	76.11	3.31	0.142
C3 Interval 1	244.00	160.54	2.26	0.284
C3 Interval 2	239.68	114.89	5.09	0.209

Dataset 3A

Load case	A	B	C	D
Steel	496.53	70.83	0.00	0.19
Aluminium	492.48	70.03	0.00	0.215
C1 Interval 2	496.62	70.65	0.00	0.196
C2 Interval 1	435.32	40.90	1.04	0.088
C2 Interval 2	480.74	57.78	3.97	0.104
C3 Interval 1	520.88	120.28	1.77	0.213
C3 Interval 2	508.69	86.23	2.45	0.219

Dataset 3B

Load case	A	B	C	D
Steel	323.15	70.69	1.30	0.184
Aluminium	323.01	69.69	1.11	0.215
C1 Interval 2	323.78	70.46	1.26	0.191
C2 Interval 1	292.68	40.85	1.86	0.051
C2 Interval 2	315.16	57.73	5.13	0.134
C3 Interval 1	334.20	120.22	4.16	0.21
C3 Interval 2	328.44	86.19	4.17	0.221

Dataset 3C

Load case	A	B	C	D
Steel	233.12	70.68	2.34	0.171
Aluminium	233.00	69.61	2.12	0.182
C1 Interval 2	233.33	70.43	2.29	0.174
C2 Interval 1	211.10	40.81	2.44	0.026
C2 Interval 2	225.21	57.94	0.00	0.118
C3 Interval 1	238.66	120.43	0.00	0.221
C3 Interval 2	236.74	86.17	5.46	0.204

4.4.3   Fourier series

As shown in Section 3.5, the complete Fourier series is found by the following calculation:

$$f(t) = \sum_{n=0}^{50} a_n \cos\left(\frac{2\pi t}{100 * 0.005s}\right) + b_n \sin\left(\frac{2\pi t}{100 * 0.005s}\right)$$

The results of curve fitting when using Fourier series is illustrated with the material properties of steel in Dataset 1A (t=0.125 and Z=4m/kg$^{1/3}$). As described in Section 3.5, curve fitting by Fourier series is only analysed for the first 0.5 seconds of the response. Further, as the output from Abaqus is given at every 0.005 seconds (Δt), the response consists of a total of 101 data points (N), for the first 0.5 seconds (this includes the first point, starting in 0, 0). These datapoints are converted to the frequency domain by a Discrete Fourier Transforms (DFT), leading to a maximum value of $n = N/2 = 50$. Leading to 50 values of both Fourier coefficients a_n and b_n.

Figure 29 shows the result of a Fourier series consisting of the total Fourier series, $\Sigma_{n=0}^{50}$, denoted as Σtot in the figure, as well as a function consisting of the first 15 terms of the Fourier series, $\Sigma_{n=0}^{15}$, denoted as Σ0-15 in the figure. As Figure 29 shows, using the maximum value of n, leads to a function that precisely mimic the response of the reaction forces, neither over- or underestimating the response at any point. This also means the Fourier series produces a function where the magnitude of the reaction force is zero, until the arrival time of the load. Figure 29 also shows that using a function consisting of $\Sigma_{n=0}^{15}$ is a good approximation of the response of the material. However, this function exaggerates the magnitude of reaction forces at certain points, most notably between 0 and 0.025 seconds and at the peaks of the oscillations. Additionally, it underestimates the negative values of the oscillations. Yet, the general response of the plate is accounted for.

Fourier series - 1A Steel
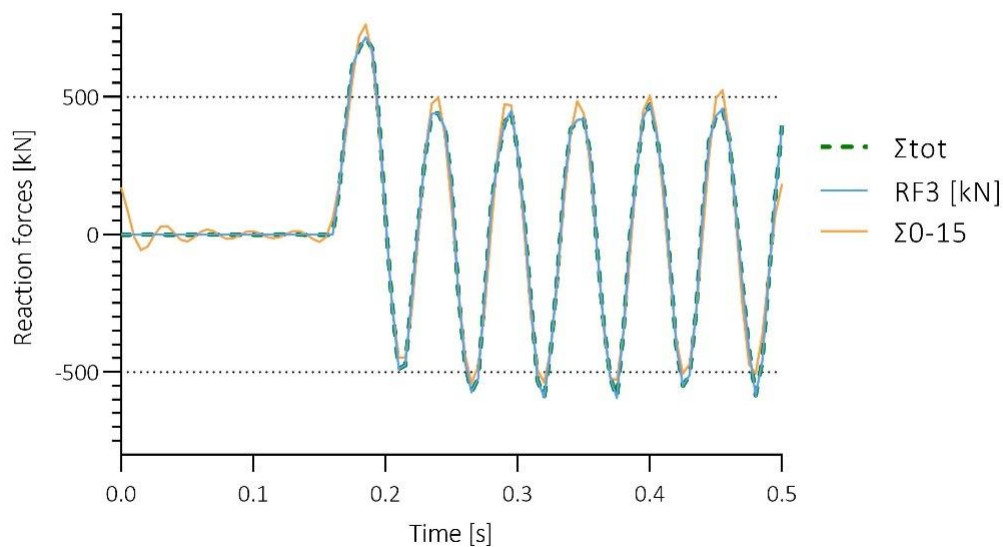
Figure 29: Curve fitting - Fourier series

As illustrated, the discrepancy between Σtot and Σ0-15 is relatively small. Both series are able to mimic the main oscillations, without severely under- nor overestimating the reaction. However, the computational cost is notably high for both functions.

As mentioned, a Fourier series using $\Sigma_{n=0}^{50}$, consists of 50 values of both a_n and b_n for every time step. Meaning the total Fourier series is the sum of $50a_n + 50b_n$ at 101 steps, as this corresponds to the number of data points. It is not given that this expression, however precise, can be simplified any further. Therefore, although the Fourier series, $\Sigma_{n=0}^{50}$, is able to calculate the response accurately, it is not a viable option at this point, with regards to composing a simplified expression of the response.

5.   Analysis

In the following sections the results are analysed. The analysis is divided into three main parts. The first part focuses on analysing the Abaqus results with regards to the peak reaction forces of each material. The second part of the analysis focuses on the vibrations of the free vibration phase. Finally, the last part of the analysis focus on the equation constants found from curve fitting. The equation constants are analysed to uncover relationships between the constant and the material definitions. In addition to analysing the part of the time history response each equation constant describes.

The numerical analysis and the vibration analysis is analysed based on the three material categories, defined in Section 3.2.1. Category 1 is not analysed in as great detail as Category 2 and 3. As it is difficult to isolate the effect of varying Young's modulus and density alone, when all the material properties vary simultaneously. Steel is used a comparison for the materials in every category. As mentioned in Section 2.3.1, the natural period, T_n, impacts the response of the plate, which means that the mass and stiffness will impact the results. Therefore, the different responses are evaluated based on the material parameters, as well as the stiffness and mass of the system. The stiffness and mass are not varied using a constant interval, as these are a product of the material parameters.

5.1   Numerical analysis

The peak reaction forces are analysed focusing on the impact of the scaled distance, thickness, Young's modulus and density. The effect of varying thickness, Young's modulus, and density is only analysed using Load case A, as the behaviour is similar for all load cases. This analysis is also supplemented with an evaluation of the reaction time, i.e., the time from arrival time t_a, to the time it takes for the plate to reach peak reaction force.

5.1.1   Scaled Distance

The effect on the reaction forces when increasing the scaled distance is illustrated in Figure 30. The figure shows the variation of the average peak reaction forces when scaled distance increases from 4 m/kg$^{1/3}$ to 6 m/kg$^{1/3}$. The average peak reaction forces are calculated using the peak reaction forces of materials within each dataset. This is used since the materials have similar behaviour when the scaled distance increases, so Figure 30 shows the behaviour for the different thicknesses.

Figure 30 shows that the different thicknesses have similar behaviour when the scaled distance increases. The figure clearly illustrates that the average peak reaction force decreases when the scaled distance increases. Load case A results in the highest reaction forces, while Load case C results in the lowest reaction forces. However, the reduction of reaction forces does not follow a linear curve from Load case A to C. The gradient of the slope is somewhat higher from Load case A to B than from Load case B to C, this phenomenon is observed for all thicknesses.
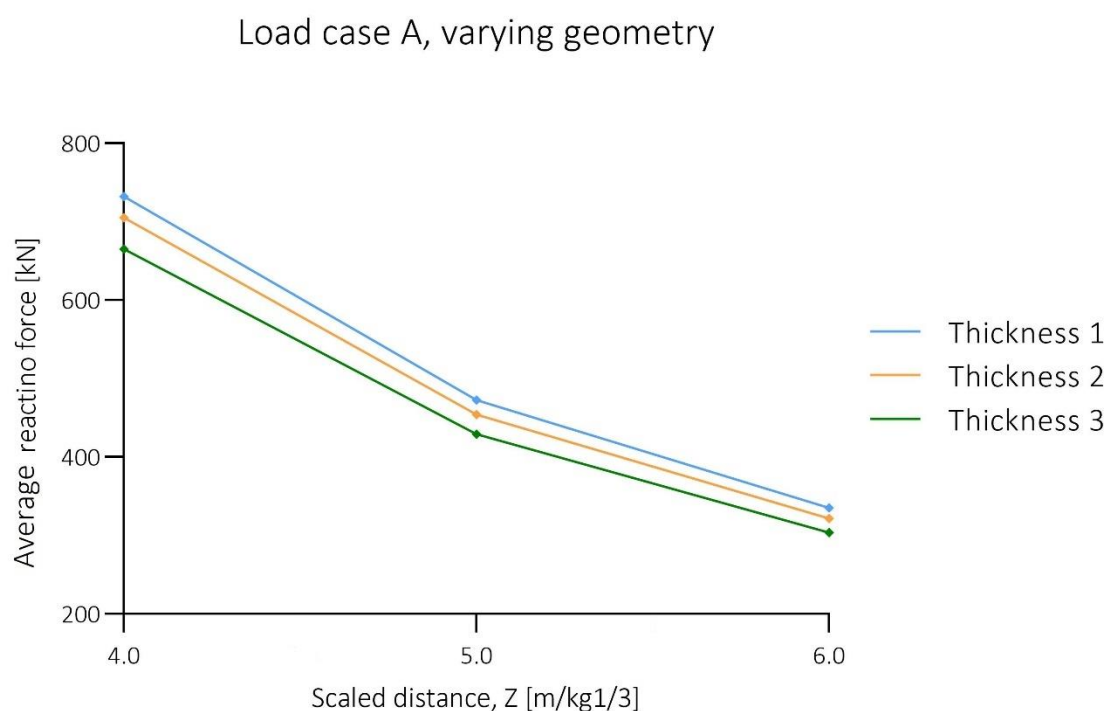
Figure 30: Average reaction forces

5.1.2   Thickness

Figure 31 shows how the peak reaction forces of the different materials vary when the thickness increases. The plate thickness has influence of both the mass and stiffness of the system, and consequently the natural frequency, described in Section 4.2.

As shown in Figure 31, the peak reaction forces of the materials in Category 1 stays almost constant when the thickness increase from 0.075 m to 0.1 m. When the thickness increases further the reaction forces increase, albeit with a lower gradient of the curve compared to the materials in Category 2 and 3.

Additionally, Figure 31 shows that the peak reaction forces in Category 2 and 3 behaves in the same manner when the thickness is 0.075 m to 0.1 m, thereafter different behaviours are registered within the two categories. For both categories the lowest peak reaction forces are found when the thickness is 0.075 m. Further, the peak reaction force increases from 0.075 m to 0.1 m for both categories. After this point the response varies somewhat. The peak reaction force of two materials continues to increase as the thickness reaches 0.125 m, while it decreases for the remaining two materials. The materials displaying decreasing reaction forces is C3 Interval 1 and C2 Interval 2.

Since the different materials exhibit different behaviours, and no clear trends are registered as the thickness increase, it indicates that peak reaction forces are depended on interaction effects from the material properties and thicknesses. However, as Figure 31 shows, it is found that the peak reaction force generally increases when the thickness is increased from 0.075 m to 0.125 m. The effects of different material properties will be analysed further in Section 5.1.3 and 5.1.4.
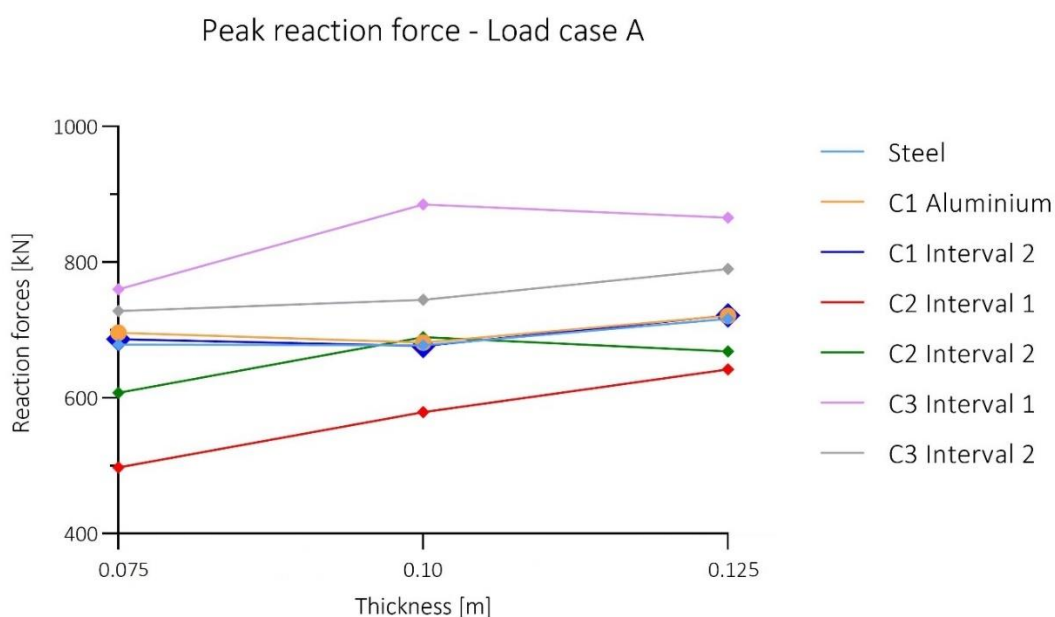
Figure 31: Peak reaction forces, Load case A

5.1.3   Young's modulus

This section analyses the results of Category 2, where the Young's modulus is varying. Figure 32 illustrates how the peak reaction forces vary as the Young's modulus increases, showing the peak reaction forces of Thickness 1, 2 and 3. In Figure 32, E=70 GPa corresponds to C2 Interval 1, while E=140 GPa and 210 GPa corresponds to C2 Interval 2 and Steel respectively.

As Figure 32 shows, the lowest peak reaction force, is found when the Young's modulus is lowest, this is seen for all thicknesses. Furthermore, Thickness 3 has the lowest reaction forces, regardless of the magnitude of the Young's modulus. The behaviour is quite similar for Thickness 1 and 3, where the peak reaction forces increase almost linearly, although with a higher gradient for Thickness 3. For both Thickness 1 and Thickness 3 the highest peak reaction force is found when E=210 GPa.

The same phenomenon is not observed for Thickness 2, where the highest peak reaction force is found when E=140 GPa. From 70 GPa to 140 GPa the peak reaction forces of Thickness 2 increase, with a curve that has the highest gradient of all datasets. Further, the peak reaction forces decrease from E=140 GPa to 210 GPa. This may indicate an interaction effect between the material properties and the thickness, which is also pointed out in the analysis of the thickness. By analysing Young's modulus effect on the peak reaction forces, the findings may indicate that the peak reaction forces generally increase as the stiffness increase. This is seen as the peak reaction forces of all thicknesses increase from E=70 GPa to E=210 GPa.
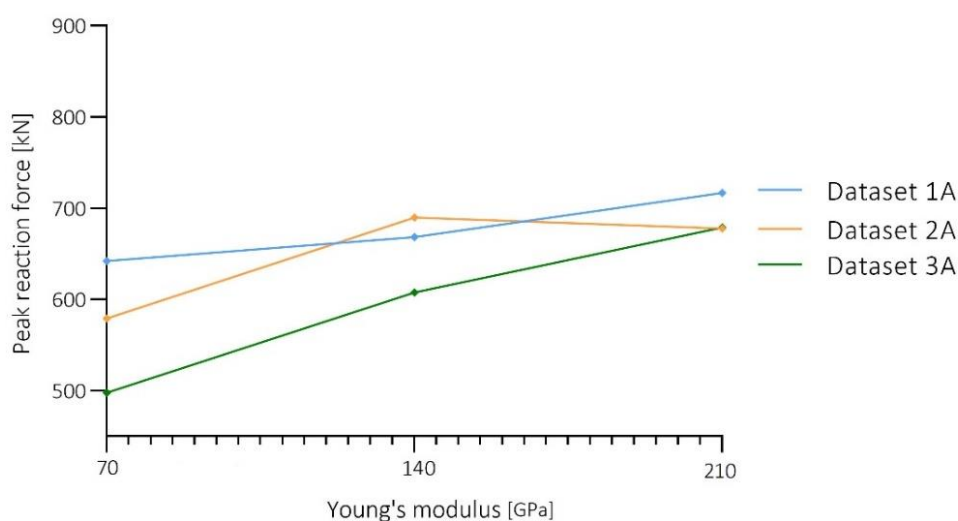
Figure 32: Peak reaction forces – Category 2

Table 17 shows the reaction time for the datasets in Category 2. It is noticeable that the different load cases do not influence the reaction time, as the values stays constant when changing the load. Though, there is one exception for steel in Dataset 2C (t=0.1 m and Z=6 m/kg$^{1/3}$). Table 17 shows that the reaction time gets shorter as the thickness increases. This may indicate that as the plate get stiffer, the reaction time decreases. Though this may also indicate that as the mass increases the reaction time get shorter. There is a general decrease in the reaction time from C2 Interval 1 to C2 Interval 2. So, as the Young's modulus gets higher, the reaction time gets shorter. Which again indicates that when the plate gets stiffer the reaction time gets shorter.

Table 17: Reaction time – Category 2

Dataset	1A	1B	1C	2A	2B	2C	3A	3B	3C
C2 Interval 1	0.035	0.035	0.035	0.04	0.04	0.04	0.055	0.055	0.055
C2 Interval 2	0.02	0.02	0.02	0.03	0.03	0.03	0.04	0.04	0.04
Steel	0.020	0.020	0.020	0.025	0.025	0.020	0.030	0.030	0.030

5.1.4   Density

This section analyses the results of the peak reaction forces in Category 3, where the density is varying. Figure 33 gives the peak reaction forces for Dataset 1A, 2A and 3A (t=0.125 m, t=0.1 m, and t=0.075 m respectively, Z=4 m/kg$^{1/3}$). In Figure 33, ρ=2700 kg/m^3 corresponds to C3 Interval 1, while ρ=5250 kg/m^3 and ρ=7800 kg/m^3 corresponds to C3 Interval 2 and Steel respectively.

As Figure 33 shows, the peak reaction forces are highest when the density is lowest, decreasing as the density increase. The peak reaction forces of both Thickness 1 and 3, decrease linearly when the density is increasing, the same behaviour is not found for Thickness 2. For Thickness 2 the peak reaction forces decrease quicker from ρ=2700 kg/m^3 to ρ=5250 kg/m^3, than from ρ=5250 kg/m^3 to ρ=7800 kg/m^3.

At the lowest density, Thickness 2 has the highest peak reaction forces, while Thickness 3 has the lowest peak reaction forces. When the density increases to ρ=5250 kg/m^3, this order changes, where Thickness 1 has highest peak reaction forces, while Thickness 3 still has the lowest peak reaction force. As the density increases further to ρ=7800 kg/m^3, the peak reaction forces of Thickness 1 is still the highest. However, with a density of ρ=7800 kg/m^3 the peak reaction forces for Thickness 2 and Thickness 3 have the same magnitude, as shown in Figure 33. This behaviour applies to all load cases.

So, when the density increases the peak reaction forces decrease. Which could indicate that as the mass decreases, the peak reaction forces decreases. These finding are true, when analysing the effect of an increased density alone.
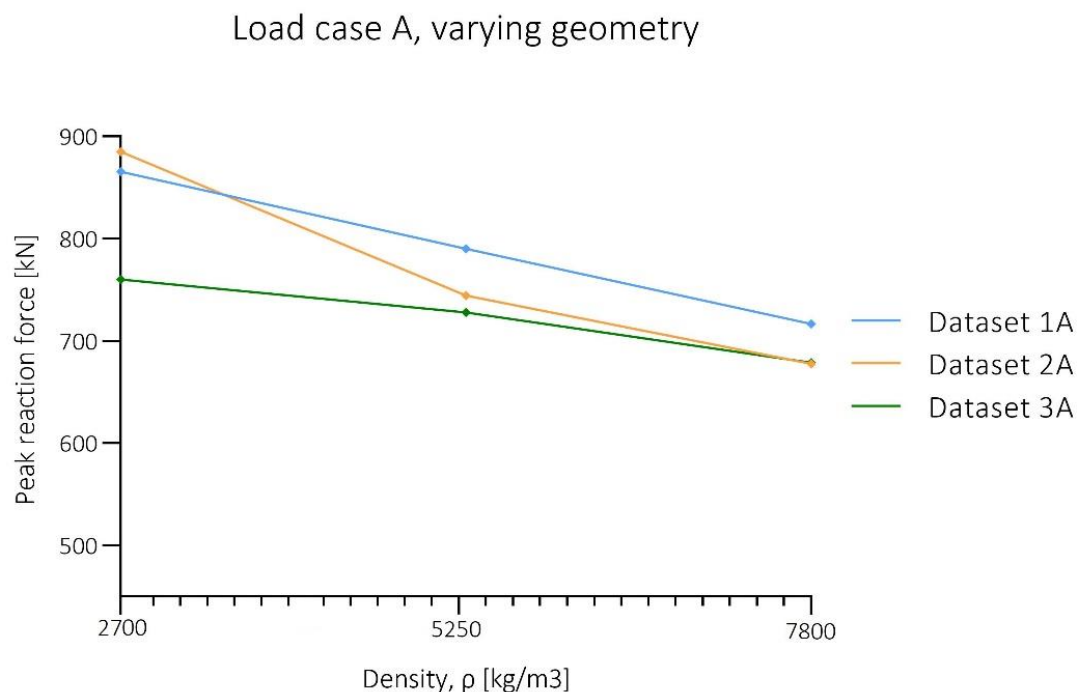
Figure 33: Peak reaction forces – Category 3

Table 18 shows the reaction time for all the datasets in Category 3. The reaction time stays constant as the load changes, and as the thickness increases the reaction time get shorter. Table 18 shows that Interval 1, lowest density, has the shortest reaction time, also compared to Category 2, and as the density increases the reaction time gets longer. To sum this up, low density results in shorter reaction time.

Table 18: Reaction time – Category 3

Dataset	1A	1B	1C	2A	2B	2C	3A	3B	3C
C3 Interval 1	0.01	0.01	0.01	0.015	0.015	0.015	0.015	0.015	0.015
C3 Interval 2	0.015	0.015	0.015	0.02	0.02	0.02	0.025	0.025	0.025
Steel	0.020	0.020	0.020	0.025	0.025	0.020	0.030	0.030	0.030

5.2   Vibration analysis

As shown in Section 4.1.3, the time history response of the reaction forces indicates the presence of multiple frequencies. However, analysing the reaction forces based on these results alone can prove difficult, as it is hard to identify the distinct oscillations and their belonging frequencies. To analyse the vibratory response, the time history response is supplemented with the results of the FFT. The time history response of the materials in every dataset is given in Appendix A, while the results of the FFT are given in Appendix B. The analysis in the following sections focuses on the free vibration phase.

Table 19 shows the number of distinct frequencies found in the FFT, and the corresponding amplitudes of these frequencies, for Dataset 1A, 2A and 3A (t=0.125 m, t=0.1 m and t=0.075 m respectively, and Z=4 m/kg$^{1/3}$). The table also give the number of peaks found in the FFT of every material, indicating the number of modes present in the response. It shows that the distinct number of modes is highest for the thinnest plate, followed by the thickest. However, some of the modes exhibits amplitudes with very low peaks, meaning these modes do not affect the overall response notably. Therefore, the analysis only focuses on the modes with the highest and second highest amplitude, as these modes dominate the response.

In Table 19 the notations D1 and D2 refers to the most dominant mode and the second most dominant mode, respectively.

Table 19: Mode frequencies and amplitude

			AMPLITUDE [kN]		FREQUENCY [Hz]	
		No. of modes	*D1 mode*	*D2 mode*	*D1 mode*	*D2 mode*
1A	*Steel*	4	357.3	42.32	18.45	36.91
	C2 Interval 1	4	362	44.56	10.97	94.26
	C2 Interval 2	2	355.7	47.5	15.46	66.83
	C3 Interval 1	2	403.9	77.31	31.92	77.31
	C3 Interval 2	3	397.9	45.83	22.94	0.9975
2A	*Steel*	2	465.8	47.48	14.96	67.33
	C2 Interval 1	3	398.9	49.26	8.479	76.31
	C2 Interval 2	2	402.7	35.16	11.97	92.27
	C3 Interval 1	2	405.8	41.04	25.44	28.93
	C3 Interval 2	3	403.3	39.34	18.45	37.41
3A	*Steel*	5	347.4	51.68	11.47	99.75
	C2 Interval 1	5	398.1	51.55	6.484	58.35
	C2 Interval 2	4	329.4	42.02	8.978	82.79
	C3 Interval 1	4	386	43.07	18.95	27.93
	C3 Interval 2	3	330.06	50.77	13.97	76.81

5.2.1   Dominant frequency

Table 19 shows that the lowest frequency of the most dominant mode is found in Category 2, while the highest frequency is found in Category 3, these trends are found for all thicknesses. This finding can be seen visually in the time history graphs as well, where the plate using the materials in Category 3 completes more periods during the time step than Category 2.

In Category 2 the frequency of the most dominant mode increases with an increasing Young's modulus, as illustrated in Table 19. An effect which also is clearly visible when analysing the time history graphs of the different materials in Category 2. C2 Interval 1, the material with the lowest Young's modulus, completes the least periods over 2 seconds of the analysis compared to C2 Interval 2. Suggesting that increasing the Young's modulus leads to a higher frequency.

Furthermore, as shown in Table 19 it is found that the frequency of the most dominant mode decreases with increasing density. This same effect can also be seen visually by the time history graphs for materials in Category 3, where C3 Interval 1 completes the more oscillations during the two seconds than C3 Interval 2. This suggests that increasing the density in a material leads to slower vibrations.

It is found that the frequency of the dominant mode increases when the thickness increases. This again can be seen visually in the time-history response, where the oscillation of the plate completes fewer periods for Thickness 3 than Thickness 1, as shown in Section 4.1.3.

5.2.2   Second most dominant mode

The time history results clearly shows that the frequency of the most dominant mode is quite easy to see visually. The second most dominant mode, however, is not as clear to isolate and analyse visually. As shown by Table 19 the frequency of the second dominant mode is generally higher than the frequency on the most dominant mode. This is true for all instances except from C3 Interval 2 in Dataset 1A (t=0.125 m and Z=4 m/kg$^{1/3}$).

The table illustrate that the discrepancy between the frequencies of the dominating mode and the second dominant mode is higher for Category 2 than Category 3. The effect of this can be seen visually in the time history graphs. In Category 2, where the discrepancy of the frequencies is high, the complete response vibrates with a somewhat stable amplitude. However, the oscillations are serrated, suggesting that the second most dominant mode generate vibrations within the oscillations of the dominant mode. An example of this effect is illustrated in Figure 34, where orange line represents the combined vibration.
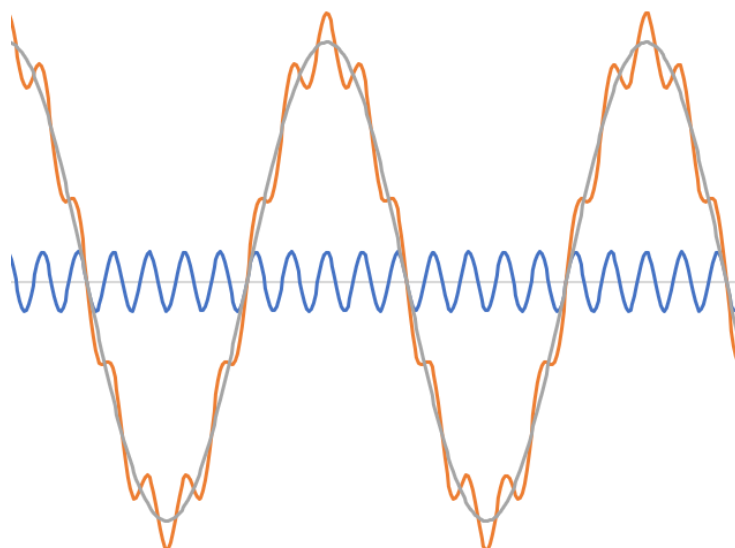
Figure 34: Combined vibration

When the discrepancy between the frequencies is low, as in Category 3, the complete response vibrates with noticeable variations in the amplitude. This suggests that the frequencies in Category 3 oscillates with a total vibration pattern that is harder to isolate, than for Category 2. Since they amplify and reduce each other, with a seemingly more random pattern.

The effect of varying thickness is not found to have a distinct effect on the second most dominant mode alone. However, as shown by the time history graphs, and described in Section 4.1.3, decreasing the thickness has a noticeable effect on the total vibration of the plate. When the thickness decreases the relationship between the most dominant mode, and the second most dominant mode changes. Causing more of the materials to exhibit a serrated or saw-toothed form. Table 20 shows how the relationship between the dominant mode and the second most dominant mode change, where $\Delta D = |D1 - D2|$. The table shows that when the thickness decreases this relationship increase, leading to a serrated form of the total response. These findings indicate that this form starts to occur when $\Delta D \approx 52$. However, for steel in Dataset 2A (t=0.1 m, Z=4 m/kg$^{1/3}$) this is not true.

Table 20: Dominant mode vs. second most dominant mode

		ΔD [Hz]	Serrated form
1A	*Steel*	18.46	
	C2 Interval 1	83.29	Yes
	C2 Interval 2	51.37	
	C3 Interval 1	45.39	
	C3 Interval 2	21.9425	
2A	*Steel*	52.37	
	C2 Interval 1	67.831	Yes
	C2 Interval 2	80.3	Yes
	C3 Interval 1	3.49	
	C3 Interval 2	18.96	
3A	*Steel*	88.28	Yes
	C2 Interval 1	51.866	Yes
	C2 Interval 2	73.812	Yes
	C3 Interval 1	8.98	
	C3 Interval 2	62.84	Yes

5.3 Curve fitting

In this section the equation constants in General equation (3) are analysed, followed by an analysis of the Fourier coefficients, a_n and b_n.

5.3.1 Equation constant A

Equation constant A describes the amplitude of the oscillations in General equation (3). The value of A, for each material, is given in Table 16. The value of Equation constant A is compared to the average amplitude of the free vibration phase, given in Table 13. The ratio between the averaged amplitude of every material and Equation constant A, is calculated by Equation (17).

A ratio of 1 means that the amplitude of the oscillations in General equation (3) is equal to the average amplitude of the free vibration phase. While a ratio above 1 means that the amplitude of the sine oscillations is lower than the average amplitude, and a ratio below 1 means the sine oscillations in General equation (3) are higher than the actual average amplitude. The ratio for every material is given in Table 21.

$$\frac{Average\ amplitude}{Equation\ constant\ A} = Ratio_A \qquad (17)$$

As shown in Table 21, the ratio is always slightly higher than 1 in Category 2, indicating that Equation constant A underestimates the true amplitude of the response. In this category the material C2 Interval 1 in Dataset 1A (t=0.125 m and Z=4 m/kg$^{1/3}$) deviates the most with a ratio of 1.11.

For Category 3, the ratio is slightly lower than 1 for every material, indicating that parameter A exaggerate the true amplitude of the response. This Category also exhibits an exception for C3 Interval 2 in Dataset 3A to 3C (t=0.075 m and Z=4 m/kg$^{1/3}$ to Z=6 m/kg$^{1/3}$).

Though both Category 2 and 3 underestimates and exaggerates the average amplitude, this deviation is small. Thus, Equation constant A relates quite closely to the average amplitudes and can be used in General equation (3) with satisfactory results.

Table 21: Results of ratio$_A$

Dataset	1A	1B	1C	2A	2B	2C	3A	3B	3C
Steel	1.00	0.99	0.99	1.01	1.01	1.02	1.06	1.04	1.03
Aluminium	1.00	0.99	0.99	1.04	1.02	1.02	1.07	1.05	1.04
C1 Interval 2	0.97	0.97	0.96	1.04	1.03	1.02	1.06	1.04	1.04
C2 Interval 1	1.11	1.05	1.04	1.07	1.05	1.05	1.10	1.08	1.08
C2 Interval 2	1.02	1.01	1.00	1.05	1.04	1.04	1.08	1.06	1.07
C3 Interval 1	0.96	0.96	0.95	0.98	0.97	0.96	0.99	0.98	0.98
C3 Interval 2	0.97	0.97	0.97	0.98	0.98	0.97	1.02	1.02	1.02

5.3.2   Equation constant *B*

Equation constant B relates to the frequency of the sine oscillations in General equation (3). Therefore, Equation constant B is compared to the natural frequency, ω_n. The value of B for every material is given in Table 16, while the natural frequency, ω_n, is given in Table 15.

As Equation constant B is approximately the same for all load cases, and the natural frequency is only dependent on the stiffness and mass of the plate, as detailed in Section 4.2, the relationship of B/ω_n are only evaluated for Thickness 1, 2 and 3 using Load case A. The results of B/ω_n are given in Table 22.

Table 22: Results of ωn/B

Thickness	1	2	3
Steel	2.071	2.069	2.083
C1 Aluminium	2.061	2.063	2.085
C1 Interval 2	2.066	2.048	2.081
C2 Interval 1	2.084	2.063	2.084
C2 Interval 2	2.070	2.057	2.082
C3 Interval 1	2.071	2.083	2.082
C3 Interval 2	2.080	2.079	2.081

The calculations shows that Equation constant B relates to the natural frequency by a constant factor of 2. The relationship found between B and ω_n is given in Equation (18).

$$B = 2\omega_n \tag{18}$$

5.3.3 Equation constant C

Equation constant C relates to the phase shift. Thus, Equation constant C is dependent on both the arrival time of the load, and the phase of General equation (3) at this time. There is not found a relationship that results in a general expression for Equation constant C.

5.3.4 Equation constant D

Equation constant D determines the relationship between the amplitude of the sine oscillations in General equation (3) and the peak reaction forces. The exponential term, $e^{(Dt_a/t)^2}$, functions as a scaling of the amplitude to reach the peak reaction force. This means that the magnitude of $e^{(Dt_a/t)^2}$ should correspond to the relationship between the actual peak reaction forces, and the average amplitude of the free vibration phase. This is evaluated based on Equation (19), where the peak reaction forces are denoted RF_{max}.

A ratio of 1 means that the scaling of the amplitude in General equation (3) is equal to the relationship between the actual peak reaction forces and the average amplitude of the free vibrations. While a ratio above 1 means that the exponential part, $e^{(Dt_a/t)^2}$, understates the scaling. The ratio for every material is given in Table 23.

$$\frac{RF_{max}/Average\ amplitude}{e^{(Dt_a/t)^2}} = Ratio_D \tag{19}$$

Table 23: Results of ratio$_D$

Dataset	1A	1B	1C	2A	2B	2C	3A	3B	3C
Steel	1.00	1.01	1.01	0.99	0.99	0.96	0.95	0.96	0.96
Aluminium	1.00	1.01	1.01	0.94	0.96	0.96	0.93	0.92	0.96
C1 Interval 2	1.03	1.03	1.04	0.93	0.95	0.95	0.95	0.95	0.96
C2 Interval 1	0.89	0.95	0.93	0.93	0.92	0.95	0.91	0.96	0.99
C2 Interval 2	0.98	0.99	1.03	0.95	0.96	1.01	0.99	0.94	0.93
C3 Interval 1	1.03	0.98	1.05	1.02	1.03	1.04	1.01	1.02	1.00
C3 Interval 2	1.02	1.02	1.02	0.99	0.99	1.00	0.96	0.96	0.96

The table shows that ratio is close to 1 for every material. Thus, the exponential term $e^{(Dt_a/t)^2}$, describes the scaling satisfactory. Meaning, the method of calculating the peak reaction forces using Equation constant D closely resembles the actual reaction forces.

5.3.5　Fourier coefficients a_n, and b_n

This part of the analysis focuses on the Fourier coefficients a_n and b_n, where the variation of the coefficients of the first 15 terms, $\Sigma_{n=0}^{15}$, is analysed. The Fourier series is analysed using the materials in Category 3 in Dataset 1A (t=0.125 m and Z=4 m/kg$^{1/3}$).

The variation of the Fourier coefficients a_n and b_n is shown in Figure 35 and Figure 36 respectively. These figures give an indication to the weight each coefficient has on the total Fourier series. A higher value results in a more pronounced effect on the total sum of the Fourier series, i.e., contributes more to the total vibration of the function.

The figures shows that the weight of the constants is quite similar for all materials, until $n = 8$. After this point the magnitude of the constants differ noticeably. It is important to note that the highest magnitude of both a_n and b_n varies for every material. To summarize, the figures indicate that some values of n, generate equation constants with a higher impact on the total result.

Dataset 1A - Parameter a_n
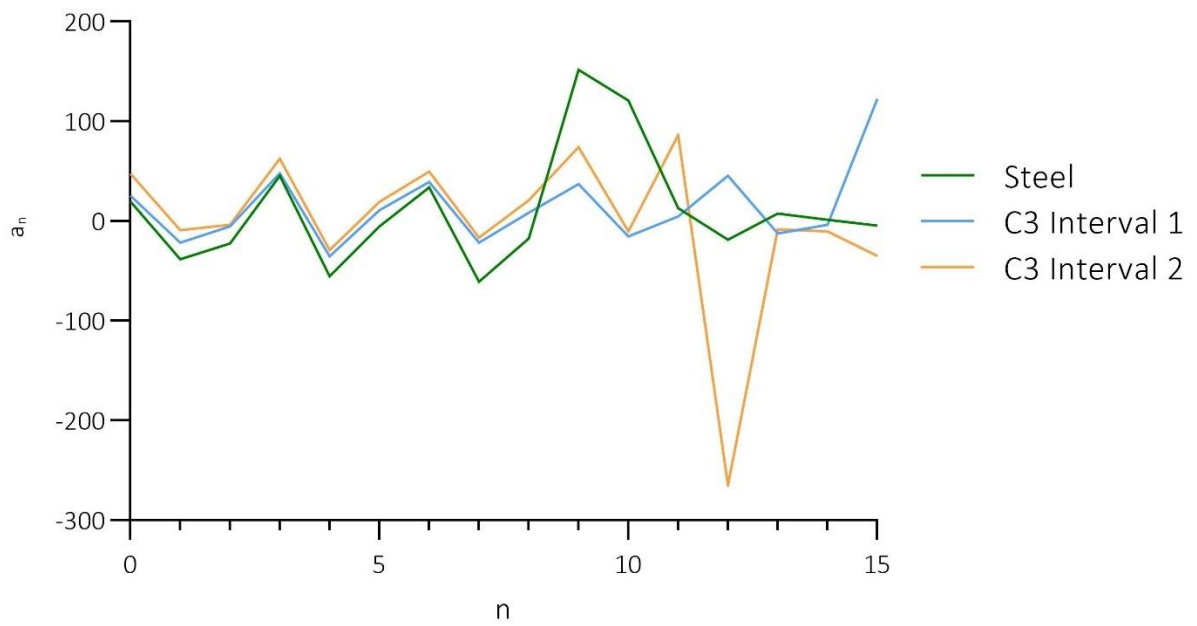
Figure 35: Variation of a_n

Dataset 1A - Parameter b_n
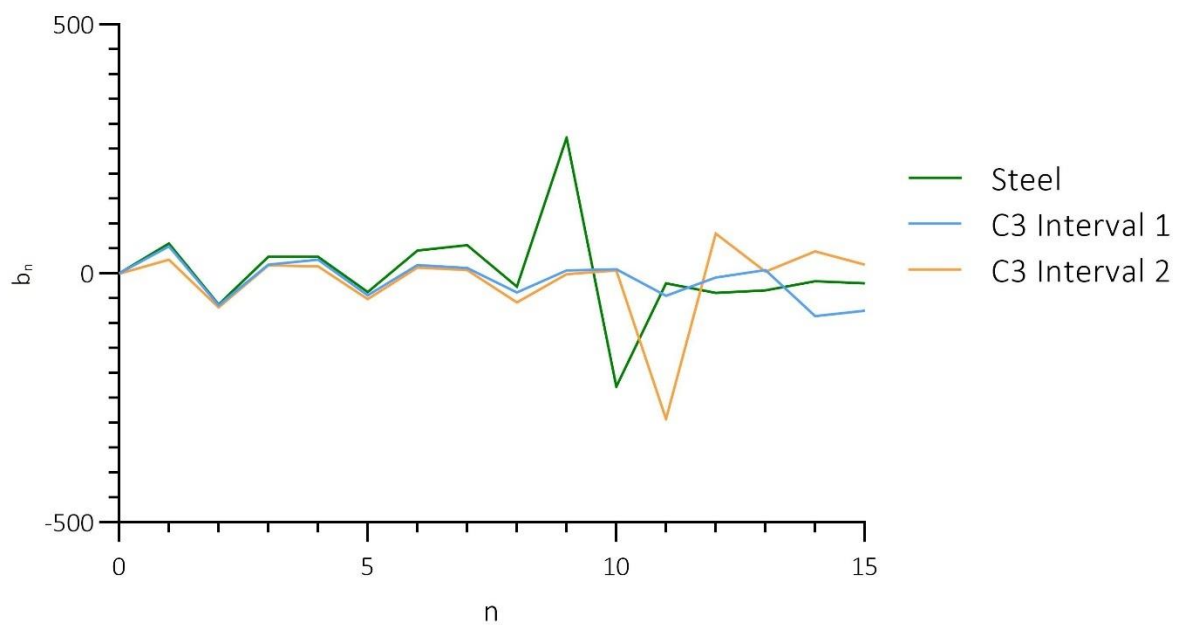
Figure 36: Variation of b_n

5.4   General findings

This section presents a summary of the general findings from the analysis.

In the analysis of the Young's modulus influence on the peak reaction forces, it is found that the peak reaction forces of Thickness 1 and 3 increase almost linearly when increasing the Young's modulus. However, Thickness 2 does not exhibit the same behaviour as its highest value is found at the middle value of Young's modulus, C2 Interval 2. The lowest peak reaction forces of the whole numerical analysis is found for C2 Interval 1 in Dataset 3C (t=0.075 m and Z=6 m/kg$^{1/3}$).

The general finding when analysing how the peak reaction forces changes as the density varies is that when density increases the reaction forces decreases. Thickness 1 and 3 shows an almost linear decrease. However, Thickness 2 has a steeper decrease in reaction forces from C3 Interval 1 to C3 Interval 2 (from the lowest to the middle density). The highest peak reaction force for the whole numerical analysis is found for C3 Interval 1 in Dataset 1A (t=0.125 m and Z=4 m/kg$^{1/3}$).

The analysis shows that when increasing the density, the peak reaction forces decrease. This indicates that increasing mass, results in lower reaction forces. The analysis also showed that if the Young's modulus increases the peak reaction forces increase, with one exception pointed out. This indicate that increasing the stiffness results in higher peak reaction forces. However, it is hard to describe the effects of the changing thickness, as the isolated effect of varying the thickness is concealed by interaction effects. Though, the overall trend shows that there is an increase in reaction forces when increasing the thickness.

Further, the analysis has shown that when the thickness and Young's modulus increase, the reaction time gets shorter. Additionally, it is found that the reaction time gets longer when the density increases, while the scaled distance has no influence on the reaction time. C3 Interval 1 Thickness 1 has the shortest reaction time, while C2 Interval 1 Thickness 3 has the longest reaction time. In other words, when the plate has a high stiffness and low density the reaction time is shortest, and when the plate has a low stiffness and high density the reaction time is longer.

The response of a system is highly dependent on its natural frequency, which is based on the mass and the stiffness of the system, as shown in Equation (8). Moreover, both the density and thickness naturally affect the total mass, while the Young's modulus and thickness affects the

stiffness. The general findings correspond with this, with some deviations, therefore, the findings are deemed appropriate.

In the vibration analysis it is found that all materials respond with more than one distinct frequency. The lowest frequency is found to dominate the response of every material, except for C3 Interval 2 in Dataset 1A ($t=0.125$ m and $Z=4$ m/kg$^{1/3}$). It is found that the frequency of the dominant mode is higher in Category 3 than Category 2, with the highest frequency of the dominant mode occurring in C3 Interval 1, and the lowest in C2 Interval 1. Further it is found that the dominant frequency increase for both an increase in the Young's modulus and in the thickness, while it decreases for an increasing density. This suggests that increasing the stiffness leads to a higher frequency of the dominant mode. It is also found that the discrepancy between the dominant mode and the second most dominant mode generally is higher in Category 2 than 3.

The analysis has shown that the reaction forces of the plate can be described using a simple sine equation. This correlation means that the method used for the curve fitting is satisfactory. However, the function only contains one repeating motion, defined by sine and an exponential part, meaning it is not able to register the presence of multiple frequencies. Yet, it does capture the most important parts of the reaction force, the peak reaction force, frequency of the dominant vibration and its amplitude. The parameter B which represents the frequency is found to be two times the natural frequency.

6.   Discussion

In this section, the numerical analysis and parametric study, is discussed. Following this, a brief discussion about the curve fitting is given.

6.1   Numerical analysis

This part focuses on the main aspects of the numerical analysis and parametric study that could have been done differently, and the effects of these changes. Following this, a discussion regarding the output frequency used, and the way this might affect the results, is presented. Thereafter the division of the parametric categories is evaluated. And lastly, the effect of including damping is briefly examined.

6.1.1   Output request

As described in detail in Section 3.2.2 the accuracy of the results depends on the frequency of the output, as it determines if the results are covered sufficiently. In this thesis the output request refinement is based on the steel analysis, using a plate thickness of 0.1 m. Using this plate definition, evenly spaced time intervals of 0.005 was deemed appropriate to capture the main response. However, if the aim was to capture all the frequencies present in the system, and not only the most dominates, a higher output frequency would be necessary.

The material properties and thickness of the steel plate used in the output refinement, results in a system with both high stiffness and mass. If the output refinement was performed using a less stiff material, i.e., C2 Interval 1 with a thickness of 0.075 m, a higher output frequency might be needed to satisfactory capture more detailed information about all the frequencies present. As this material and thickness exhibited a serrated vibration. So, a higher output frequency can lead to more detailed information regarding the distinct frequencies of the modes in the response.

Further, increasing the output frequency might be needed to produce a manual or standard with as detailed calculations as the equations provided in the European Standards. Thus, if the general expression of the reaction forces is to include multiple modes, it is pertinent to evaluate the output frequency for additional materials, to ensure that all frequencies of the response is covered in extensive detail.

The frequency of the output request should also be evaluated based on the reaction forces during the positive phase duration. As described previously, a blast load is a rapid dynamic load, with a very short positive phase. In the analyses in this thesis the positive phase lasts for

0.07 seconds to 0.055 seconds, from Load case A to C. With the output requested every 0.005 seconds, this results in a total of 14 outputs in Load case A and 11 outputs in Load case C, during the positive phase. Given the high velocity of the pressure wave it is possible that the peak reaction force is not covered by these outputs, as it could occur between the requested outputs. Thus, using a higher output request could mean that the output covers the reaction forces better, giving a higher value of the reaction forces.

6.1.2   Analyses time and computational time

Some adjustments regarding the modelling of the load could be implemented to reduce the computational cost considerably. As the model uses a CONWEP definition of the load, the analyses include calculations of the wave propagating from the explosion to the façade Resulting in many calculations before the load arrives at the façade. Furthermore, given that the stand-off distance used in these analyses is quite high, the pressure load can be regarded as almost evenly distributed. Therefore, to reduce the computational time, the time history of the pressure wave at the middle of the façade, can be applied as an evenly distributed pressure load, where the time history before arrival time is neglected. This way, the computational time of each analysis could be reduced, without negatively affecting the results.

Further, the numerical analysis in this thesis presents results for a timestep of two seconds. Through the analyses in this thesis, it was shown that this is an adequate duration to capture more than one mode on the time history graph. However, if the peak and the most dominant mode is the main focus for analysis, a shorter timestep could be used.

6.1.3   Categories

As meticulously detailed, the numerical analysis covers three distinct parametric categories, described, and defined in Section 3.2.1. From the results described in Section 5.1, some discussion points arise regarding the categories. Firstly, the material intervals used in Category 1 is not a very efficient way of studying the effects of each material property. When all the material parameters are changed simultaneously the effect of each individual parameter is concealed by each other. Therefore, this category could be disregarded all together, reducing the computational cost of both running the analysis in Abaqus and analysing the results. Alternatively, this category could be used to uncover interaction effects. Secondly, the results show that it could be beneficial to use more intervals in each category. By incorporating several more materials in each category, more datapoints is available to uncover complex relationships.

To enable an analysis of the effect of each material parameters this thesis focuses on quite simple façade elements, using a homogenous cross-section and simple geometries. However, in reality most façades have more complex geometries, often fitted with windows etc. Additionally, façade elements commonly consist of multiple layers, resulting in an inhomogeneous cross-section. Therefore, it could be beneficial to define the parametric categories based on the total stiffness and mass. This would enable the results to be transferable to a vast range of both geometries and cross-sections. Yet, even though, the geometries and load cases analysed in this thesis are quite limited, compared to the many possible variations of both façades and loads, the analysis has focused on uncovering the most important aspect of the load transfer to possibly find a general expression.

6.1.4   Damping

As mentioned in Section 1.2.1, this thesis does not cover the effect of damping, as this does not have an impact on the peak reaction force. However, when damping is disregarded in the Abaqus model the façade element will seemingly oscillate forever, without any reduction of the amplitude. This does not reflect the true behaviour of a vibrating façade, where the vibrations in reality eventually would be phased out. However, if damping is included it could prove difficult to isolate the distinct frequencies in the total response, as the vibration would diminish over time.

Additionally, incorporating damping in the model impacts the results of the curve fitting. The proposed general equation, General equation (3), does not produce a satisfactory output if damping is included. If future guidelines aim at capturing the most realist response of the system, damping should be included, and consequently more complex functions should be evaluated.

6.2   Curve fitting

In this section, the constants in General equation (3) and the possibility of using more complex functions to describe the reaction forces is evaluated. The implementation of Fourier series is also discussed.

6.2.1   Simple sinusoidal functions

General equation (3), include four equation constants, thoroughly described in Section 5.3. The intent of this function is to express a general equation related to the response of a plate with an arbitrary material, thickness, and scaled distance. However, only one of these equation

constants is further expressed by the general state of the façade, as shown by the analysis. The constant B is found as $B = 2\omega_n$, where ω_n is the natural frequency, while the value of the remaining Equation constants is found empirically. Even though this analysis did not find a specific relationship between the general state of the façade and the Equation constants A, C and D, such a relationship may exist. It is important to note that the general expression found can be used for similar situations, as presented in these analyses. For façades designed with the same materials, geometries, and scaled distances the results presented in Section 4.4.2 are applicable.

To reach the detailed level of the European Standards, more aspects than just the peak reaction forces and the dominant mode should be evaluated. General equation (3) is able to capture one frequency. To cover the reaction forces of the system more precisely, an equation consisting of two oscillations might be more fitting. Such a function might be able to capture not only the dominating frequency, but the second most dominant frequency as well. An example of this is a function consisting of sine and cosine, $F(t) = A\sin(Bt) + C\cos(Dt)$. However, as the analysis in Section 5.2.2 showed, the second most dominant frequency vary greatly. Therefore, even if an equation is found to describe every material more precisely, it might prove difficult to find a relationship between the equation constants of each material.

6.2.2   Fourier series

The results presented in Section 4.4.3 shows that a Fourier series can be a viable option when deriving a detailed expression precise enough to be included in a future guidelines or Standards. However, there are two considerations important to highlight.

Firstly, using a Fourier series with a high value of n leads to a more precise function. However, this also means that the function is more complex. Thus, for high values of n it can become quite hard (if not impossible) to find a relationship between the many equation constants. Leading to a complex and time-consuming equation.

Secondly, the Fourier series presented in this thesis is only fitted to match 0.5 seconds of the response. If a longer response period is chosen the value n naturally increases. Thus, the computational cost of using Fourier series increases drastically for when increasing the total time analysed. To reduce the computational cost of a Fourier series, while still analysing longer time periods an equation could be derived based on fewer data points, with longer time intervals between them. However, this means that some of the response might be lost.

However, the computational cost of a Fourier series could possibly be reduced by compiling a general expression based only some of the term found by a Fourier series. Pointed out in Section 5.3.5, the weight of the Fourier coefficients a_n and b_n vary greatly. Leading to a few terms being more influential in the total Fourier series than others. Therefore, the possibility of compiling a general expression based on only the highest weighted terms in the Fourier series should be investigated. This way the complete general expression might consist of a simplification of the Fourier series.

7.   Conclusion

Due to an increased interest in designing structures to resist actions from external explosions, a deeper understanding of the load transfer from a façade to the supporting structure is needed. From this the following research question was presented:

What are the effects of varying the scaled distance, façade thickness, Young's modulus, and density, on the reaction forces of a façade element subjected to a blast load, and to what extent can the response be expressed by an empirical equation?

Some general effects regarding scaled distance, Young's modulus, density and façade thickness were found. The scaled distance only affects the magnitude of the reaction force, where the reaction forces decreases when the scaled distance increase. When the Young's modulus increases, so does the peak reaction force and the frequency of the free vibration phase, while the reaction time shortens. This indicates that an increase in stiffness leads to increases in peak reaction force and frequency, and a shorter reaction time. When the density increases, both the peak reaction force and frequency of the free vibration phase decrease, while the reaction time gets longer. This indicates that as the mass increases the peak reaction forces and frequency decreases, and the reaction time gets longer.

It is also shown that for thinner plates, the free vibrations exhibit a more serrated form, and the reaction time gets shorter. When the thickness increased, there was a general tendency of increase in peak reaction forces, with some notable deviations. These deviations indicate that there is an interaction effect between the material properties and the thickness. As the thickness has a larger effect on the stiffness than the mass, it supports the finding that higher stiffness results in higher peak reaction forces.

These findings shows that the response of the system is highly dependent on both the stiffness and mass, i.e., the natural frequency of the system, as well the scaled distance. Theory presented in Section 2.2.3 and 2.3 confirms these findings

Further, it is possible to express the response by a simple, yet accurate, empirical equation. The proposed equation predicts the peak reaction force and the free vibration phase satisfactory. However, more complex functions can also be used, resulting in more detailed predictions. Yet, the empirical equations given in this thesis, with the stated equation constants, can be directly used to predict the response of a steel or aluminium plate, with the same geometries as presented in this thesis, using the same scaled distance.

To summarise, the findings of this thesis highlight the individual effect of varying the scaled distance, Young's modulus, density, and thickness. The thesis has found that the reaction forces of a plate subjected to a blast load are highly dependent on the natural frequency of the system and the scaled distance. Moreover, the findings show that the response consists of multiple frequencies, yet, can still be approximated by a simple empirical function. The findings of this thesis functions as a solid building block for future research, e.g., to develop design guidelines for blast resistant structures.

8.   Further work

Research and guidelines focusing on load transfer or reaction forces of façade elements subjected to blast loads, are quite limited, as highlighted in Section 1.1. The findings of this thesis are valuable for future research that can build on the presented findings. Some specific recommendations regarding future work are presented in the following sections.

8.1   Parameter study and factorial design

For further research focusing on load transfer of plates subjected to blast loads, it can be beneficial to include more intervals between the material properties, the thicknesses, and the loads. The results can function as a basis for future work, where more intervals are supplemented to the already existing analysis.

Future work can also benefit from structuring the division of the material parameters to fit the format of a statistical analysis, such as factorial design or a sensitivity analysis. The effect of each material property can be described more precisely, and possible interaction effects could be uncovered. To use factorial design, the analysis must be structured around a required format. It is therefore important to clearly understand the basis of factorial design, when determining the categorization of the material properties.

8.2   Stiffness

Further research can also benefit from analysing more complex façades. To enable this, future work can focus on analysing the response based on the total stiffness and mass of the structure, as opposed to the effects of each unique material parameter. Such a categorization of the analysis can yield more general results, as the findings are applicable for a wider range of geometries and cross-sections.

8.3   Multidisciplinary focus

Future work would benefit from multidisciplinary collaboration. As shown in Chapter 5 and Chapter 6, developing equations to describe the reaction forces requires thorough knowledge of multiple disciplines. In future work, a mathematician could provide stronger insight with regards to curve fitting and simplification of complex mathematical terms. This should be combined with a thorough understanding of material science, to enable a detailed analysis of the behaviour of the façade, and the importance of each material parameter. These disciplinary focuses combined with structural engineering could prove beneficial.

References

[1]   T. Krauthammer, *Modern Protective Structures* (Civil and environmental engineering). Baton Rouge: Baton Rouge: CRC Press, 2008.

[2]   E. Commission. "About the EN Eurocodes." https://eurocodes.jrc.ec.europa.eu/showpage.php?id=1 (accessed 15.05, 2022).

[3]   V. Karlos and G. Solomos, "Calculation of blast loads for application to structural components," *Luxembourg: Publications Office of the European Union,* p. 5, 2013.

[4]   U. DoD, "UFC 3-340-02: Structures to Resist the Effects of Accidental Explosions," *US DoD.: Washington, DC, USA,* p. 83, 2008.

[5]   Forsvarsbygg. "OM OSS." https://www.forsvarsbygg.no/no/om-oss/ (accessed 15.05, 2022).

[6]   A. K. Chopra, *Dynamics of Structures: Theory and applications to earthquake engineering.*, 5. ed. Hoboken, NJ: Pearson Education Inc, 2017.

[7]   P. K. Larsen, *Dimensjonering av stålkonstruksjoner*, 3 ed. Bergen: Fagbokforlaget, 2020.

[8]   R. D. Cook and W. C. Young, *Advanced mechanics of materials*, 2. ed. Upper Saddle River, N.J: Prentice Hall, 1999.

[9]   S. W.-K. Timoshenko, S., *Theory of Plates and Shells*, 2. ed. New York: McGraw-Hill Book Company, Inc., 1959.

[10]   D. Cormie, G. Mays, and P. Smith, *Blast Effects on Buildings (3rd Edition)*. ICE Publishing.

[11]   M. V. Dharaneepathy, M. N. K. Rao, and A. R. Santhakumar, "Critical distance for blast-resistant design," *Computers & Structures,* vol. 54, no. 4, pp. 587-595, 1995/02/17/ 1995, doi: https://doi.org/10.1016/0045-7949(94)00380-L.

[12]   D. O. Dusenberry, *Handbook for blast resistant design of buildings*. John Wiley & Sons, 2010.

[13]   G. F. Kinney and K. J. Graham, *Explosive Shocks in Air*. Berlin, Heidelberg, GERMANY: Springer Berlin / Heidelberg, 1985.

[14]   V. Karlos, G. Solomos, and M. Larcher, "Analysis of the blast wave decay coefficient using the Kingery–Bulmash data," *International journal of protective structures,* vol. 7, no. 3, pp. 409-429, 2016, doi: 10.1177/2041419616659572.

[15]   V. S. Karlos, George; Larcher, Martin, "Analysis of blast parameters in the near-field for spherical free-air explosions," Ispra (VA), Italy, 2016.

[16]   D. Jeon, K. Kim, and S. Han, "Modified Equation of Shock Wave Parameters," *Computation,* vol. 5, no. 3, p. 41, 2017. [Online]. Available: https://www.mdpi.com/2079-3197/5/3/41.

[17]   M. Mukhopadhyay, *Structural Dynamics: Vibrations and Systems*. Cham: Cham: Springer International Publishing.

[18]   A. M. Kabe and B. H. Sako, "Chapter 6 - Multi-degree-of-freedom systems," in *Structural Dynamics Fundamentals and Advanced Applications*, A. M. Kabe and B. H. Sako Eds.: Academic Press, 2020, pp. 333-435.

[19]   E. M. van de Vrie, H. G. ter Morsche, J. C. van den Berg, and R. J. Beerends, *Fourier and Laplace Transforms*, 1. ed. Cambridge: Cambridge University Press, 2003.

[20]   R. D. Cook, D. S. Malkus, M. E. Plesha, and R. J. Witt, *Concepts and applications of finite element analysis*, 4. ed. New York: John Wiley & Sons, Inc., 2002.

[21]   Dassault Systèmes Simulia Corp, "Abaqus 6.11 Theory Manual," RI, USA, 2011. [Online]. Available: http://130.149.89.49:2080/v6.11/pdf_books/THEORY.pdf

[22]   D. Systèms. "Acoustic and shock loads." https://help.3ds.com/2020/English/DSSIMULIA_Established/SIMACAEPRCRefMap/simaprc-c-acoustic.htm?contextscope=all (accessed 07.04, 2022).

[23]   S. Mendes and C. Liling, "Analysis Method for Reinforcing Circular Openings in Isotropic Homogeneous Plate-Like Structures Subjected to Blast Loading," *Advances in Civil Engineering,* vol. 2018, p. 4071732 (21 pp.), / 2018, doi: 10.1155/2018/4071732.

[24]   A. Markose and C. L. Rao, "Effectiveness of Polyurea Coated Steel Plates in Blast Mitigation in Vehicles," in *Second International Conference on Structural Integrity (ICONS 2018), 14-17*

Dec. 2018, Singapore, Singapore, 2020: Springer, in Structural Integrity Assessment. ICONS 2018. Proceedings: Lecture Notes in Mechanical Engineering (LNME), pp. 153-64, doi: 10.1007/978-981-13-8767-8_12. [Online]. Available: http://dx.doi.org/10.1007/978-981-13-8767-8_12

[25] K. P. Dharmasena, H. N. G. Wadley, X. Zhenyu, and J. W. Hutchinson, "Mechanical response of metallic honeycomb sandwich panel structures to high-intensity dynamic loading," *International Journal of Impact Engineering,* vol. 35, no. 9, pp. 1063-74, 2008, doi: 10.1016/j.ijimpeng.2007.06.008.

[26] T. F. Henchie, S. Chung Kim Yuen, G. N. Nurick, N. Ranwaha, and V. H. Balden, "The response of circular plates to repeated uniform blast loads: An experimental and numerical study," *International Journal of Impact Engineering,* vol. 74, pp. 36-45, 2014, doi: 10.1016/j.ijimpeng.2014.02.021.

[27] K. Ackland, C. Anderson, and T. D. Ngo, "Deformation of polyurea-coated steel plates under localised blast loading," *International Journal of Impact Engineering,* vol. 51, pp. 13-22, 2013/01/01/ 2013, doi: https://doi.org/10.1016/j.ijimpeng.2012.08.005.

[28] N. S. A. Razak and A. Alias, "The Response of Steel Plates Subjected to Close-in Blast Loads," in *4th National Conference on Wind & Earthquake Engineering, 16-17 Oct. 2020*, UK, 2021, vol. 682: IOP Publishing, in IOP Conf. Ser., Earth Environ. Sci. (UK), p. 012036 (8 pp.), doi: 10.1088/1755-1315/682/1/012036. [Online]. Available: http://dx.doi.org/10.1088/1755-1315/682/1/012036

[29] S. C. K. Yuen and G. N. Nurick, "Experimental and numerical studies on the response of quadrangular stiffened plates. Part I: Subjected to uniform blast load," *International Journal of Impact Engineering,* vol. 31, no. 1, pp. 55-83, 2005, doi: 10.1016/j.ijimpeng.2003.09.048.

[30] A. Markose and C. L. Rao, "Failure analysis of V-shaped plates under blast loading," *Procedia Engineering,* vol. 173, pp. 519-25, / 2017, doi: 10.1016/j.proeng.2016.12.080.

[31] D. D. Truong, B.-S. Jang, and H.-B. Ju, "Development of simplified method for prediction of structural response of stiffened plates under explosion loads," *Marine Structures,* vol. 79, p. 103039, 2021/09/01/ 2021, doi: https://doi.org/10.1016/j.marstruc.2021.103039.

[32] P. E. Prueter, "Using Explicit Finite Element Analysis to Simulate Blast Loading on Hazardous Chemical Storage Tanks," presented at the SIMULIA Community Conference Rhode Island Convention Center 20-22 may 2014, 2014. [Online]. Available: https://ifwe.3ds.com/modules/custom/ifwe/ifwe_specific/dynamic_infographic/pdfs/Equity_Engineering.pdf.

[33] K. Arge, "Generalitet, fleksibilitet ogelastisitet i kontorbygninger," Norges byggforskningsinstitutt, Oslo, Prosjektrapport 340 - 2003 2003. [Online]. Available: https://www.sintef.no/globalassets/upload/byggforsk/publikasjoner/prosjektrapport-340.pdf?fbclid=IwAR1jNDLio2it9DRXJiEDnZteeIsrHYY5752bdemBI8Aqr96n2cV6tRDSf8w

[34] *Eurokode 3: Prosjektering av stålkonstruksjoner - Del 1-1: Allmenne regler og regler for bygninger*, NS-EN 1993, 2015.

[35] *Eurokode 9: Prosjektering av aluminiumskonstruksjoner - Del 1-1: Allmenne regler*, NS-EN 1999, 2009.

[36] MathWorks. "fft Fast Fourier transform." https://se.mathworks.com/help/matlab/ref/fft.html (accessed 25.04, 2022).

[37] G. U. o. Technology. "Fourier analysis of real data sets." http://lampx.tugraz.at/~hadley/num/ch3/3.3a.php (accessed 20.04, 2022).

[38] P. Nayuki. "Free small FFT in multiple languages." https://www.nayuki.io/page/free-small-fft-in-multiple-languages (accessed 20.04, 2022).

# Appendix A

DATASET 1A

1A - Steel
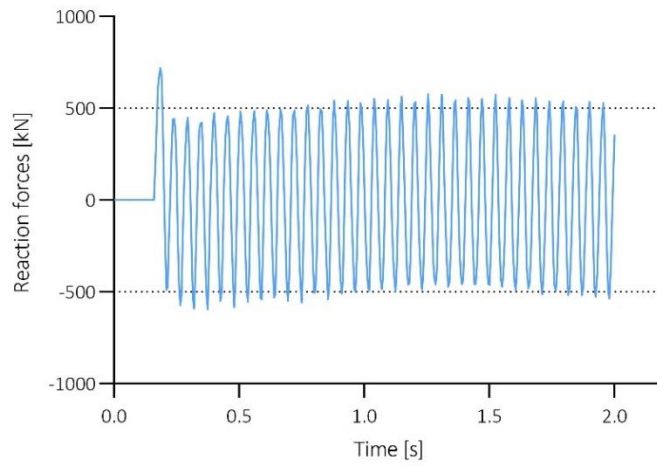
1A C1 - Aluminium
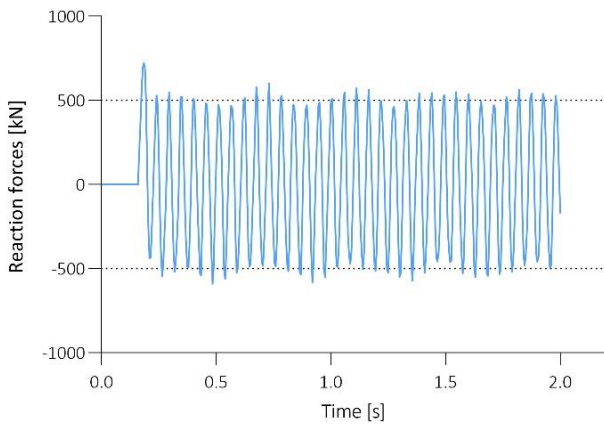
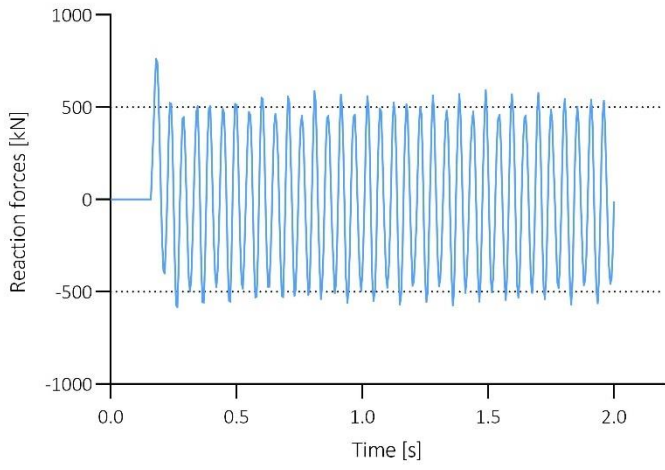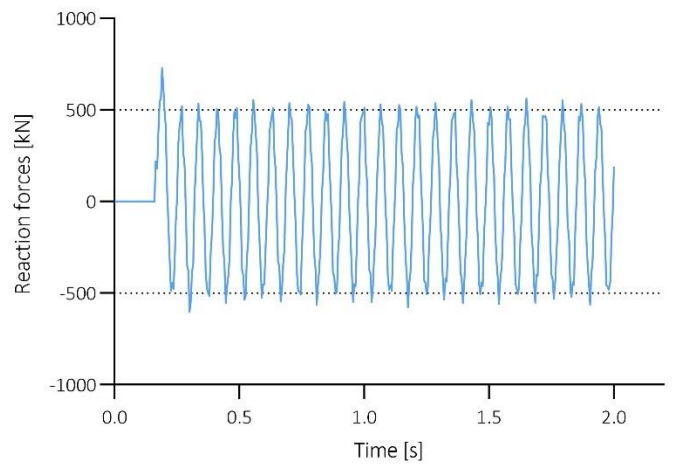### 1A C1 - Interval 2
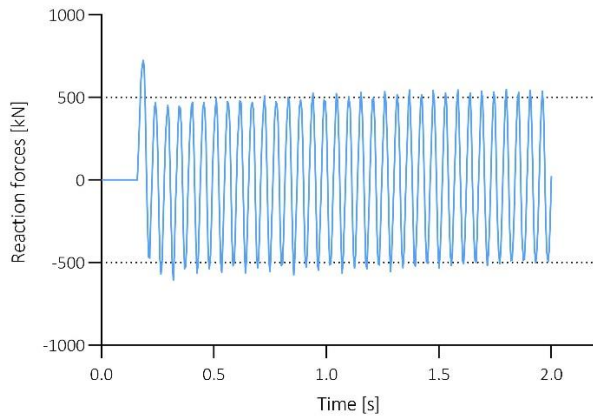
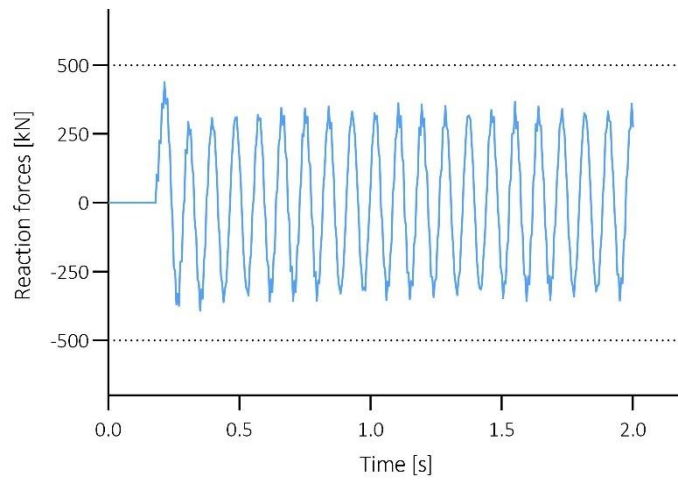

1A C2 - Interval 1
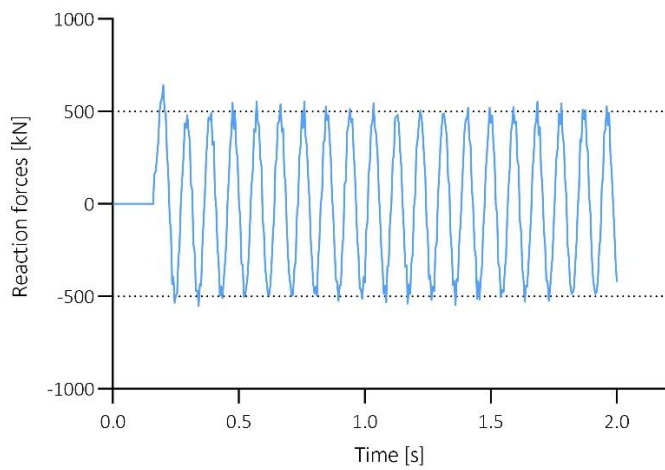
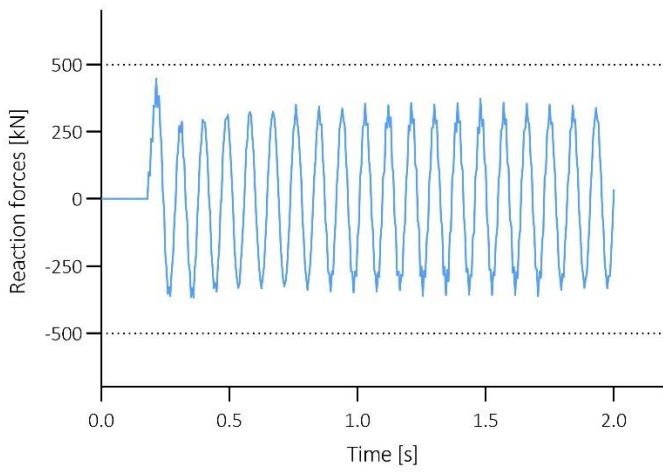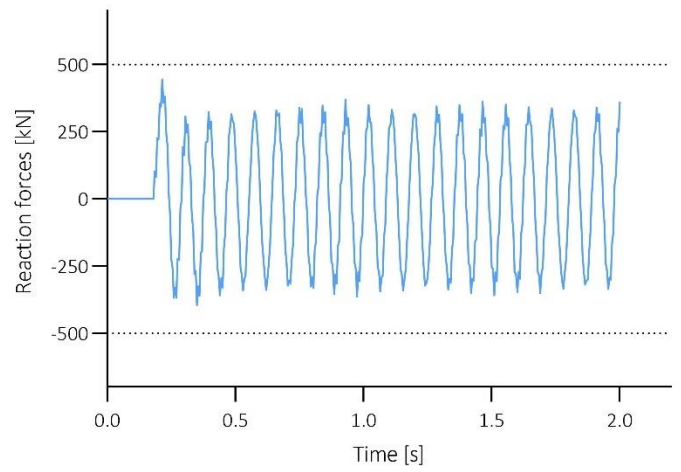### 1A C2 - Interval 2
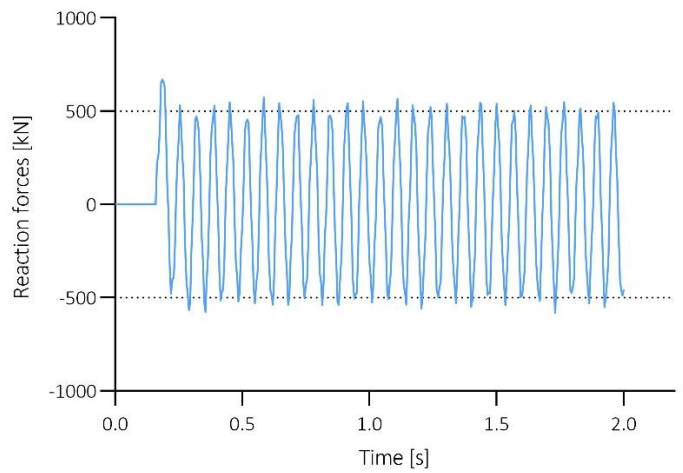
1A C3 - Interval 1
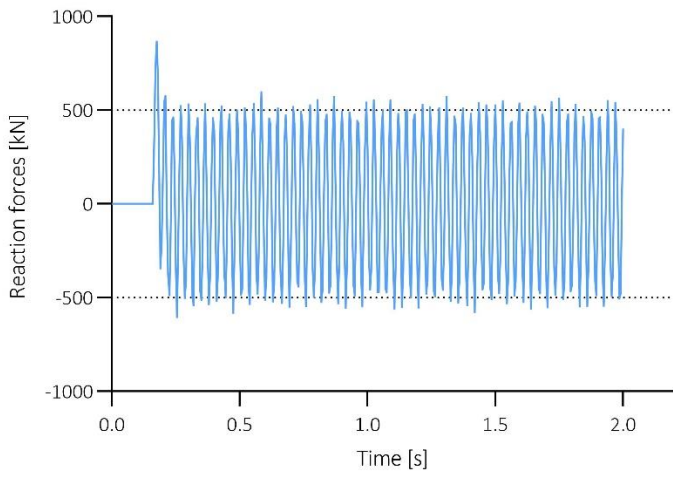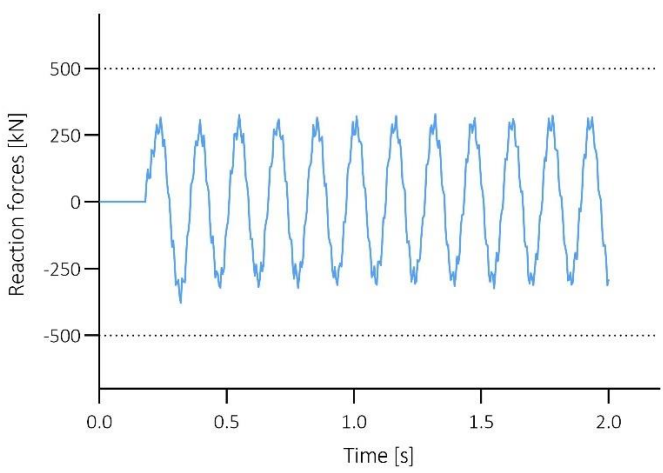
1A C3 - Interval 2
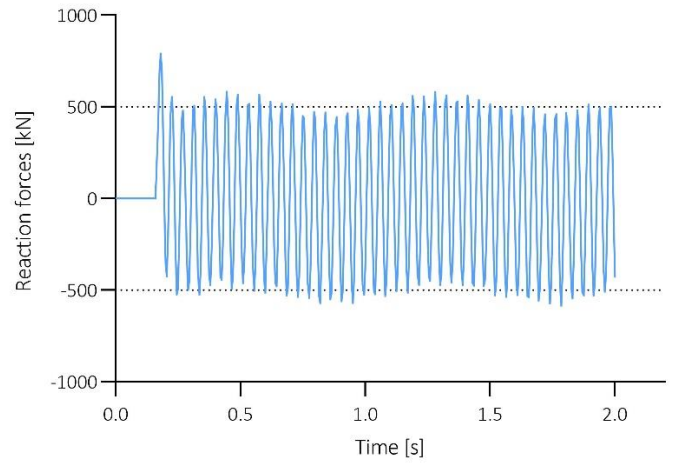
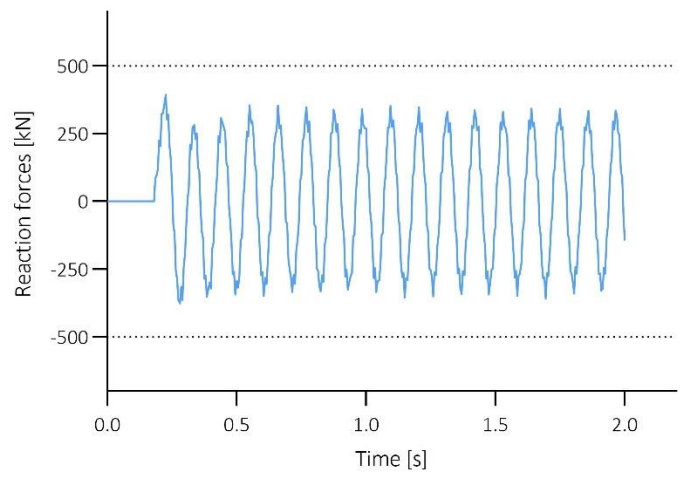# DATASET 1B

1B - Steel
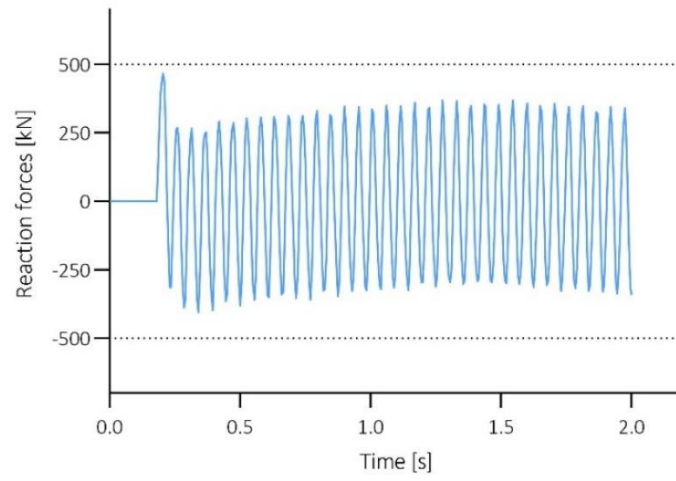
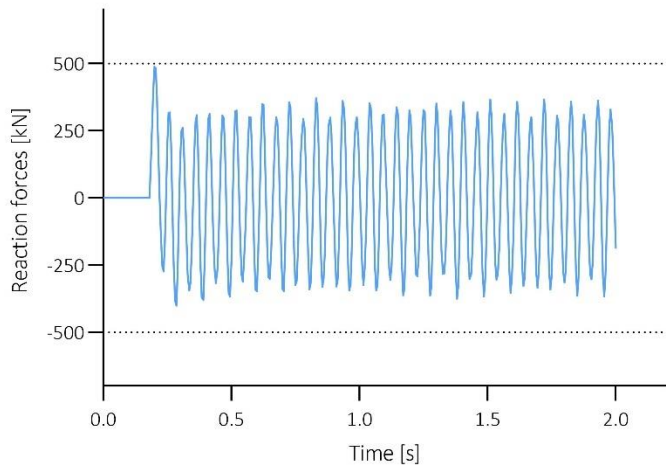## 1B C1 - Aluminium
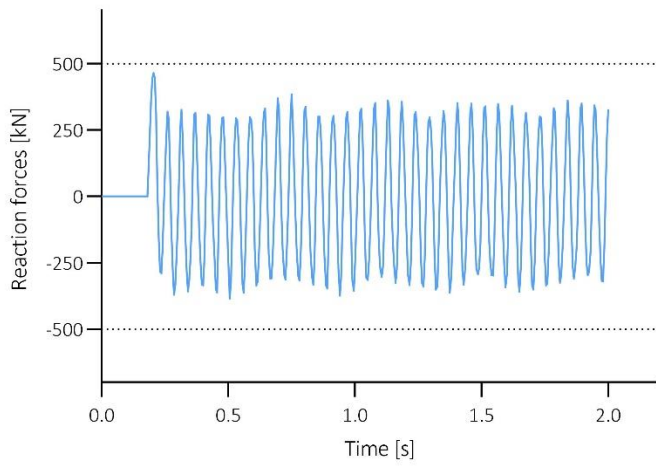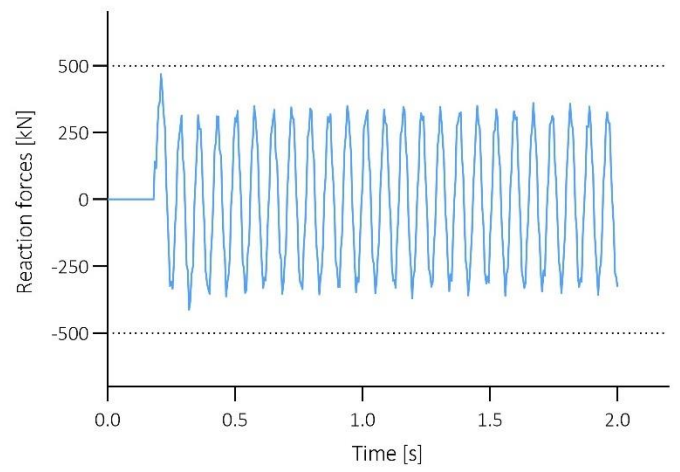

1B C1 - Interval 2
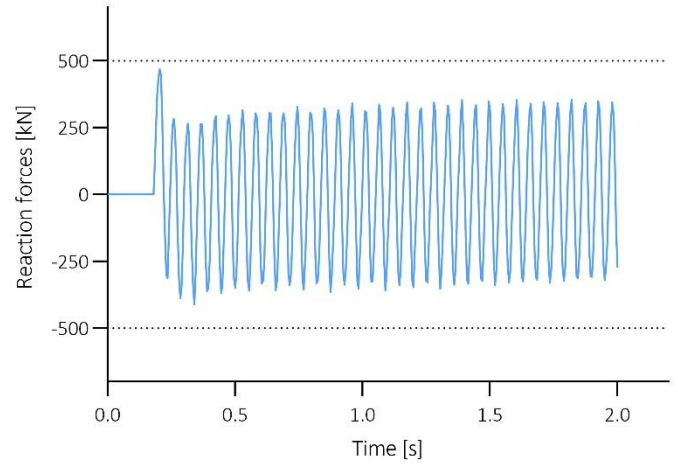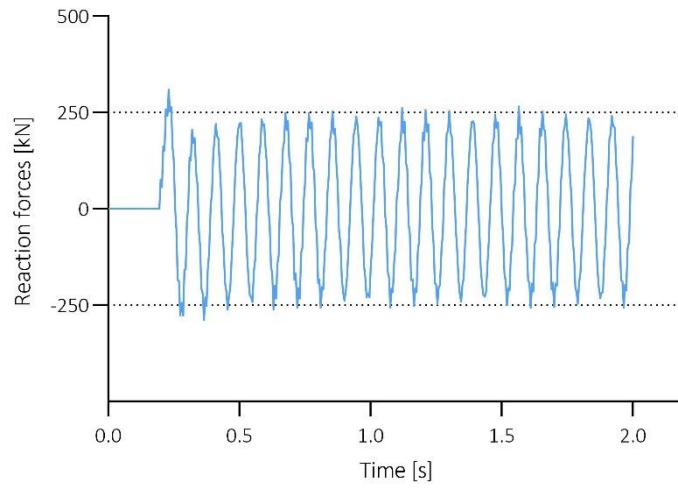

1B C2 - Interval 1
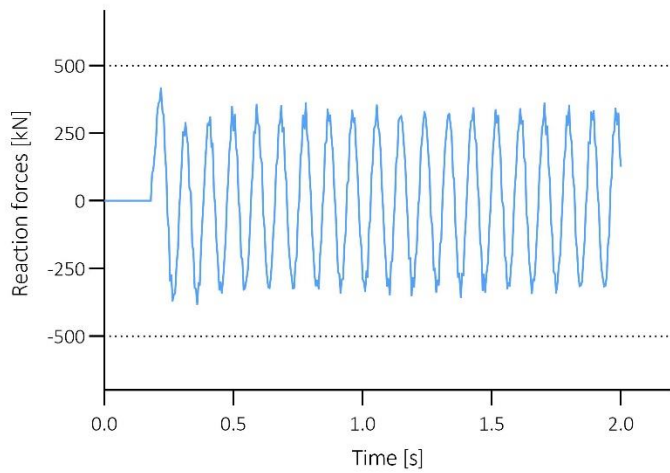
1B C2 - Interval 2
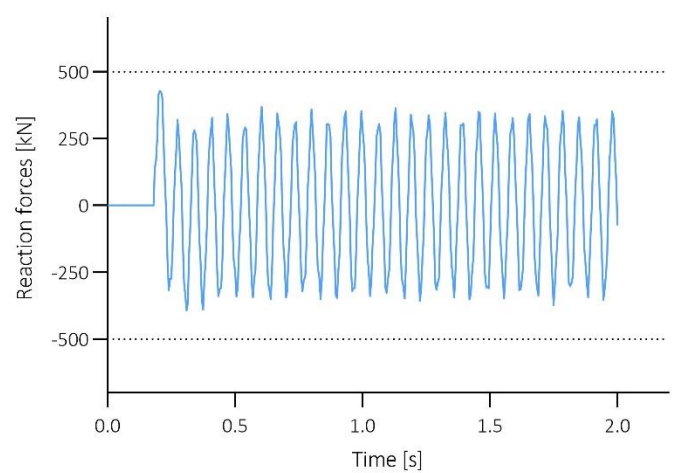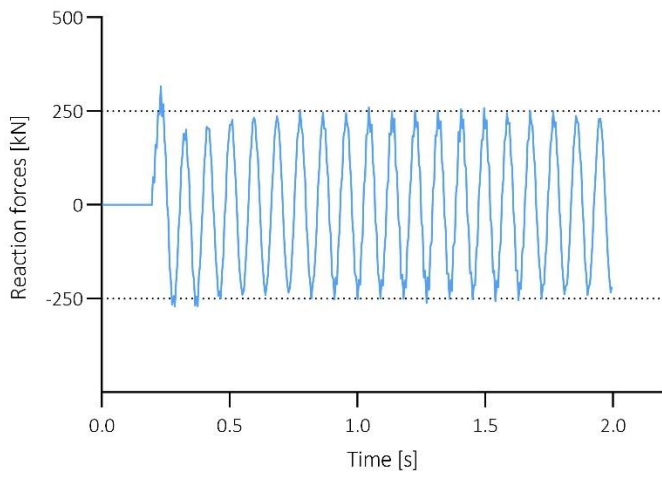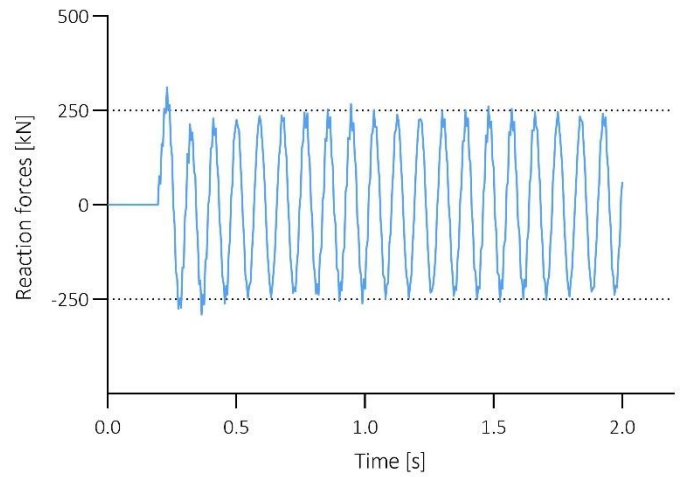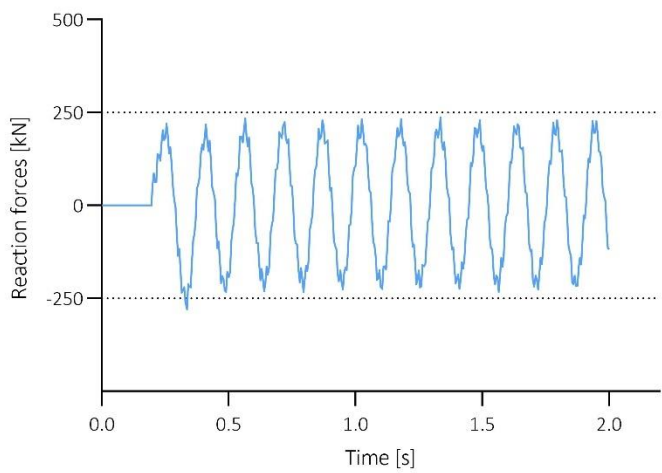
1B C3 - Interval 1
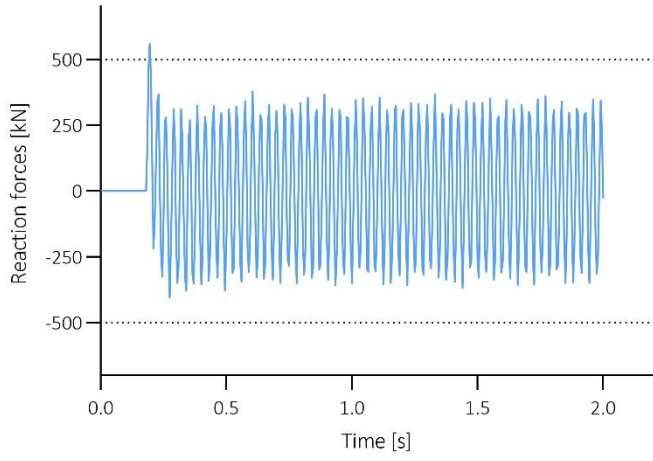
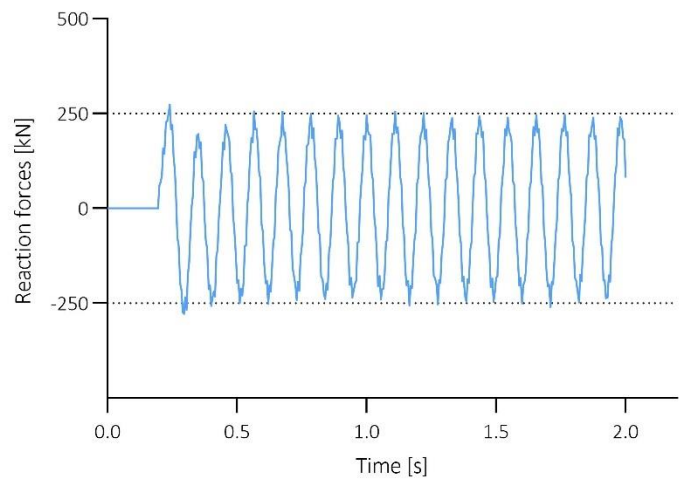1B C3 - Interval 2
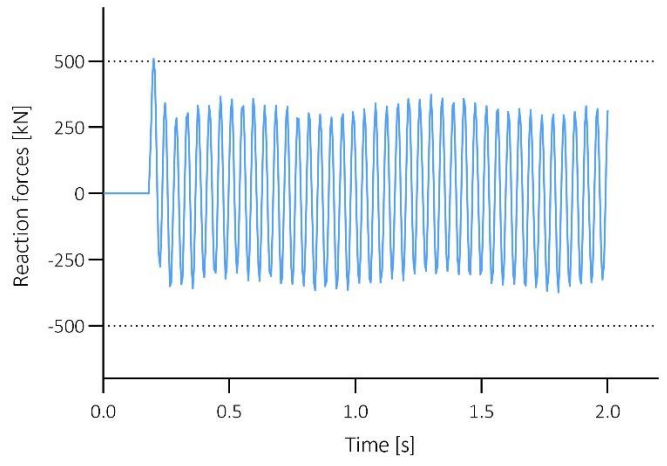
DATASET 1C

## 1C - Steel
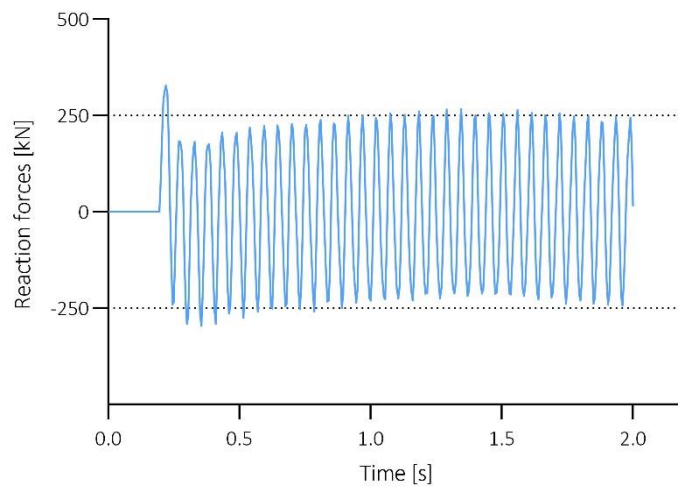
1C C1 - Aluminium
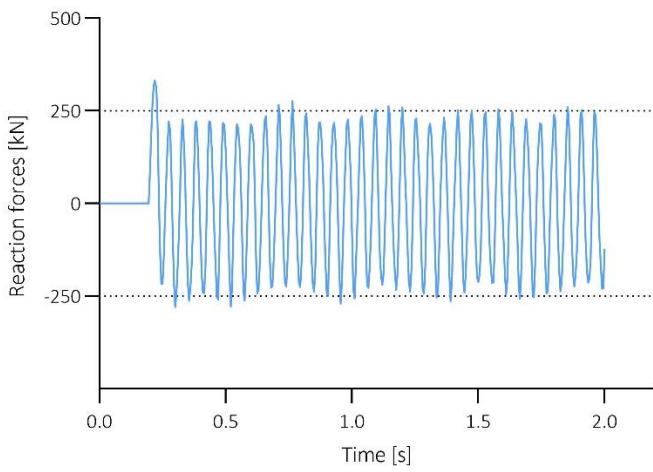
1C C1 - Interval 2
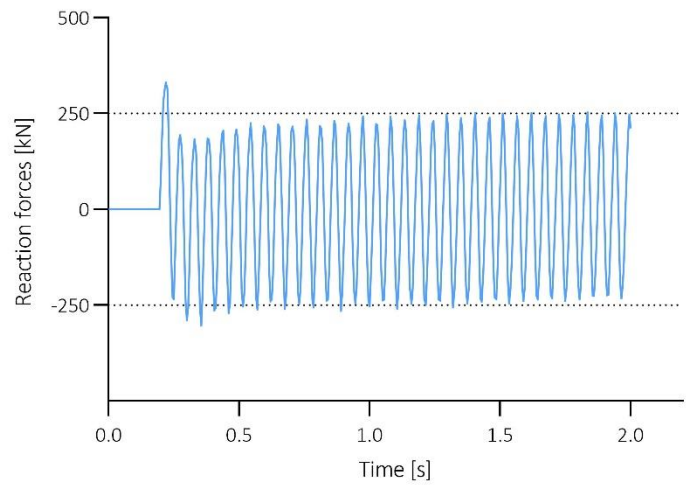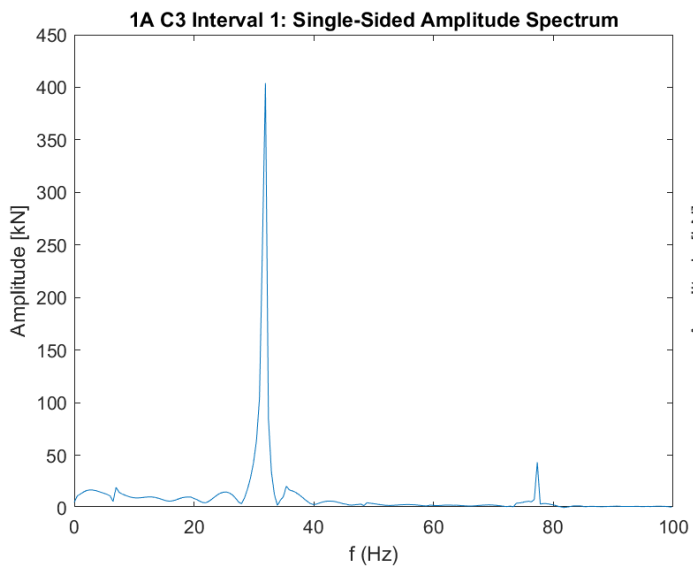

1C C2 - Interval 1
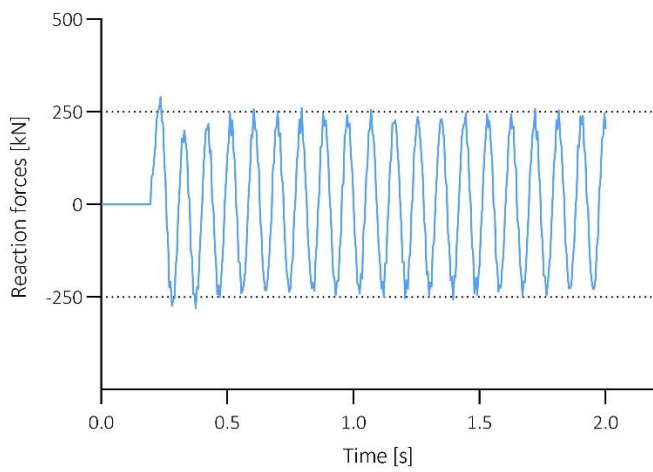
1C C2 - Interval 2
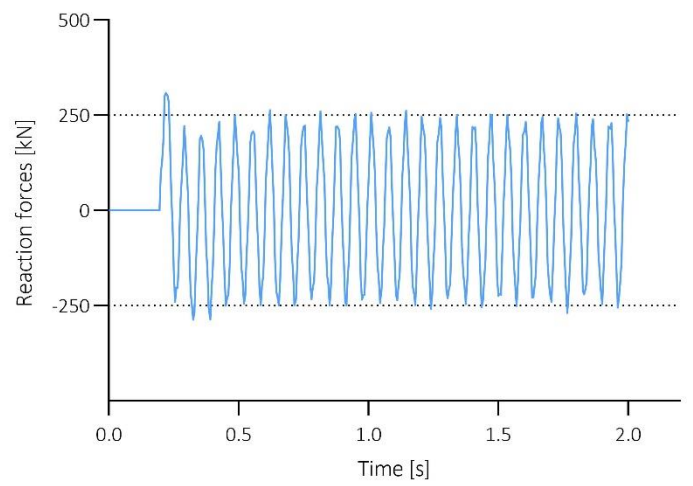
1C C3- Interval 1
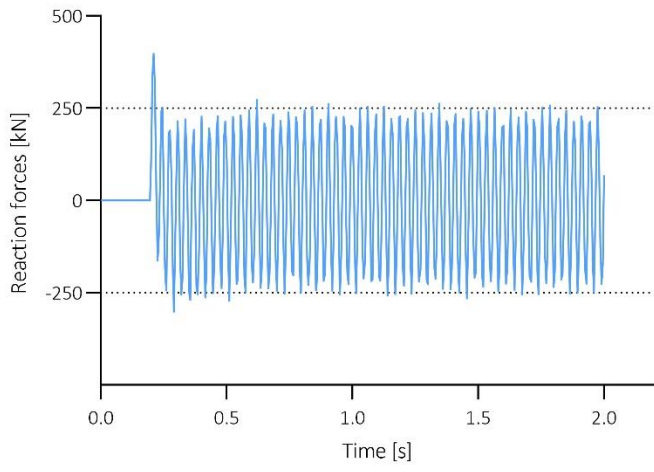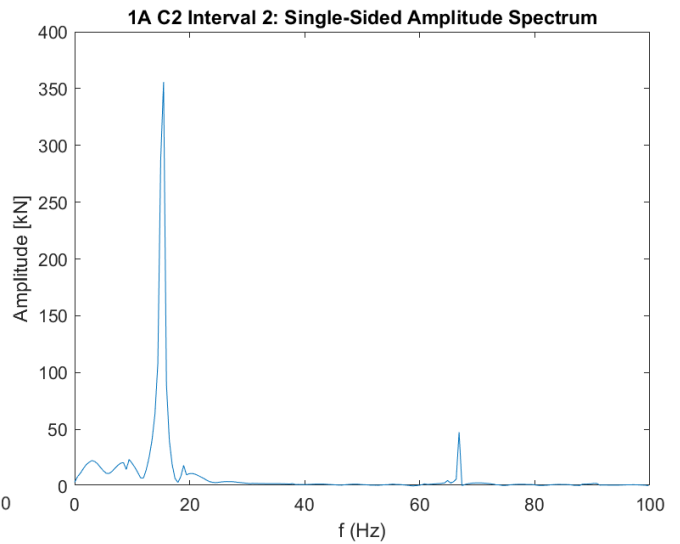
1C C3 - Interval 2
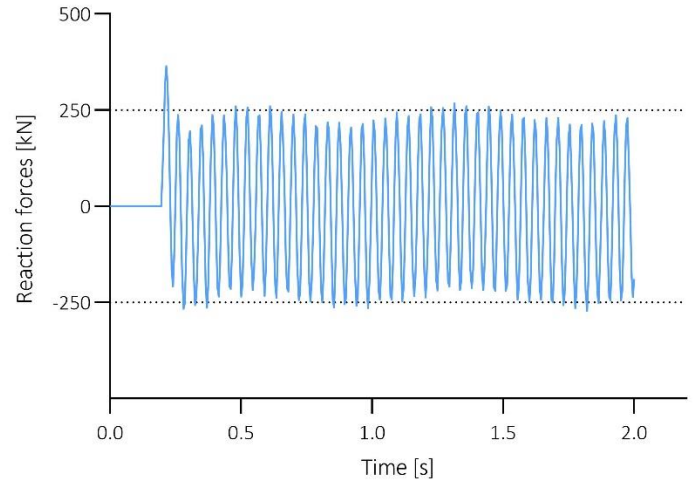
DATASET 2A

2A - Steel
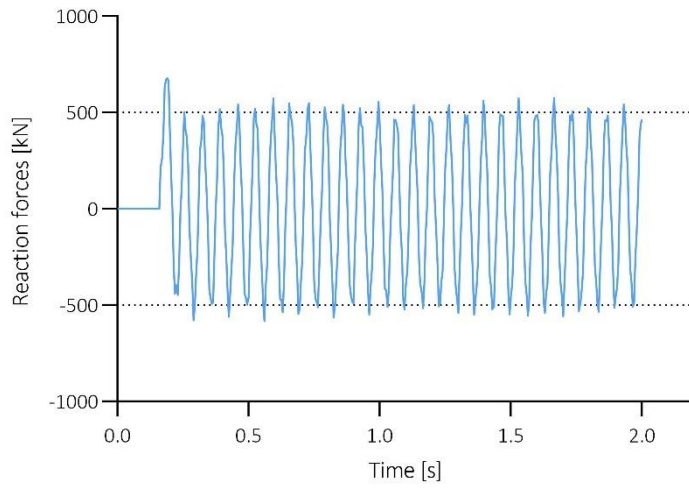
2A C1 - Aluminium
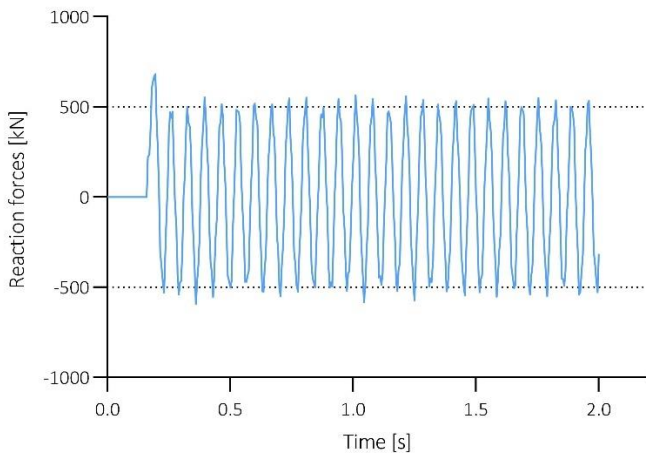
2A C1 - Interval 2
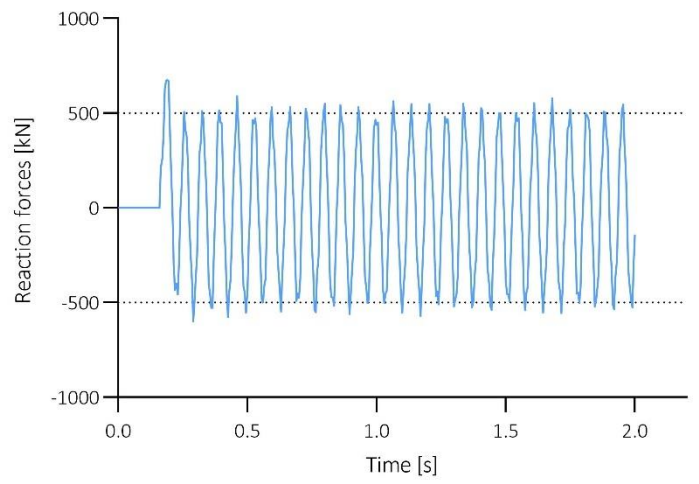
2A C2 - Interval 1
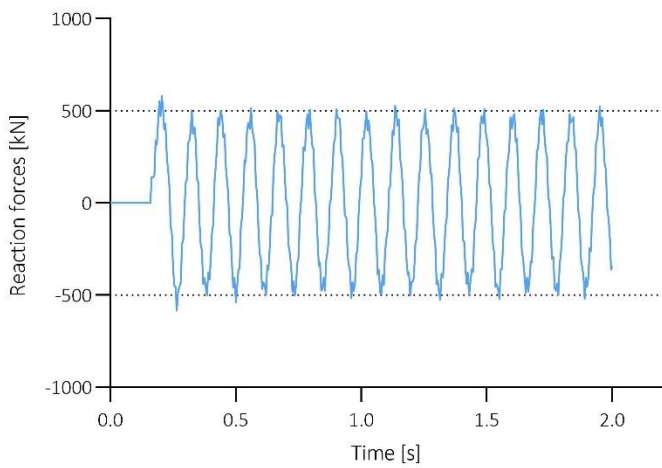
2A C2 - Interval 2
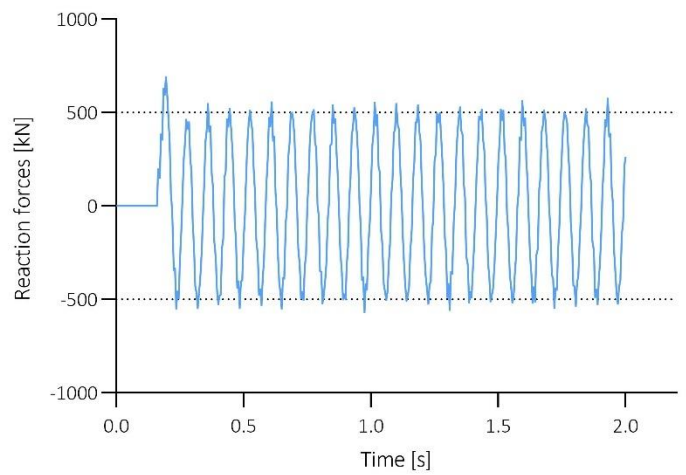
2A C3 - Interval 1
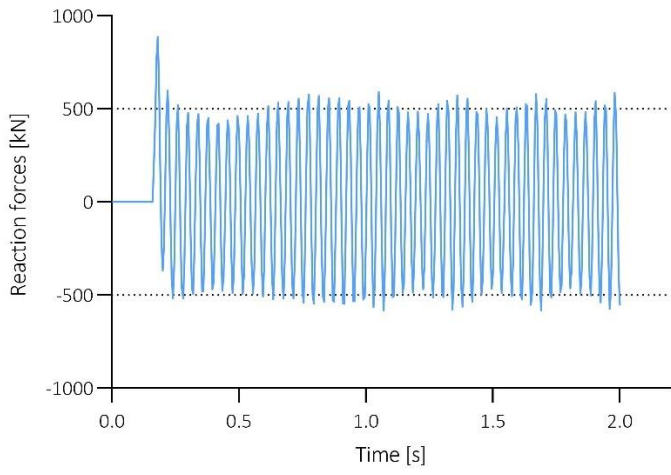
2A C3 - Interval 2
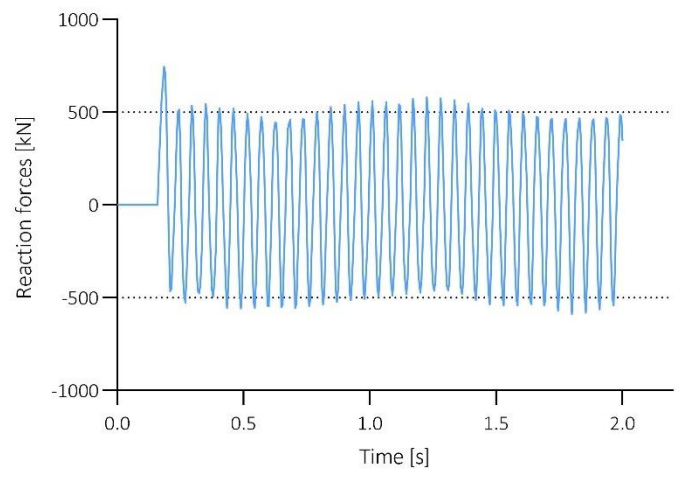
DATASET 2B

2B - Steel
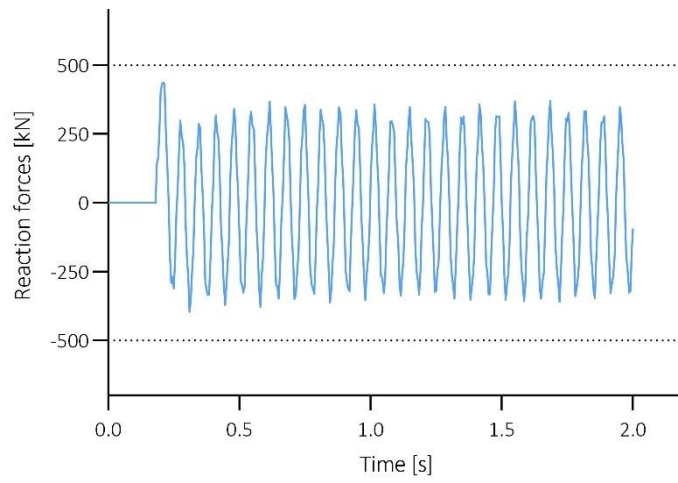
2B C1 - Aluminium
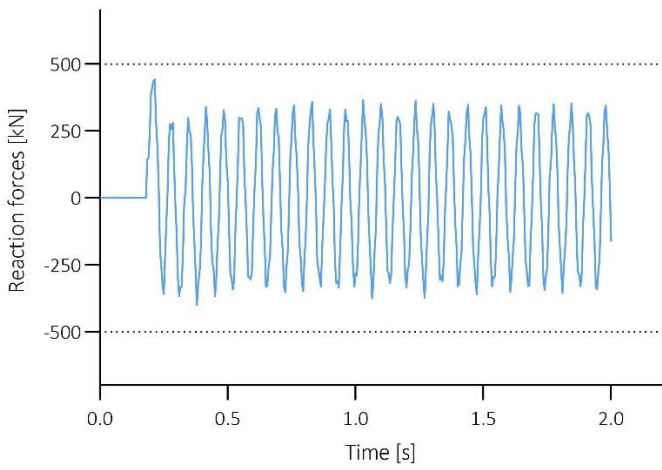
2B C1 - Interval 2
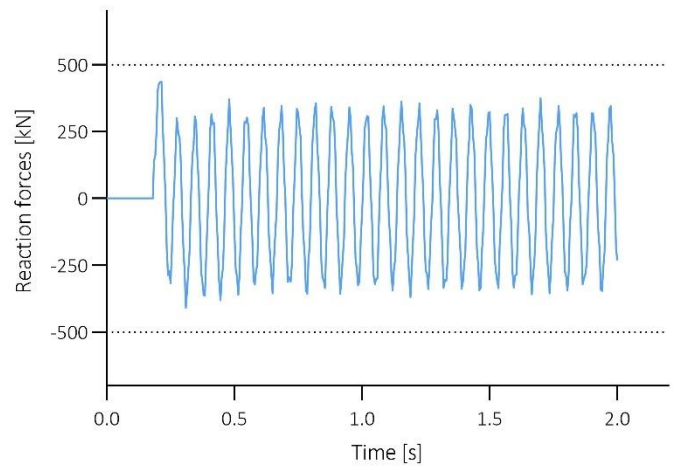
2B C2 - Interval 1
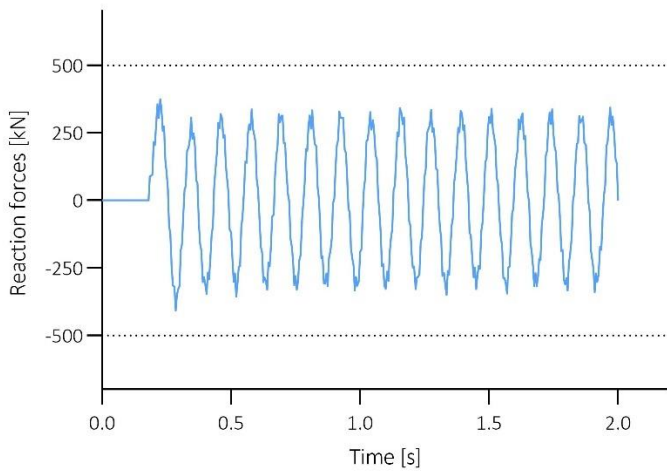
2B C2 - Interval 2

2B C3 - Interval 1

Reaction forces [kN] vs Time [s]

2B C3 - Interval 2

Reaction forces [kN] vs Time [s]
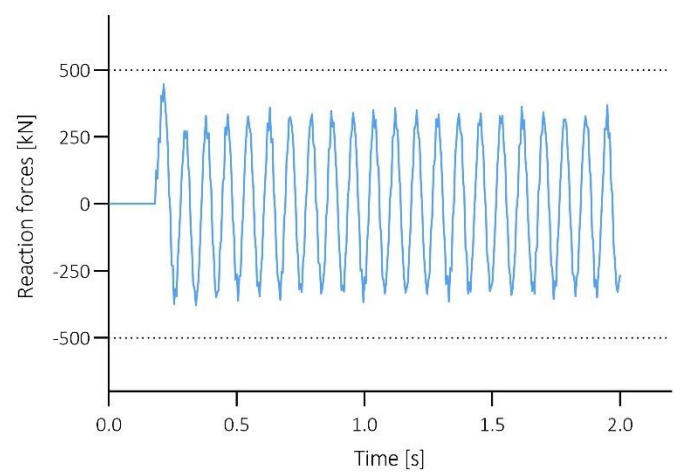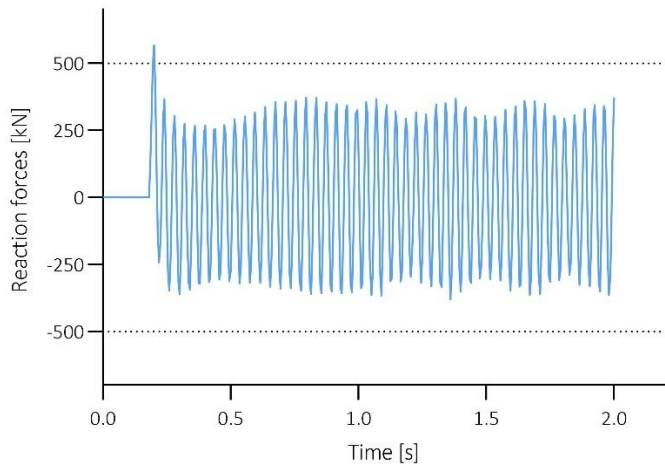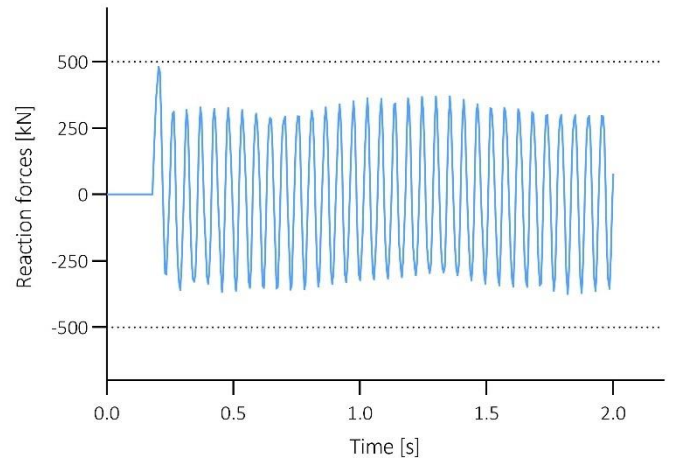
DATASET 2C

2C - Steel
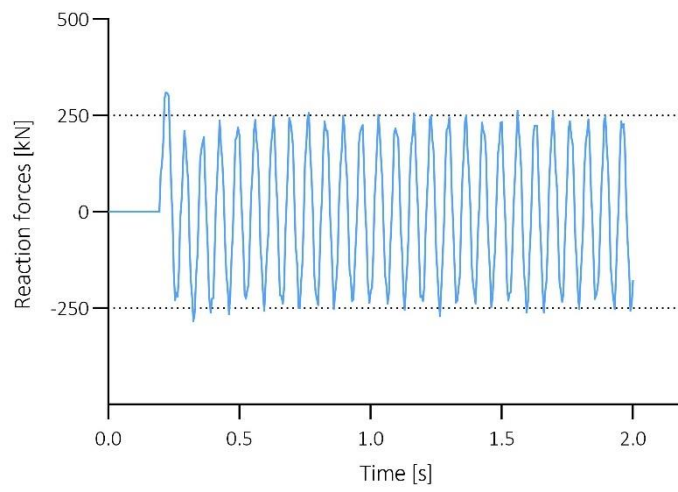
2C C1 - Aluminium
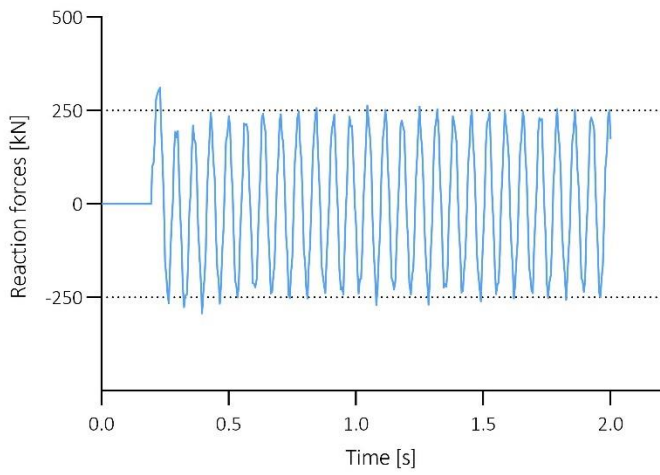
2C C1 - Interval 2
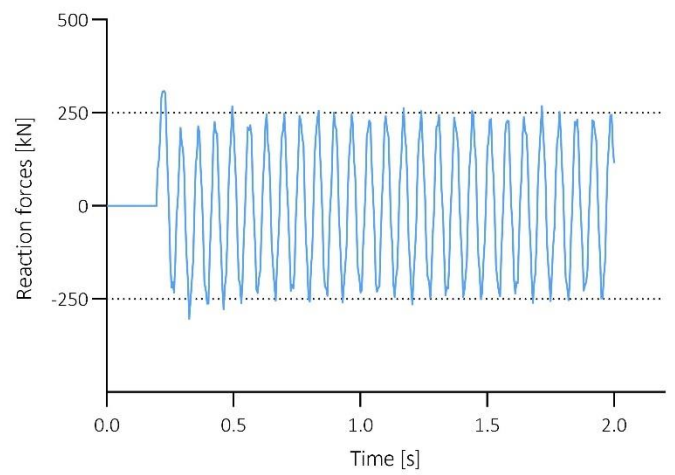
2C C2 - Interval 1
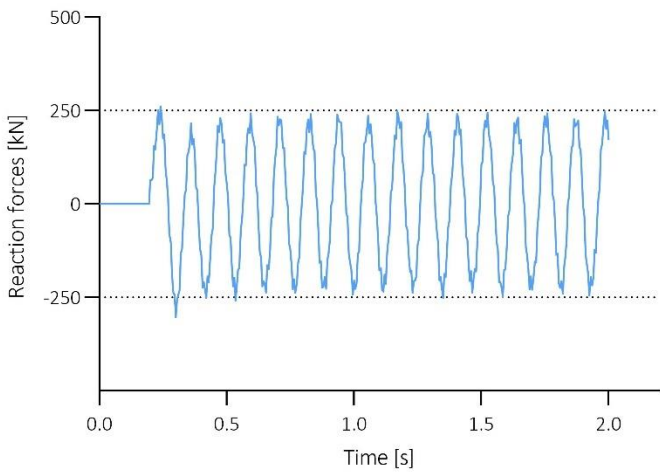
2C C2 - Interval 2
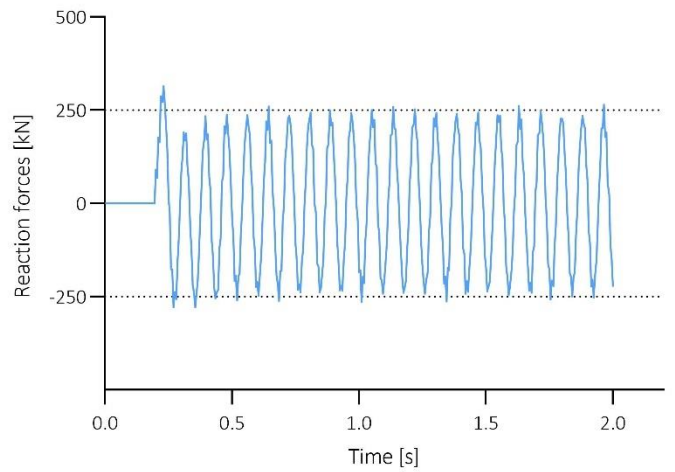
2C C3- Interval 1
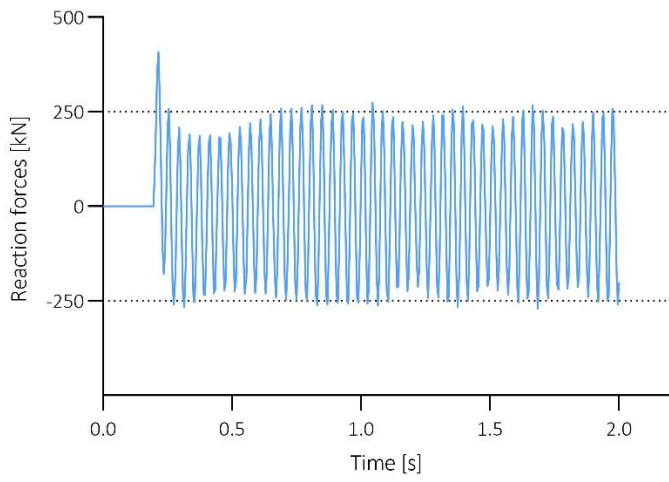
2C C3- Interval 2
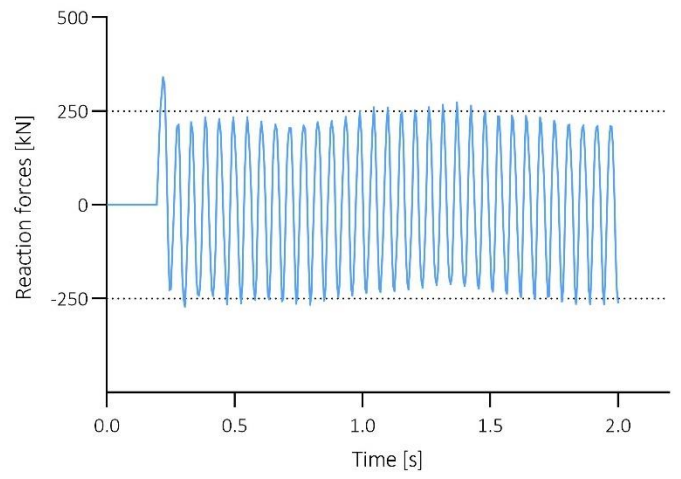
DATASET 3A

3A - Steel
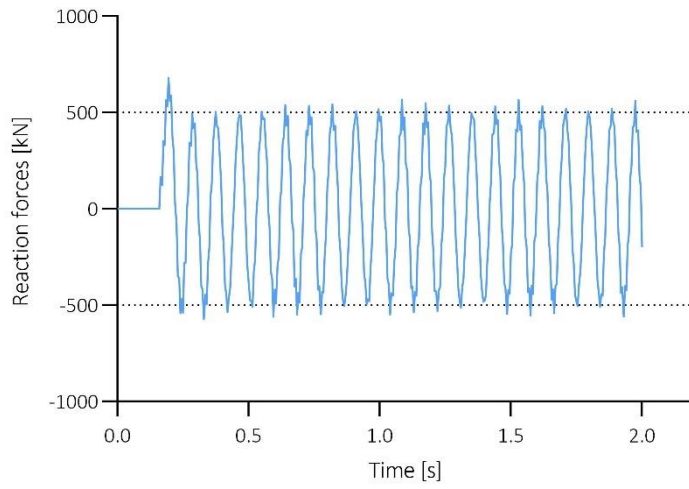
3A C1 - Aluminium
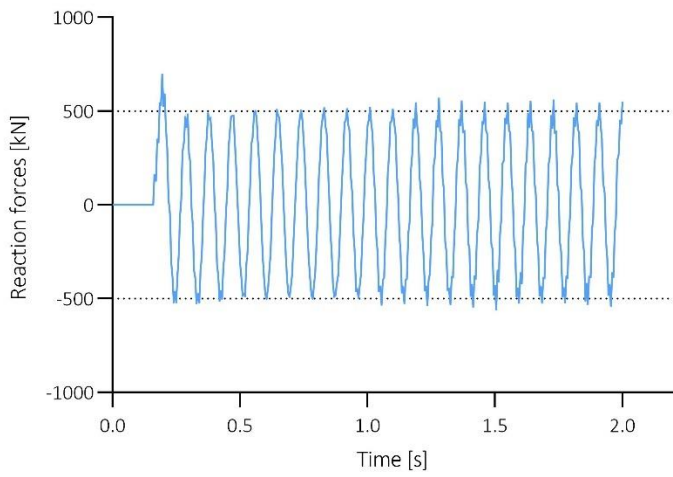
3A C1 - Interval 2
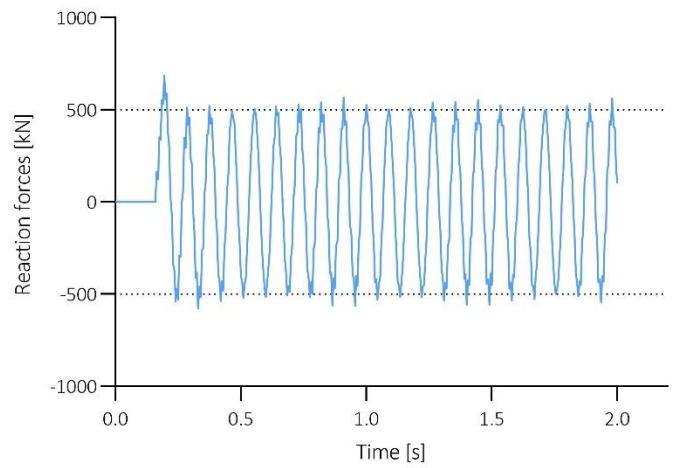
3A C2 - Interval 1
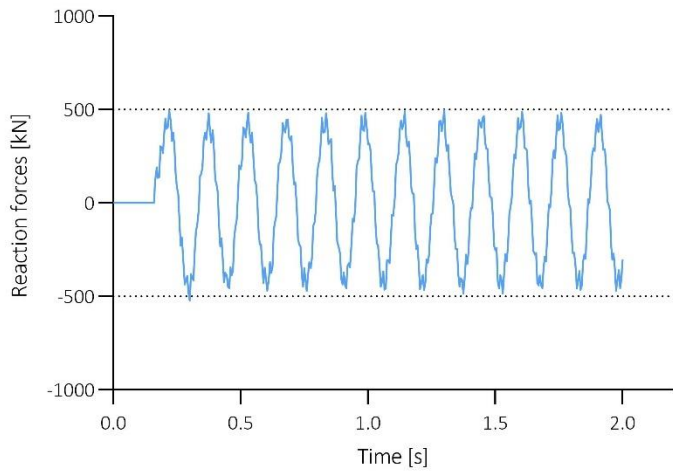
3A C2 - Interval 2
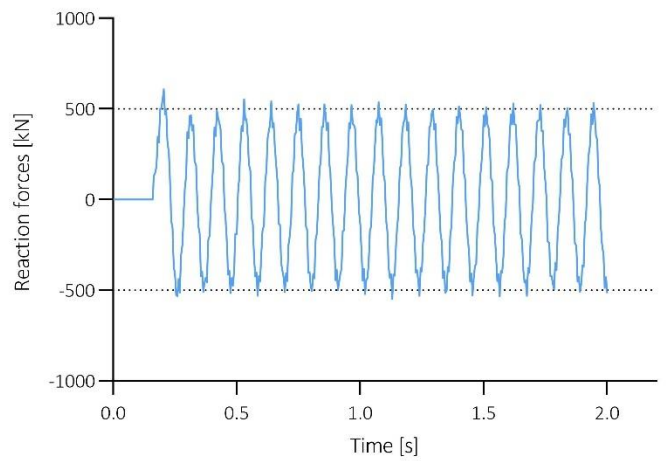
3A C3- Interval 1

3A C3 - Interval 2

DATASET 3B

3B - Steel

3B C1 - Aluminium

3B C1 - Interval 2

3B C2 - Interval 1

3B C2 - Interval 2

3B C3 - Interval 1

3B C3 - Interval 2

DATASET 3C

3C - Steel

3C C1 - Aluminium

3C C1 - Interval 2

3C C2 - Interval 1
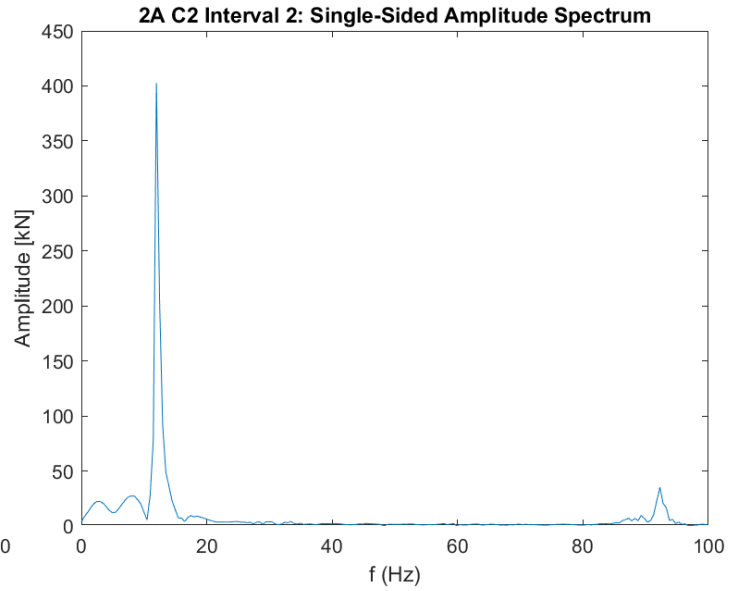

3C C2 - Interval 2
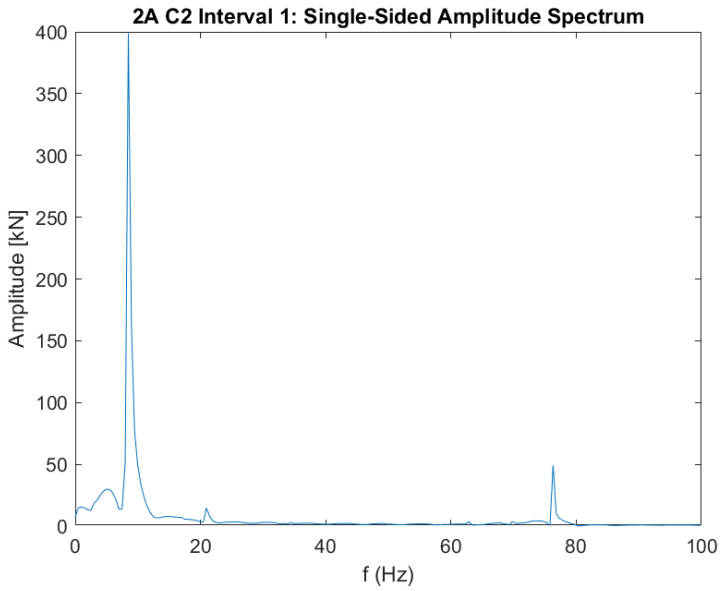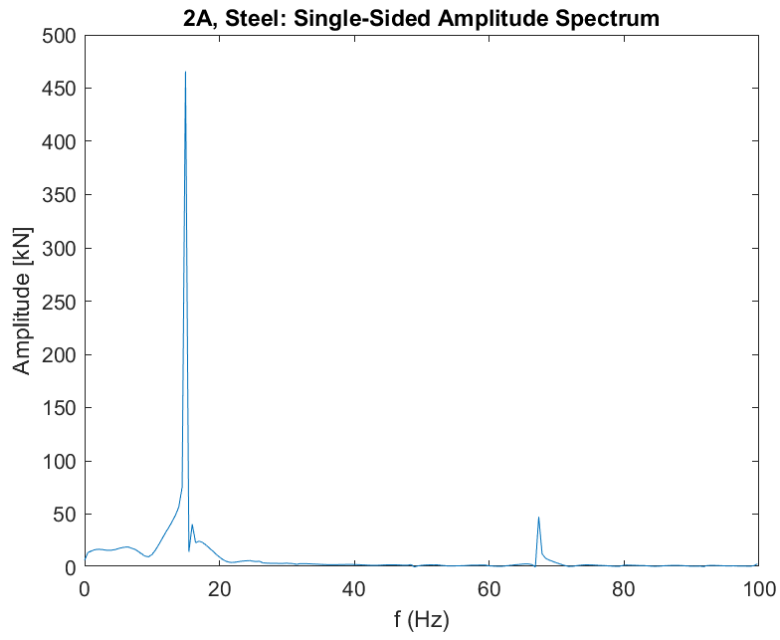
3C C3 - Interval 1
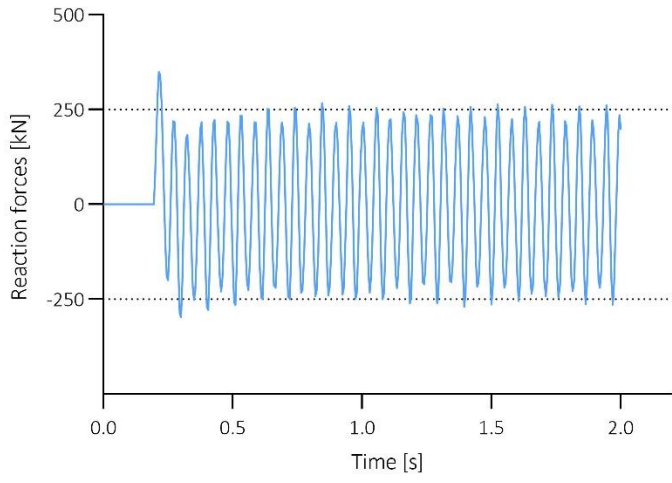
3C C3 - Interval 2
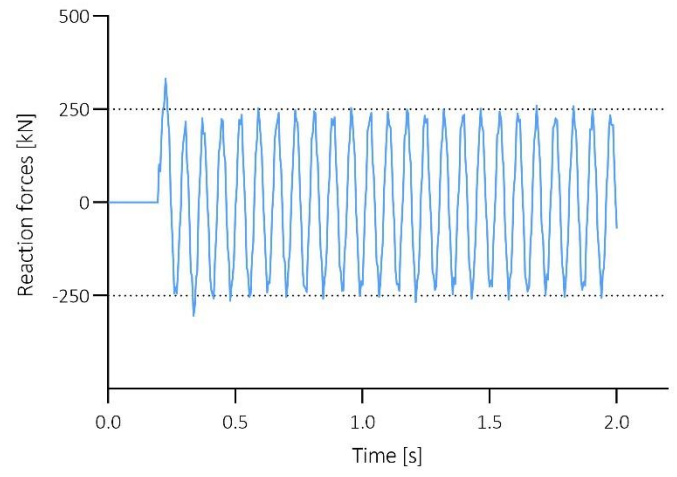
Appendix B

FFT – DATASET 1A
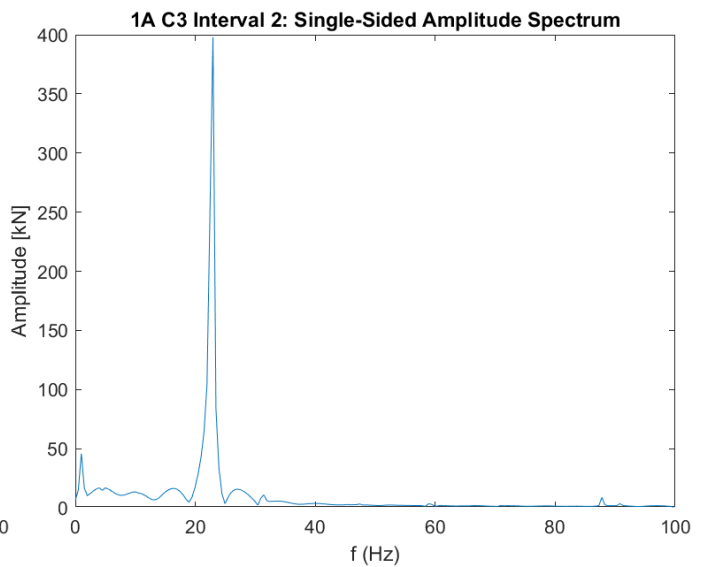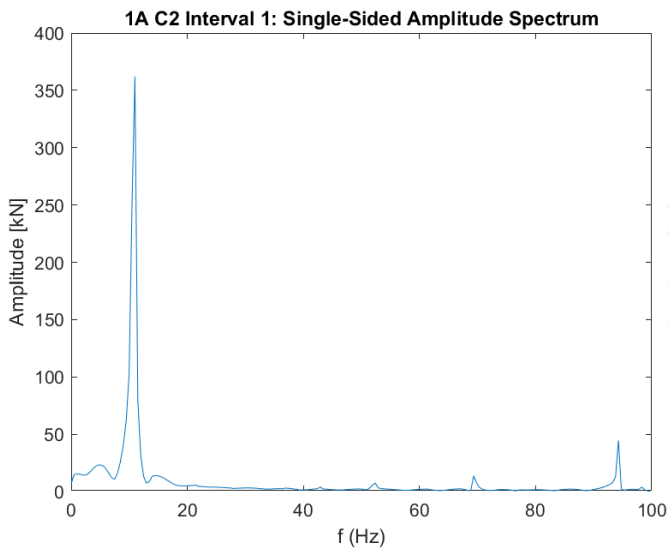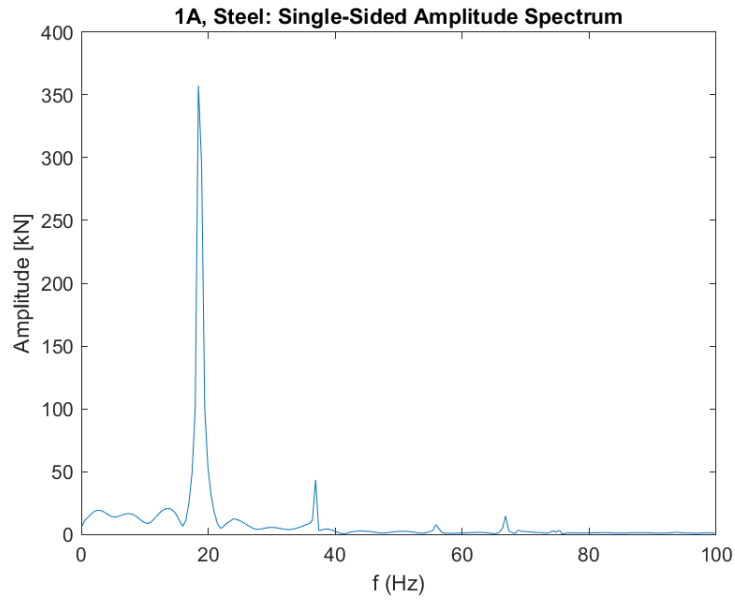
FFT – DATASET 2A

FFT – DATASET 3A